ARL-TR-10010 • Oct 2024

A Universal Continuum Theory and Shock Wave Analysis for Biologic Solids and Fluids

by John D Clayton

NOTICES

Disclaimers

The findings in this report are not to be construed as an official Department of the Army position unless so designated by other authorized documents.

Citation of manufacturer's or trade names does not constitute an official endorsement or approval of the use thereof.

Destroy this report when it is no longer needed. Do not return it to the originator.

ARL-TR-10010 ● OCT 2024

A Universal Continuum Theory and Shock Wave Analysis for Biologic Solids and Fluids

John D Clayton
DEVCOM Army Research Laboratory

REPORT DOCUMENTATION PAGE

1. REPORT DATE	2. REPORT TYPE	3. DATES COVERED	
		START DATE	END DATE
October 2024	Technical Report	01 August 2024	31 October 2024

4. TITLE AND SUBTITLE

A Universal Continuum Theory and Shock Wave Analysis for Biologic Solids and Fluids

5a. CONTRACT NUMBER	5b. GRANT NUMBER	5c. PROGRAM ELEMENT NUMBER
5d. PROJECT NUMBER	**5e. TASK NUMBER**	**5f. WORK UNIT NUMBER**

6. AUTHOR(S)

John D Clayton

7. PERFORMING ORGANIZATION NAME(S) AND ADDRESS(ES)

DEVCOM Army Research Laboratory
ATTN: FCDD-RLA-TB
Aberdeen Proving Ground, MD 21005-5066

8. PERFORMING ORGANIZATION REPORT NUMBER

ARL-TR-10010

9. SPONSORING/MONITORING AGENCY NAME(S) AND ADDRESS(ES)	10. SPONSOR/MONITOR'S ACRONYM(S)	11. SPONSOR/MONITOR'S REPORT NUMBER(S)

12. DISTRIBUTION/AVAILABILITY STATEMENT

DISTRIBUTION STATEMENT A. Approved for public release: distribution unlimited.

13. SUPPLEMENTARY NOTES

primary author's email: <john.d.clayton1.civ@army.mil>
ORCID: John D Clayton 0000-0003-4107-6282

14. ABSTRACT

Soft biologic tissues comprise one or more solid and fluid phases and may exhibit nonlinear anisotropic elastic, viscoelastic, thermoelastic, and poroelastic behaviors. Tissues can tear or rupture when loading is severe. A mixture theory is formulated to account for finite deformations, thermal effects, phase interactions, and degradation of tissues. Physical mechanisms are encompassed in a universal, thermodynamically consistent formulation that combines the continuum theory of mixtures with phase-field mechanics of fracture. A metric tensor of generalized Finsler geometry provides insight on rearrangements of microstructure; for example, degrading collagen fibers and remnant strains. Energy potentials capture isotropic and anisotropic behaviors pertinent to fibrous-tissue microstructures. Kinetic equations consistent with derived conservation laws and the dissipation inequality describe viscoelasticity, fracture, and exchanges of mass, momentum, and energy among coexisting phases. Shock waves are modeled as surfaces of singularity. Hugoniot states and shock decay are quantified, the latter by a new analytical solution encompassing dissipation from viscoelasticity, damage, and phase interactions that reduce shock amplitudes over time. Agreement of calculations and experimental data is respectable, validating theory and parameters. Materials studied include water, extracellular fluid, blood, skeletal muscle, liver, lung, and skin.

15. SUBJECT TERMS continuum mechanics, nonlinear elasticity, mixture theory, phase field, damage mechanics, differential geometry, soft matter, biologic tissue, shock physics, Terminal Effects

16. SECURITY CLASSIFICATION OF:			17. LIMITATION OF ABSTRACT	18. NUMBER OF PAGES
a. REPORT	b. ABSTRACT	C. THIS PAGE		
UNCLASSIFIED	UNCLASSIFIED	UNCLASSIFIED	UU	136

19a. NAME OF RESPONSIBLE PERSON	19b. PHONE NUMBER *(Include area code)*
John D Clayton	410-278-5966

STANDARD FORM 298 (REV. 5/2020)
Prescribed by ANSI Std. Z39.18

Contents

List of Figures

List of Tables

Acknowledgments

The author acknowledges support from the US Army Combat Capabilities Development Command (DEVCOM) Army Research Laboratory (ARL).

This report encompasses and extends work recently published by the author[1] in the journal *Physical Review E*. The theoretical presentation with supporting discussion and references are enhanced. New content on modeling the dynamic response and shock decay in skin tissue is included. In this new analysis, skin is treated either as a two-phase mixture of an anisotropic fibrous solid and an extracellular fluid or as a single-phase, anisotropic viscoelastic material with homogenized mechanical and thermodynamic properties of its solid and fluid constituents. Some content of this report was also recently presented at an international conference on Finsler geometry.[2]

[1] Clayton J. Universal phase-field mixture representation of thermodynamics and shock wave mechanics in porous soft biologic continua. Physical Review E. 2024;110:035001.

[2] Clayton J. Generalized Finsler geometry for physics of ferromagnetic crystals and soft biologic tissues (invited plenary lecture). New Methods in Finsler Geometry IV; 2024 Sep 2–6; Brasov, Romania.

1. Introduction

A nonlinear constitutive theory—for example, the one set forth in a recent article[1] that is a precursor to the present, more comprehensive, technical report—is required to model the complex physics of soft biological tissue when subject to mechanical and thermal loading. Soft tissues of relevance to the current study include skin, muscle, connective tissue, blood vessels, and the internal organs. These materials are often simultaneously nonlinear anisotropic elastic, viscoelastic, thermoelastic, and poroelastic.[2,3]

For traumatic scenarios involving dynamic impact or blast, extreme deformation magnitudes and rapid loading rates arise.[2,4–9] Large deformations manifesting nonlinear mechanical response occur frequently even under normal physiological activity, necessitating a geometrically nonlinear theory.[2,3] Medical events involving disease and surgery incur deterioration, cutting, or tearing (i.e., fracture) of the tissue, requiring a treatment of damage mechanics. Understanding soft-tissue damage is paramount for development and validation of injury criteria[10–12] important for forensic science, sports medicine, and military and law enforcement communities, as well as efforts toward trauma mitigation in engineering biomechanics.[2]

Microstructures are often hierarchical and highly complex.[2,3,13] Materials consist of multiple solid- and fluid-like phases. The liver includes the spongy parenchyma, connective tissue, blood vessels and ducts, plus blood and bile.[14,15] Skeletal and cardiac muscles contain fibers (i.e., cells), connective tissue, blood, and interstitial fluid.[3,16] Skin includes dermal tissue layers, cells, and interstitial fluid.[17] Lung includes parenchyma (e.g., alveoli and ducts), air, and surfactant fluid, as well as stiffer elements of the bronchiole structure.[2] Membraneous tissues (e.g., in skin) contain ground substance, elastin, and collagen fibers.[18] Blood has cells immersed in the extracellular plasma.[3,19,20] Cells themselves can include solid-like walls and internal fluids.[21,22]

Contemporary constitutive treatments of mechanics of soft tissues most often focus on their nonlinear elastic response.[16,23,24] Effects of fluids are included implicitly in the energy densities and parameters, perhaps augmented with viscoelasticity or other dissipation elements.[25–27] Even in the nondissipative case, sophisticated models are needed to account for anisotropy and nonlinearity; for example, due to preferred distributions of collagen fibers.[28–30] If tearing or degradation occurs, con-

tinuum damage mechanics theories are fairly standard,[8,31–36] whereby phenomenological kinetic equation(s) are prescribed for internal state variable(s) measuring local loss of stress-bearing capacity.

In contrast to the former method, the phase-field approach has been more recently advocated for modeling tearing of soft biologic tissues.[37–39] Diffuse-interface modeling has witnessed use over a broad application space; models with elasticity include phase changes, twinning, and dislocations in crystals.[40–44] The method appeared for brittle fracture around 25 years ago,[45–49] typically for isotropic elasticity theory at small strains. Finite-strain approaches for fracture appeared not long thereafter.[50,51] Fluid cavitation[52] and fluid injection[53] have been modeled, as has coupling of fracture to other deformation mechanisms.[54–56] From the perspective of numerical simulation, advantages of phase-field methods include an intrinsic regularization length to mitigate mesh sensitivity and preserve compatibility with standard finite element meshing technology. The latter feature, since mesh topology is preserved, contrasts cohesive-zone finite element methods popular for modeling interfacial separation.[57–61] Rate- and pressure-dependence of fracture kinetics can be modeled with the phase-field method.[62,63]

Continuum mixture theories and porous media theories emerged in the mid-20th century.[64–68] Microstructure details are smeared, but these models distinguish among stresses and deformations of each constituent and capture transfers of mass, momentum, and energy between phases. Mixture- and porous-media theories introduce length and time scales that are absent in single-phase viscoelasticity.[69,70] Although porous media models have been used for soft tissues,[14,15,69,71–74] they have not been routinely combined with the phase-field fracture approach for the class of soft biologic materials. Finite strains[75] and thermal exchange effects[76] have, however, been considered previously with phase-field fracture of brittle porous media.

The theory of porous media classically models a two-phase system of one solid and one fluid, though models with multiple fluids exist. The fully dense solid and fluid phases are usually treated as incompressible, but the mixture overall is compressible as fluid is locally squeezed out.[14,69,71] Solid and fluid are usually, but not always,[15] treated as inviscid individually, but interactions of viscous origin between phases are captured by hydraulic conductivity and dissipation from fluid transport (e.g., Darcy's law). An effective stress principle[77] decomposes total stress into solid

skeleton stress and pore pressure. Constitutive equations are supplied for the solid skeleton (i.e., drained material) and fully dense fluid rather than for partial stresses of mixture components. This method has proven successful for soil and rock mechanics in which the distinction between solid and fluid(s) is clear (e.g., water flowing through sand or porous rock), and it has been used elsewhere for porous tissues.[69,71,78]

The effective stress principle with solid-skeleton concept[72,77] is not implemented here for several reasons. First, tissue may consist of multiple solid and fluid phases. For example, the liver has the parenchyma, blood vessels, and connective tissue (which might be tied or displace independently), and distinct fluids of blood and bile. Second, designation of a constituent as a "solid" or "fluid" may be ambiguous; for example, the extracellular matrix of tissue or blood demonstrating both viscous (fluid-like) and viscoelastic (solid-like) physics.[19,20,79] With no single true solid or fluid phase, the soil mechanics analogy is tenuous. Cracking in ambiguously soft materials also shows richer physics than in brittle elastic solids due to stochastic bond opening and closure (i.e., healing).[80]

A continuum mixture theory similar to those of Bowen,[67] Bowen and Wright,[81] Baer and Nunziatio,[82] Madjarevic et al.,[83] and Madjarevic and Simic[84] is advocated here[1] instead, with constituent energies formulated on a per-unit-mass basis. Complexity in thermodynamic derivations is reduced since partial stresses are used instead of effective stress and pore pressure. However, potential difficulty can arise in ascertaining properties of isolated phases because experiments might measure responses of only some (e.g., fluid) phase(s) and the mixture as a whole. This issue is rectified by example in Section 4.

The typical assumption[85] of incompressibility of individual phases is abandoned herein to resolve bulk sound waves and longitudinal shocks. Furthermore, in a two-phase nonreactive mixture of a solid and fluid, incompressibility of the "real" solid phase restricts local volumetric compression to not exceed the porosity (i.e., an initial fluid volume fraction).[86,87] For biologic systems modeled in this report, with porosity on the order of 10%, solid incompressibility is incompatible with strong shock loading.[88] If the system is closed (i.e., no mass flux across boundaries), no interphase mass reactions occur, and if all constituents are truly incompressible, then any volumetric compression of the system as a whole is impossible. Incom-

pressibility is also unrealistic if materials locally dilate under shock loading[89,90] or undergo cavitation; for example, tensile or spall damage.[52,60,91]

Augmenting the original presentation,[1] a unified framework is formulated in Sections 2 and 3. This universal framework synthesizes continuum mixture theory, nonlinear anisotropic thermoelasticity, viscosity, viscoelasticity, and phase-field fracture mechanics for biologic systems. Prior to the original article,[1] a universal, thermodynamically consistent theory containing all such features relevant to soft-tissue mechanics for intense rapid loading did not seem to exist. Another unique aspect is generalized Finsler geometry[92–94] describing the material manifold with evolving microstructure.[95–97]

Traditional continuum models[65] are couched in ambient Euclidean 3-space. Residual stresses from growth and remodeling have been considered using theories of Riemannian geometry with a material metric having nonvanishing curvature tensor.[98–100] Geometric methods have similarly long been used to study crystal lattices and crystal defects; see representative works[101–104] and historic references cited therein. A recent approach[94,95,105] accounts for effects of microstructure using a generalized Finsler metric[92] as opposed to a Riemannian metric. In addition to residual stress from growth and remodeling,[105] the Finsler-geometric approach on the material manifold has been used to describe changes in local configurations of collagen fibers as tissues degrade and tear.[97] A Finsler metric was used elsewhere to quantify effects of fiber orientations on mechanical responses of soft tissues in a discrete bond-based model[106,107] rather than a continuum physics approach as herein. The Finsler-geometric theory has similarities to micropolar theory,[108–110] but the former is more general.[93,95,97,111] Much past work focused on hard crystalline solids.[96,112–115]

Shock waves in soft tissues are analyzed in the preceding article[1] and this report with the mixture theory and constitutive frameworks. Hugoniot solutions and evolution equations are derived for compressive shocks, extending prior works[87,116–118] to simultaneously account for internal state variables (e.g., order parameters) and the Finsler metric that, in the present application, can be transformed to an osculating Riemannian metric.[97,119,120] The osculating Riemannian description, when admissible, can simplify some derivations and calculations. But the Finslerian description offers a clearer delineation of effects of microstructure on geometry and

material response and enables more broad classes of physical behaviors via a wider selection of linear and nonlinear connection coefficients.[97,105,113]

Dissipation from viscoelasticity, momentum and energy transfer between phases, and degradation due to shear-induced tearing all potentially affect shock amplitudes over time. Treatment of shocks as singular surfaces of velocity[65,87,116–118,121–123] differs from those of continuous waves in nonlinear materials.[124] Shock structures (e.g., shapes of continuous wave forms) have been analyzed elsewhere for nonlinear solids[125] and fluids.[84,126]

Modeled in the precursor study[1] and Section 4 of this report are three soft-tissue systems: skeletal muscle with interstitial fluid, liver with blood, and lung with air. Prior to modeling such two-constituent systems, an equation of state (EOS) entering the theory is validated for describing the shock Hugoniot response of water, extracellular fluid (ECF), and blood. The ideal gas model used for air is standard[127] and was verified in prior work[87] on lung mechanics. Solutions to physical problems involving tension, compression, or shock-wave loading grant new understanding of the physics demonstrated by these biological materials and their constituents.

New theory and results in Section 4.4.2 describe the dynamic response of skin tissue. The quasi-static, nonlinear elastic, 2-D orthotropic framework of a recent article,[97] which invokes generalized Finsler geometry to describe rearrangement and degradation of collagen fibers, is adapted to 3-D and augmented to account for viscoelasticity, poromechanics, and thermal effects. Skin is modeled either as a two-phase system of solid tissue and interstitial fluid[17] or a single-phase system with homogenized physical properties. Shock evolution in different directions with respect to fiber orientations is analyzed for both model representations. Conclusions follow in Section 5. A list of terminology and notation is included after the bibliography.

In the current applications, like most prior settings of continuum theory,[16,25–28,128] the transient uncoiling, recruitment, and nonaffine deformations of collagen-fiber families witnessed in some experiments[18,129] are not modeled explicitly. Rather, such dynamic "remodeling" effects are included implicitly in functions and material parameters that dictate the fibers' contributions to strain energy, viscoelasticity, and damage. A more physically realistic approach—one that should consider ideas from other theoretical studies on soft tissues,[105,130–136] some including poromechan-

ics with anelasticity[137,138] or phase-field type kinetics[86]—remains to be developed for remodeling of tissue under severe dynamic loading conditions (i.e., high strain rates). Whether or not such remodeling processes have sufficient time to occur over durations pertinent to shock and impact is presently unknown, but very brief time scales would seem to limit their extent. On the other hand, growth and remodeling processes that equilibrate *before* severe dynamic loading can always induce residual stresses or other heterogeneities that would likely affect the subsequent dynamic response.[98,105,139] This phenomenon, and transient remodeling, have been recently predicted[105] using a Finsler-geometric continuum theory, albeit in the context of quasi-statics (i.e., incremental equilibrium states rather than dissipative dynamics with inertia).

In nearly all applications reported in Section 4, initial stresses differing from ambient atmospheric pressure, residual stresses, and material heterogeneities are omitted in model representations. The lone exception is active muscle tension prescribed as one kind of initial condition for stimulated skeletal muscle. However, the general framework outlined in Sections 2 and 3 of this report should accommodate growth and remodeling if physically suitable state variables with kinetic laws and their effects on system energy and geometry (e.g., metric tensors) can all be prescribed.

2. Governing Equations

The present theory builds significantly on the finite-strain mixture theories of Bowen and Clayton.[67,68,87] This framework of Bowen,[67] with origins in the treatise of Truesdell and Toupin[65] and consistent with the rational thermodynamics philosophy of Truesdell,[140] is used as starting point for several reasons. First, this framework is of sufficient generality, upon several augmentations discussed shortly, to describe all physical phenomena of present interest. Second, although other rigorous mixture theories exist and numerous generalizations and specializations of the Bowen–Truesdell framework have been postulated, especially with regard to thermodynamics (see discussions in Rajagopal and Tao[141] and Hall and Rajagopal,[142] and references therein), the original theory was then, and still is, widely accepted as physically credible and mathematically "correct."[67]

To the same extent as the original theories,[65–67,140] the present framework obeys the three principles of mixture theory emphasized by Truesdell,[140] paraphrased as follows:

1. All properties of the mixture are mathematically obtained from properties of its constituents.

2. Each constituent's behaviors can be described by governing equations for that single constituent, provided these equations account for its interactions with other constituents.

3. Behavior of the mixture obeys governing equations of the same form as those for a single-constituent body.

The third principle constrains interactions and suggests definitions for "average" quantities of the mixture as a whole. The latter are not unique,[143,144] nor even do all exist. For example, average (e.g., tensor-valued) quantities referred to "material" coordinates may not exist, there being no unique material/reference configuration of the mixed system when velocity histories of constituents differ or mass supplies exist.[145,146] Average temperature is not well-defined in Bowen[67] unless all constituents share the same temperature, but it has been defined elsewhere.[147]

Two enhancements are incorporated here. First, time-dependent general internal state vectors are introduced. Elements of these vectors are associated with history-dependent mechanisms in the material microstructure, namely viscoelasticity, active tension, and damage, all generally anisotropic. A dependence of energy potentials on internal state and the gradient of internal state is permitted, with terms associated with internal state gradients properly incorporated in the balance of energy and boundary conditions. This enables a phase-field type representation when the internal variables of gradient type are interpreted as order parameters,[40,42,148] suitable for modeling regularized fracture.[38,50,51,75]

Second, metric tensors on spatial and material manifolds are permitted to depend on internal state and can be time-dependent. Distances measured in the material can include remnant strains from dissipative processes, or internal strains from biologic growth and remodeling, if the latter physics are resolved by state variables. If internal-state dependence of metrics is explicit and distinct from coordinate dependence, a generalized Finsler representation emerges.[94,95] If internal-state dependence is implicit and state vectors are (time-dependent) functions of position,[149] then an osculating Riemannian geometry[97,105,120] is obtained. In the Riemannian setting, similarities with theoretical studies of Takamizawa and Matsuda,[98]

Takamizawa and Nakayama,[139] and Yavari[99] are noted.

2.1 Geometry and Kinematics

A mixture of $N \geq 1$ constituents is considered, where at time t, these occupy a shared infinitesimal control volume $\mathrm{d}\Omega$ centered at spatial position $\mathbf{x}$. Greek superscripts $\alpha = 1, \ldots, N$ denote constituents having reference coordinates $\mathbf{X}^\alpha$; constituents coincident at $\mathbf{x}$ may occupy different $\mathbf{X}^\alpha$ due to diffusion processes. Motions are

$$\mathbf{x} = \boldsymbol{\chi}^\alpha(\mathbf{X}^\alpha, t). \tag{1}$$

A spatial manifold comprising the material body, parameterized by one or more coordinate charts $\{x^k\}$, is $\mathfrak{m}$. Referential manifold(s) $\mathfrak{M}^\alpha$ are parameterized by coordinate chart(s) $\{(X^\alpha)^K\}$ corresponding to reference positions of constituent α. Denote by $\{\boldsymbol{\xi}^\alpha(\mathbf{x}, t)\}$ and $\{\boldsymbol{\Xi}^\alpha(\mathbf{X}^\alpha, t)\}$ sets of internal state variables viewed as auxiliary coordinates over $\mathfrak{m}$ and $\mathfrak{M}^\alpha$, respectively.[96,97] Metric tensors $\mathbf{g}$ and $\mathbf{G}^\alpha$ with components g_{ij} and G^α_{IJ} are permitted to be coordinate- and time-dependent in the general functional forms

$$\mathbf{g} = \mathbf{g}(\mathbf{x}, t) = \tilde{\mathbf{g}}(\mathbf{x}, \{\boldsymbol{\xi}^\alpha(\mathbf{x}, t)\}), \tag{2}$$

$$\mathbf{G}^\alpha = \mathbf{G}^\alpha(\mathbf{X}^\alpha, t) = \tilde{\mathbf{G}}^\alpha(\mathbf{X}^\alpha, \{\boldsymbol{\Xi}^\alpha(\mathbf{X}^\alpha, t)\}). \tag{3}$$

The $\sim$ notation denotes the generalized Finsler description[92,94,95] of metrics on $\mathfrak{m}$ and $\mathfrak{M}^\alpha$, whereas unadorned versions are interpreted as osculating Riemannian metric tensors[97,105,119,120] at any fixed time t. Determinants are written $g = \det \mathbf{g}$ and $G^\alpha = \det \mathbf{G}^\alpha$.

The partial time derivative at fixed $\mathbf{x}$ is $\partial_t(\cdot)$; the material time derivative at fixed $\mathbf{X}^\alpha$ is $D^\alpha_t(\cdot)$, related by

$$D^\alpha_t(\cdot) = \partial_t(\cdot) + \nabla(\cdot) \cdot \boldsymbol{\upsilon}^\alpha, \qquad (\upsilon^\alpha)^k = D^\alpha_t(\chi^\alpha)^k. \tag{4}$$

Particle velocity is $\boldsymbol{\upsilon}^\alpha$, and $\nabla(\cdot)$ is the covariant derivative with respect to $\mathbf{x}$ where Christoffel symbols are those of the Levi-Civita connection derived from g_{ij}. The covariant derivative with respect to $\mathbf{X}^\alpha$ on $\mathfrak{M}^\alpha$ is $\nabla^\alpha_0(\cdot)$. Spatial and referential gradient operators obey

$$\nabla(\cdot) = \partial(\cdot)/\partial x^k \otimes \mathbf{g}^k, \qquad \nabla^\alpha_0(\cdot) = \partial(\cdot)/\partial (X^\alpha)^K \otimes (\mathbf{G}^\alpha)^K. \tag{5}$$

When used on *typical* scalars, vectors, and tensors, $\partial_t(\cdot)$ and $D_t^\alpha(\cdot)$ are performed with natural basis vectors $\mathbf{g}_k = \partial\mathbf{x}/\partial x^k$ held fixed with respect to t at $\mathbf{x}$ and $\mathbf{G}_K^\alpha = \partial\mathbf{X}^\alpha/\partial(X^\alpha)^K$ held fixed with respect to t at $\mathbf{X}^\alpha$, so $\partial_t\mathbf{g}_k$ and $D_t^\alpha\mathbf{G}_K^\alpha$ vanish in such circumstances. These definitions of partial spatial and material time differentiations produce the following commutation rules:

$$\nabla[\partial_t(\cdot)] = \partial_t[\nabla(\cdot)], \qquad \nabla_0^\alpha[D_t^\alpha(\cdot)] = D_t^\alpha[\nabla_0^\alpha(\cdot)]. \tag{6}$$

The deformation gradient $\mathbf{F}^\alpha$ and Jacobian determinant J^α are defined as follows, the former giving a relation between reference and spatial gradient operators:

$$(F^\alpha)^i_J = \frac{\partial(\chi^\alpha)^i}{\partial(X^\alpha)^J}, \qquad J^\alpha = \det[(F^\alpha)^i_J]\sqrt{g/G^\alpha}, \tag{7}$$

$$\mathbf{F}^\alpha = (F^\alpha)^i_J\mathbf{g}_i \otimes (\mathbf{G}^\alpha)^J, \qquad \nabla_0^\alpha(\cdot) = \nabla(\cdot)\mathbf{F}^\alpha. \tag{8}$$

The velocity gradient $\mathbf{l}^\alpha$ and its trace are

$$\mathbf{l}^\alpha = \nabla\boldsymbol{v}^\alpha = D_t^\alpha\mathbf{F}^\alpha(\mathbf{F}^\alpha)^{-1}, \qquad \nabla\cdot\boldsymbol{v}^\alpha = \mathrm{tr}\mathbf{l}^\alpha. \tag{9}$$

Spatial and material volume elements, respective $\mathrm{d}\Omega$ and $\mathrm{d}\Omega_0^\alpha$, obey

$$\mathrm{d}\Omega(\mathbf{x}(\mathbf{X}^\alpha,t),t) = J^\alpha(\mathbf{X}^\alpha,t)\mathrm{d}\Omega_0^\alpha(\mathbf{X}^\alpha,t). \tag{10}$$

Time derivatives of local volume elements allow for time dependence of metric tensors, extending the theory of Yavari,[99] for example, as*

$$\partial_t(\mathrm{d}\Omega) = \tfrac{1}{2}\mathrm{tr}(\partial_t\mathbf{g})\mathrm{d}\Omega = \partial_t(\ln\sqrt{g})\mathrm{d}\Omega, \tag{11}$$

$$D_t^\alpha(\mathrm{d}\Omega_0^\alpha) = \tfrac{1}{2}\mathrm{tr}(D_t^\alpha\mathbf{G}^\alpha)\mathrm{d}\Omega_0^\alpha = D_t^\alpha(\ln\sqrt{G^\alpha})\mathrm{d}\Omega_0^\alpha, \tag{12}$$

$$\begin{aligned} D_t^\alpha(\mathrm{d}\Omega) &= (D_t^\alpha J^\alpha + J^\alpha D_t^\alpha \ln\sqrt{G^\alpha})\mathrm{d}\Omega_0^\alpha \\ &= (\nabla\cdot\boldsymbol{v}^\alpha + \partial_t\ln\sqrt{g})\mathrm{d}\Omega. \end{aligned} \tag{13}$$

In Eq. 13, $D_t^\alpha\sqrt{g/G^\alpha}$ is included in $D_t^\alpha J^\alpha$, and $\partial_t g = D_t^\alpha g$ since ∇g vanishes for a Levi-Civita connection.[150] The partial time derivative of the spatial metric

*In Eqs. 11–13, local volume elements and the Jacobian determinant do not behave as typical "scalars" if metric components comprising $g(\boldsymbol{x},t) = \det(\boldsymbol{g}_i\cdot\boldsymbol{g}_j)$ and $G^\alpha(\boldsymbol{X}^\alpha,t) = \det(\boldsymbol{G}_I^\alpha\cdot\boldsymbol{G}_J^\alpha)$ are regarded as originating from time-dependent basis vectors $\{\boldsymbol{g}_k,\boldsymbol{G}_K^\alpha\}$. These quantities are not invariant under changes of intrinsic coordinate nets whose tangents on spatial and material manifolds furnish the (time-dependent) basis vectors.

tensor in Eq. 11 is defined as $\partial_t \boldsymbol{g} = \partial_t g_{ij}\, \boldsymbol{g}^i \otimes \boldsymbol{g}^j$; the time derivative $\partial_t(\cdot)$ does not commute here with the trace $\mathrm{tr}(\cdot)$ when the inverse metric components g^{ij} are time dependent at $\boldsymbol{x}$. Analogous statements apply for material time derivatives of the referential metric tensors.

In contrast, for other standard (e.g., vector and tensor) quantities, basis vectors are held fixed during spatial and material time differentiation, unless noted otherwise. In such typical cases, this implies that metric components are also held fixed, and thus $\partial_t(\cdot)$ commutes with raising or lowering indices of a standard object via $\boldsymbol{g}$, and $D_t^\alpha(\cdot)$ commutes with raising or lowering indices of a standard object via $\boldsymbol{G}^\alpha$. Furthermore, since covariant derivatives of $\boldsymbol{g}$ and $\boldsymbol{G}^\alpha$ vanish, each particular metric tensor's spatial and material time derivatives are equal via Eq. 4. Thus, this commutation applies in both reference and current configuration coordinate charts, regardless of which time derivative is used. The special cases in Eqs. 11–13 constitute exceptions to these rules.

The spatial mass density of constituent α is $\rho^\alpha(\mathbf{x}, t)$. Referential mass density at a fixed time $t = t_0$ is $\rho_0^\alpha(\mathbf{X}^\alpha)$ with metric $\mathbf{G}_0^\alpha(\mathbf{X}^\alpha)$ and mass element $\mathrm{d}m_0^\alpha(\mathbf{X}^\alpha) = \rho_0^\alpha \sqrt{G_0^\alpha / G^\alpha}\mathrm{d}\Omega_0^\alpha$. At an arbitrary time t, the local mass element is, dropping arguments from the right side for brevity,

$$\mathrm{d}m^\alpha(\mathbf{X}^\alpha, t) = \rho^\alpha \mathrm{d}\Omega = \rho^\alpha J^\alpha \mathrm{d}\Omega_0^\alpha. \tag{14}$$

2.2 Continuous Processes

Define the following, all generally fields of $(\mathbf{x}, t)$: partial Cauchy stress tensor $\boldsymbol{\sigma}^\alpha$, traction vector $\mathbf{t}^\alpha = \boldsymbol{\sigma}^\alpha \cdot \mathbf{n}$, body force per unit mass $\mathbf{b}^\alpha$, partial internal energy per unit mass u^α, heat source per unit mass r^α, heat flux vector $\mathbf{q}^\alpha$, mass supply rate c^α, linear momentum exchange $\mathbf{h}^\alpha$, and energy exchange rate ϵ^α.

A global energy balance for each constituent is posited on a region of $\mathfrak{m}$ occupying a transient control volume Ω, enclosed by oriented boundary $\partial\Omega$ with unit outward normal $\mathbf{n}$. Velocity and heat flux normal to $\partial\Omega$ are $v_n^\alpha = \boldsymbol{v}^\alpha \cdot \mathbf{n}$ and $q_n^\alpha = \mathbf{q}^\alpha \cdot \mathbf{n}$, respectively. The global balance per constituent extends that of Bowen[67] to account for energy supplies of generalized tractions $\{\mathbf{z}^\alpha\} = \{\boldsymbol{\zeta}^\alpha \cdot \mathbf{n}\}$ work-conjugate to rates

of auxiliary variables $\{D_t^\alpha \boldsymbol{\xi}^\alpha\}$ on $\partial\Omega$, similarly to the philosophy of Gurtin[148]:

$$\begin{aligned}
&\partial_t \int_\Omega \rho^\alpha (u^\alpha + \tfrac{1}{2}|\boldsymbol{\upsilon}^\alpha|^2) \mathrm{d}\Omega + \oint_{\partial\Omega} \rho^\alpha (u^\alpha + \tfrac{1}{2}|\boldsymbol{\upsilon}^\alpha|^2) \upsilon_n^\alpha \mathrm{d}\partial\Omega \\
&= \oint_{\partial\Omega} (\mathbf{t}^\alpha \cdot \boldsymbol{\upsilon}^\alpha + \{\mathbf{z}^\alpha\} \cdot \{D_t^\alpha \boldsymbol{\xi}^\alpha\} - q_n^\alpha) \mathrm{d}\partial\Omega \\
&\quad + \int_\Omega [\rho^\alpha (\mathbf{b}^\alpha \cdot \boldsymbol{\upsilon}^\alpha + r^\alpha) + \mathbf{h}^\alpha \cdot \boldsymbol{\upsilon}^\alpha + \epsilon^\alpha + c^\alpha (u^\alpha + \tfrac{1}{2}|\boldsymbol{\upsilon}^\alpha|^2)] \mathrm{d}\Omega. \qquad (15)
\end{aligned}$$

Angular momentum exchange between constituents[67] is omitted herein. When $\{\boldsymbol{\zeta}^\alpha\} \to \{\mathbf{0}\}$, Eq. 15 matches the Bowen–Truesdell theory.[65,67] Working of $\{\mathbf{z}^\alpha\}$ is necessary to enable derivation of Ginzburg–Landau (i.e., Allen–Cahn) kinetic laws for internal variables of gradient type.[148,151]

Field variables in Eq. 15 are assumed sufficiently smooth on Ω such that the divergence theorem applies on $\mathfrak{m}$. Energy conservation under rigid motions (i.e., various time-dependent translations and rigid-body rotations[152,153]) of the entire mixture (i.e., all constituents assigned the same velocity history) then furnishes local conservation laws for mass, momenta, and energy:

$$\partial_t \rho^\alpha + \nabla \cdot (\rho^\alpha \boldsymbol{\upsilon}^\alpha) = c^\alpha - \rho^\alpha \partial_t \ln \sqrt{g} = \hat{c}^\alpha, \qquad (16)$$

$$\nabla \cdot \boldsymbol{\sigma}^\alpha + \rho^\alpha \mathbf{b}^\alpha + \mathbf{h}^\alpha = \rho^\alpha D_t^\alpha \boldsymbol{\upsilon}^\alpha, \qquad \boldsymbol{\sigma}^\alpha = (\boldsymbol{\sigma}^\alpha)^\mathsf{T}, \qquad (17)$$

$$\rho^\alpha D_t^\alpha u^\alpha = \boldsymbol{\sigma}^\alpha : \nabla \boldsymbol{\upsilon}^\alpha + \nabla \cdot (\{\boldsymbol{\zeta}^\alpha\} \cdot \{D_t^\alpha \boldsymbol{\xi}^\alpha\}) - \nabla \cdot \mathbf{q}^\alpha + \rho^\alpha r^\alpha + \epsilon^\alpha. \qquad (18)$$

Differentiation $\partial_t(\cdot)$ is at fixed coordinates $\{x^k\}$, but volume element $\mathrm{d}\Omega(x^k, t)$ may vary with time due to time dependence of $\mathbf{g}$ in Eq. 2, producing Eq. 11 and $\partial_t \int (\cdot) \mathrm{d}\Omega = \int [\partial_t(\cdot) + (\cdot)\partial_t \ln \sqrt{g}] \mathrm{d}\Omega$. This yields the $\rho^\alpha \partial_t \ln \sqrt{g}$ term in Eq. 16, where the latter can also be written as follows using Eq. 4 and $\nabla g_{ij}(x^k, t) = 0$:

$$D_t^\alpha \rho^\alpha + \rho^\alpha \nabla \cdot \boldsymbol{\upsilon}^\alpha = c^\alpha - \rho^\alpha D_t^\alpha \ln \sqrt{g} = \hat{c}^\alpha. \qquad (19)$$

The $\rho^\alpha \partial_t \ln \sqrt{g}$ term only explicitly enters Eqs. 16 or 19 and not Eq. 17 or Eq. 18. It vanishes from the latter two according to steps in the derivation of the local laws, whereby local mass conservation is obtained first and then eliminated in the process of deriving local momentum and energy balances.[67] All concur with invariance of the global energy balance under rigid-body motions,[152] extending derivations in spatial coordinates of Marsden and Hughes[153] and similar to (e.g., covariance) arguments in material coordinates with transient material metrics for growth given

more recently.[99,100]

The same local governing equations can be derived from separately posited global conservation laws of mass, linear momentum, and angular momentum, in addition to energy of Eq. 15, for each constituent, application of the divergence theorem, and localization of each result, as in Bowen.[67] The current procedure obviates the need for prescription of such separate global laws a priori. It also avoids the need for integration of vector fields inherent in global linear and angular momentum equations, an operation that requires existence of shifter tensors[103,154] to a global frame with spatially uniform basis vectors.

The c^α account for mass transfer between constituents when all of the internal variables $\{\boldsymbol{\xi}^\beta\}, \beta = 1, \dots, N$ affecting the metric $\boldsymbol{g}$ through Eq. 2 are held fixed. The $\rho^\alpha \partial_t \ln \sqrt{g}$ measure density changes manifesting from rates of these internal variables, which could include growth or damage, the latter considered an opposite of remodeling. The net mass supply rate for both sources is $\hat{c}^\alpha = c^\alpha - \rho^\alpha \partial_t \ln \sqrt{g}$. In Section 4, the restriction $\hat{c}^\alpha = 0 \, \forall \, \alpha = 1, \dots, N$ is typically invoked, meaning mass of each constituent is preserved. Under this restriction, when $\boldsymbol{g}$ and its determinant are explicitly time dependent, c^α is necessarily nonzero such that the net mass supply rate vanishes.

Denote by η^α the local entropy per unit mass and $\theta^\alpha > 0$ the absolute temperature of constituent α. As in works by Bowen[67] and the present author,[87] an entropy inequality for each constituent is avoided in lieu of an inequality for the whole mixture:

$$\partial_t \int_\Omega \sum_\alpha \rho^\alpha \eta^\alpha \mathrm{d}\Omega + \oint_{\partial\Omega} \sum_\alpha \rho^\alpha \eta^\alpha \upsilon_n^\alpha \mathrm{d}\partial\Omega \geq \int_\Omega \sum_\alpha \frac{\rho^\alpha r^\alpha}{\theta^\alpha} \mathrm{d}\Omega - \oint_{\partial\Omega} \sum_\alpha \frac{q_n^\alpha}{\theta^\alpha} \mathrm{d}\partial\Omega. \tag{20}$$

Note Eq. 20 is identical to that of the Bowen–Truesdell theory.[67,155] From the divergence theorem, Eq. 16, and localization,*

$$\sum_\alpha [\rho^\alpha D_t^\alpha \eta^\alpha + \frac{\nabla \cdot \mathbf{q}^\alpha}{\theta^\alpha} - \frac{\mathbf{q}^\alpha \cdot \nabla \theta^\alpha}{(\theta^\alpha)^2} - \frac{\rho^\alpha r^\alpha}{\theta^\alpha} + c^\alpha \eta^\alpha] \geq 0. \tag{21}$$

*Misprints in Eqs. (2.15), (4.1), $(4.19)_1$, $(4.30)_3$, (4.45), (4.63), $(5.2)_2$, $(5.13)_2$ of a prior article[87] are corrected herein.

Let ψ^α be Helmholtz free energy per unit mass, whereby substitution of Eq. 18 into Eq. 21 yields

$$\psi^\alpha = u^\alpha - \theta^\alpha \eta^\alpha, \tag{22}$$

$$\sum_\alpha (1/\theta^\alpha)[\boldsymbol{\sigma}^\alpha : \nabla \boldsymbol{\upsilon}^\alpha + \nabla \cdot (\{\boldsymbol{\zeta}^\alpha\} \cdot \{D_t^\alpha \boldsymbol{\xi}^\alpha\}) - (\mathbf{q}^\alpha \cdot \nabla \theta^\alpha)/\theta^\alpha + \epsilon^\alpha + c^\alpha \theta^\alpha \eta^\alpha - \rho^\alpha (D_t^\alpha \psi^\alpha + \eta^\alpha D_t^\alpha \theta^\alpha)] \geq 0. \tag{23}$$

2.3 Singular Surfaces

2.3.1 Eulerian Description

Now consider a propagating singular surface $\Sigma(t)$ in $\mathfrak{m}$, with image $\Sigma^\alpha(t)$ in $\mathfrak{M}^\alpha$. The Eulerian function ϕ defines this surface, from which the unit normal $\mathbf{n}$ and Eulerian speed $\mathcal{U} > 0$ in the direction of $\mathbf{n}$ follow:

$$\phi(\mathbf{x}, t) = 0, \qquad \mathbf{n} = \nabla\phi/|\nabla\phi|, \qquad \mathcal{U} = -\partial_t \phi/|\nabla\phi|. \tag{24}$$

Let $(\cdot)^+$ and $(\cdot)^-$ label limiting values of $(\cdot)$ as Σ is approached from either side; $\mathbf{n}$ is directed from the $(\cdot)^-$ side (behind Σ) to the $(\cdot)^+$ side (ahead of Σ). The jump of a scalar, vector, or tensor quantity across Σ is written as

$$[\![(\cdot)]\!] = (\cdot)^- - (\cdot)^+. \tag{25}$$

Across a shock front Σ, each $\boldsymbol{\chi}^\alpha$ is continuous, but space-time derivatives of $\boldsymbol{\chi}^\alpha$ are not necessarily so. Nor always are other field variables such as ρ^α, $\boldsymbol{\sigma}^\alpha$, θ^α, etc. With $\mathbf{n}$ defined per Eq. 24, the normal velocity, heat flux, and tractions are, respectively,

$$\upsilon_n^\alpha = \boldsymbol{\upsilon}^\alpha \cdot \mathbf{n}, \qquad q_n^\alpha = \mathbf{q}^\alpha \cdot \mathbf{n}, \qquad \mathbf{t}^\alpha = \boldsymbol{\sigma}^\alpha \cdot \mathbf{n}, \qquad \{\mathbf{z}^\alpha\} = \{\boldsymbol{\zeta}^\alpha \cdot \mathbf{n}\}. \tag{26}$$

Conservation laws for mass, linear momentum, and energy, and the entropy imbalance, across Σ are derived using principles established or described by Truesdell and Toupin,[65] Grinfeld,[156] and Casey.[157]

Specifically, a closed region Ω of $\mathfrak{m}$ is partitioned by Σ at an instant in time into two sub-bodies, within which the local continuum balance laws of Eqs. 16–18 and 21 hold. These continuum laws are integrated over Ω and then over each sub-body, the

latter accounting for possible boundary contributions on Σ from tractions and heat flux. Integrals are assumed to be physically meaningful even if $\mathfrak{m}$ is non-Euclidean. The total mass rate, linear momentum rate, energy rate, and entropy production rate are required to be equal for Ω and the summed contributions of each sub-body with boundary Σ. Application of a form of Reynolds' transport theorem[111,157] derived from the divergence theorem and Eq. 13 then gives analogs of Eqs. 16–18 across Σ for each α:

$$[\![\rho^\alpha(v_n^\alpha - \mathcal{U})]\!] = 0, \tag{27}$$

$$[\![\rho^\alpha \boldsymbol{v}^\alpha(v_n^\alpha - \mathcal{U})]\!] = [\![\mathbf{t}^\alpha]\!], \tag{28}$$

$$[\![\rho^\alpha(u^\alpha + \tfrac{1}{2}|\boldsymbol{v}^\alpha|^2)(v_n^\alpha - \mathcal{U})]\!] = [\![\mathbf{t}^\alpha \cdot \boldsymbol{v}^\alpha + \{\mathbf{z}^\alpha\} \cdot \{D_t^\alpha \boldsymbol{\xi}^\alpha\} - q_n^\alpha]\!]. \tag{29}$$

A jump equation for angular momentum can be derived, but it encompasses nothing beyond Eq. 28. Similarly, arguments from Casey[157] applied to Eq. 21 furnish a local entropy inequality across Σ for the mixture:

$$\sum_\alpha [\![\rho^\alpha \eta^\alpha(\mathcal{U} - v_n^\alpha) - q_n^\alpha/\theta^\alpha]\!] \geq 0. \tag{30}$$

Now consider one-dimensional (1-D) loading conditions: $n_k \to n_1 = 1$, $x^k \to x^1 = x$, $(\chi^\alpha)^k \to (\chi^\alpha)^1 = \chi^\alpha$, $(F^\alpha)^i_J \to (F^\alpha)^1_1 = \partial\chi^\alpha/\partial X^\alpha = F^\alpha$, $(v^\alpha)^k \to (v^\alpha)^1 = v_n^\alpha = v^\alpha$, $(t^\alpha)_k \to (t^\alpha)_1 = (\sigma^\alpha)^1_1 = t^\alpha$, $\{(z^\alpha)_k\} \to \{(z^\alpha)_1\} = \{(\zeta^\alpha)^1_1\} = \{z^\alpha\}$, $\{(\xi^\alpha)^k\} \to \{(\xi^\alpha)^1\} = \{\xi^\alpha\}$, and $(q^\alpha)^k \to (q^\alpha)^1 = q_n^\alpha = q^\alpha$. The shock is planar, with Eulerian speed $\mathcal{U}$. Eulerian forms of Rankine–Hugoniot Eqs. 27–30 reduce to

$$[\![\rho^\alpha(v^\alpha - \mathcal{U})]\!] = 0, \tag{31}$$

$$[\![\rho^\alpha v^\alpha(v^\alpha - \mathcal{U})]\!] = [\![t^\alpha]\!], \tag{32}$$

$$[\![\rho^\alpha(u^\alpha + \tfrac{1}{2}|v^\alpha|^2)(v^\alpha - \mathcal{U})]\!] = [\![t^\alpha v^\alpha + \{z^\alpha\}\{D_t^\alpha \xi^\alpha\} - q^\alpha]\!], \tag{33}$$

$$\sum_\alpha [\![\rho^\alpha \eta^\alpha(\mathcal{U} - v^\alpha) - q^\alpha/\theta^\alpha]\!] \geq 0. \tag{34}$$

2.3.2 Lagrangian Description

A Lagrangian description of a singular surface, denoted $\Sigma^\alpha(t)$ for each constituent α, is, analogously to Eq. 24,

$$\Phi^\alpha(\mathbf{X}^\alpha, t) = 0, \qquad \mathbf{N}^\alpha = \nabla_0^\alpha \Phi^\alpha / |\nabla_0^\alpha \Phi^\alpha|, \qquad \mathcal{U}^\alpha = -D_t^\alpha \Phi^\alpha / |\nabla_0^\alpha \Phi^\alpha|. \quad (35)$$

In 1-D, Eulerian and Lagrangian shock speeds are[118]

$$\mathcal{U}(t) = \mathrm{d}\Sigma(t)/\mathrm{d}t, \qquad \mathcal{U}^\alpha(t) = \mathrm{d}\Sigma^\alpha(t)/\mathrm{d}t. \quad (36)$$

From the 1-D inverse motion $X^\alpha(\chi^\alpha, t) = (\chi^\alpha)^{-1}(x, t)$,[118]

$$\Sigma^\alpha(t) = (\chi^\alpha)^{-1}(\Sigma(t), t) \quad \Rightarrow \quad \mathcal{U}^\alpha = (F^\alpha)^{-1}(\mathcal{U} - v^\alpha), \quad (37)$$

with $(F^\alpha)^{-1} = \partial(\chi^\alpha)^{-1}/\partial x$.

Now assume a continuous referential density field $\rho_0^\alpha(X^\alpha)$ exists and can be related in 1-D to any other spatial density field $\rho^\alpha(x, t)$ via $\rho_0^\alpha = F^\alpha \rho^\alpha$. Sufficient conditions for the latter consistent with mass conservation are $c^\alpha = \rho^\alpha \partial_t \ln \sqrt{g}$ with $g(\chi^\alpha(X^\alpha, t), t) = G^\alpha(X^\alpha, t)$. In this case, Eq. 31 with Eq. 37 and $[\![\rho_0^\alpha]\!] = 0$ produces $[\![\mathcal{U}^\alpha]\!] = 0$. Thus, noting that $\mathcal{U}^\alpha$ is intrinsic and Eq. 37 should hold at all $(\cdot)^\pm$ states, the following Lagrangian forms of the 1-D Rankine–Hugoniot equations are derived:

$$\rho_0^\alpha \mathcal{U}^\alpha [\![1/\rho^\alpha]\!] = -[\![v^\alpha]\!], \quad (38)$$

$$\rho_0^\alpha \mathcal{U}^\alpha [\![v^\alpha]\!] = -[\![t^\alpha]\!], \quad (39)$$

$$\rho_0^\alpha \mathcal{U}^\alpha [\![u^\alpha + \tfrac{1}{2}|v^\alpha|^2]\!] = -[\![t^\alpha v^\alpha + \{z^\alpha\}\{D_t^\alpha \xi^\alpha\} - q^\alpha]\!], \quad (40)$$

$$\sum_\alpha (\rho_0^\alpha \mathcal{U}^\alpha [\![\eta^\alpha]\!] - [\![q^\alpha/\theta^\alpha]\!]) \geq 0. \quad (41)$$

Routine algebra produces velocity jumps and Lagrangian shock speeds in terms of jumps in stress and mass density:

$$[\![v^\alpha]\!] = ([\![t^\alpha]\!][\![1/\rho^\alpha]\!])^{1/2}, \quad \rho_0^\alpha \mathcal{U}^\alpha = ([\![t^\alpha]\!]/[\![1/\rho^\alpha]\!])^{1/2}. \quad (42)$$

Also, since $\rho_0^\alpha/\rho^\alpha = F^\alpha$ by construction,

$$[\![v^\alpha]\!] = -\mathcal{U}^\alpha [\![F^\alpha]\!], \qquad [\![t^\alpha]\!] = \rho_0^\alpha (\mathcal{U}^\alpha)^2 [\![F^\alpha]\!]. \quad (43)$$

The Rankine–Hugoniot energy balance follows by eliminating particle and shock velocities from Eq. 40:

$$\llbracket u^\alpha \rrbracket = \langle t^\alpha \rangle \llbracket 1/\rho^\alpha \rrbracket - \frac{\llbracket \{z^\alpha\}\{D_t^\alpha \xi^\alpha\} - q^\alpha \rrbracket}{(\llbracket t^\alpha \rrbracket / \llbracket 1/\rho^\alpha \rrbracket)^{1/2}}. \tag{44}$$

where $\langle(\cdot)\rangle = \frac{1}{2}[(\cdot)^+ + (\cdot)^-]$ is the average across Σ^α.

The displacement derivative $\delta_t(\cdot)$ is defined as follows in 1-D,[65] consistently with Eqs. 4 and 36:

$$\delta_t(\cdot) = \partial_t(\cdot) + \mathcal{U}\partial(\cdot)/\partial x = D_t^\alpha(\cdot) + \mathcal{U}^\alpha \partial(\cdot)/\partial X^\alpha. \tag{45}$$

This is the time derivative of a quantity measured by an observer moving with the shock front.

2.3.3 Steady Wave Forms

Jump equations can be derived for conservation of mass, momentum, and energy between any two points in a structured steady wave form.[121,151] In the 1-D Lagrangian description, let $\mathcal{D}^\alpha$ be a constant steady wave speed, such that for a differentiable function $f(X^\alpha, t)$, within the steady wave form,

$$f(X^\alpha, t) = f(X^\alpha - \mathcal{D}^\alpha t) = f(Y^\alpha), \tag{46}$$

$$\partial f/\partial X^\alpha = \mathrm{d}f/\mathrm{d}Y^\alpha, \quad D_t^\alpha f = -\mathcal{D}^\alpha \mathrm{d}f/\mathrm{d}Y^\alpha. \tag{47}$$

Applying Eq. 47 to 1-D equations $D_t^\alpha F^\alpha = \partial \upsilon^\alpha/\partial X^\alpha$ and

$$\rho_0^\alpha D_t^\alpha \upsilon^\alpha = \partial t^\alpha/\partial X^\alpha + \rho_0^\alpha b^\alpha + (\partial \chi^\alpha/\partial X^\alpha) h^\alpha, \tag{48}$$

which is the first of Eq. 17, gives

$$\mathrm{d}\upsilon^\alpha/\mathrm{d}Y = -\mathcal{D}^\alpha \mathrm{d}F^\alpha/\mathrm{d}Y, \tag{49}$$

$$\mathrm{d}t^\alpha/\mathrm{d}Y = -\rho_0^\alpha \mathcal{D}^\alpha \mathrm{d}\upsilon^\alpha/\mathrm{d}Y - \rho_0^\alpha b^\alpha - F^\alpha h^\alpha. \tag{50}$$

Select two points at steady-wave coordinates $Y^\pm$, and define the jump in a quantity between these points as in Eq. 25: $\llbracket f(Y) \rrbracket = f(Y^-) - f(Y^+)$. Direct integration of

Eq. 49 over $Y^- \to Y^+$ and substitution into Eq. 50 gives

$$[\![\upsilon^\alpha]\!] = -\mathcal{D}^\alpha [\![F^\alpha]\!], \tag{51}$$

$$[\![t^\alpha]\!] = \rho_0^\alpha (\mathcal{D}^\alpha)^2 [\![F^\alpha]\!] + \int_-^+ (\rho_0^\alpha b^\alpha + F^\alpha h^\alpha) \mathrm{d}Y. \tag{52}$$

Using the same procedure for 1-D continuum laws of energy conservation and entropy production, Eqs. 18 and 21,

$$\rho_0^\alpha D_t^\alpha u^\alpha = t^\alpha \partial \upsilon^\alpha / \partial X^\alpha + \partial (\{z\}^\alpha \} \{D_t^\alpha \xi^\alpha\}) / \partial X^\alpha - \partial q^\alpha / \partial X^\alpha + \rho_0^\alpha r^\alpha + (\partial \chi^\alpha / \partial X^\alpha) \epsilon^\alpha, \tag{53}$$

$$\sum_\alpha [\rho_0^\alpha D_t^\alpha \eta^\alpha + \partial (q^\alpha / \theta^\alpha) / \partial X^\alpha - \rho_0^\alpha r^\alpha / \theta^\alpha + (\partial \chi^\alpha / \partial X^\alpha) c^\alpha \eta^\alpha] \geq 0, \tag{54}$$

produces jumps between two points $Y^\pm$ in a steady wave:

$$\rho_0^\alpha \mathcal{D}^\alpha [\![u^\alpha + \tfrac{1}{2} |\upsilon^\alpha|^2]\!] = -[\![t^\alpha \upsilon^\alpha + \{z^\alpha\} \{D_t^\alpha \xi^\alpha\} - q^\alpha]\!] + \int_-^+ \{\rho_0^\alpha (r^\alpha + b^\alpha \upsilon^\alpha) + F^\alpha (\epsilon^\alpha + h^\alpha \upsilon^\alpha)\} \mathrm{d}Y, \tag{55}$$

$$\sum_\alpha (\rho_0^\alpha \mathcal{D}^\alpha [\![\eta^\alpha]\!] - [\![q^\alpha / \theta^\alpha]\!]) - \int_-^+ (\rho_0^\alpha r^\alpha / \theta^\alpha - F^\alpha c^\alpha \eta^\alpha) \mathrm{d}Y \} \geq 0. \tag{56}$$

The relation derived in Eq. 51 is identical to the mass conservation law for a singular surface in the first of Eq. 43 when $\mathcal{D}^\alpha \to \mathcal{U}^\alpha$. That derived in Eq. 52 is then identical to the momentum conservation law in the second of Eq. 43 when the integral on the far right of Eq. 52 vanishes (e.g., constant body force and null drag). In such cases, the Eulerian jump conditions in Eqs. 31 and 32 can be recovered for a steady wave form of Eulerian speed $\mathcal{D}$ where $f(x,t) = f(x - \mathcal{D}t)$ when $\mathcal{D} = F^\alpha \mathcal{D}^\alpha + \upsilon^\alpha = \mathrm{constant}$. The relation derived in Eq. 55 is identical to the energy conservation law in Eq. 40 when its integral terms vanish, and Eq. 56 is identical to the entropy inequality of Eq. 41 when its integral terms involving heat and mass supplies vanish.

2.4 Total Expressions for the Mixture

The spatial mass density of the mixture ρ, mean velocity of the mixture $\boldsymbol{v}$, and diffusion velocities $\boldsymbol{\mu}^\alpha$ are

$$\rho = \sum_\alpha \rho^\alpha, \quad \boldsymbol{v} = \frac{1}{\rho}\sum_\alpha \rho^\alpha \boldsymbol{v}^\alpha, \quad \boldsymbol{\mu}^\alpha = \boldsymbol{v}^\alpha - \boldsymbol{v} \quad \Rightarrow \quad \sum_\alpha \rho^\alpha \boldsymbol{\mu}^\alpha = \mathbf{0}. \tag{57}$$

Define the material time derivative of $\square$ with respect to the mixture as

$$\dot{\square} = \partial_t(\square) + \nabla(\square)\cdot\boldsymbol{v} \;\Rightarrow\; D_t^\alpha(\square) = \dot{\square} + (\nabla\square)\cdot\boldsymbol{\mu}^\alpha. \tag{58}$$

Summing Eq. 16 over α then gives the total mass balance for the mixture at space-time location $(\mathbf{x}, t)$:

$$\dot\rho + \rho\nabla\cdot\boldsymbol{v} = \hat{C}, \qquad \hat{C} = \sum_\alpha c^\alpha - \rho\,\partial_t \ln\sqrt{g}. \tag{59}$$

Define, respectively, the total Cauchy stress tensor, total body force vector, total internal energy density, total entropy density, total heat supply, total heat flux, total internal state vector, and total conjugate force vector:

$$\boldsymbol{\sigma} = \sum_\alpha(\boldsymbol{\sigma}^\alpha - \rho^\alpha\boldsymbol{\mu}^\alpha\otimes\boldsymbol{\mu}^\alpha), \qquad \mathbf{b} = \frac{1}{\rho}\sum_\alpha \rho^\alpha \mathbf{b}^\alpha, \tag{60}$$

$$u = \frac{1}{\rho}\sum_\alpha \rho^\alpha\left[u^\alpha + \tfrac{1}{2}|\boldsymbol{\mu}^\alpha|^2\right], \tag{61}$$

$$\eta = \frac{1}{\rho}\sum_\alpha \rho^\alpha\eta^\alpha, \qquad r = \frac{1}{\rho}\sum_\alpha \rho^\alpha r^\alpha, \tag{62}$$

$$\mathbf{q} = \sum_\alpha(\mathbf{q}^\alpha - \boldsymbol{\sigma}^\alpha\cdot\boldsymbol{\mu}^\alpha + \rho^\alpha u^\alpha\boldsymbol{\mu}^\alpha + \frac{\rho^\alpha}{2}|\boldsymbol{\mu}^\alpha|^2\boldsymbol{\mu}^\alpha), \tag{63}$$

$$\{\boldsymbol{\xi}\} = (\{\boldsymbol{\xi}\}^1,\ldots,\{\boldsymbol{\xi}\}^N), \qquad \{\boldsymbol{\zeta}\} = (\{\boldsymbol{\zeta}\}^1,\ldots,\{\boldsymbol{\zeta}\}^N). \tag{64}$$

Recall from Eq. 16 that $\hat{c}^\alpha = c^\alpha - \rho^\alpha\partial_t\ln\sqrt{g}$ and impose the constraints

$$\sum_\alpha \hat{c}^\alpha = \hat{C} = 0, \qquad \sum_\alpha(\mathbf{h}^\alpha + \hat{c}^\alpha\boldsymbol{\mu}^\alpha) = \mathbf{0}, \tag{65}$$

$$\sum_\alpha[\epsilon^\alpha + \mathbf{h}^\alpha\cdot\boldsymbol{\mu}^\alpha + \hat{c}^\alpha(u^\alpha + \tfrac{1}{2}|\boldsymbol{\mu}^\alpha|^2)] = 0. \tag{66}$$

In classical mixture theory,[67] the body consisting of all $\alpha = 1,\ldots,N$ phases is

viewed as a closed system in Euclidean space, $\partial_t \ln \sqrt{g} = 0$, and c^α account exclusively for exchange of mass between phases, locally summing to zero. In many theoretical models of biologic growth and remodeling, the material is treated as an open system[99,158–160]: mass is injected or extracted due to chemical–biological interactions with a background environment. In that open-system interpretation, even in a single-phase material, $\sum_\alpha \hat{c}^\alpha(\mathbf{x}, t)$ could be nonzero. Here, per the first of Eq. 65, a closed-system viewpoint is accepted: total mass comprised by all phases is constant, giving $\hat{C} = 0$.

2.4.1 Continuous Processes

Given Eqs. 57–64 with constraints of Eqs. 65 and 66, the total balances of mass, linear momentum, angular momentum, and energy and the dissipation inequality are obtained by accumulating Eqs. 16–18 and 21 over $\alpha = 1, \ldots, N$, following steps detailed by Bowen,[67] with the addition of work contributions from Eq. 64 whose individual entries are defined as orthogonal:

$$\dot{\rho} + \rho \nabla \cdot \boldsymbol{v} = 0, \quad \nabla \cdot \boldsymbol{\sigma} + \rho \mathbf{b} = \rho \dot{\boldsymbol{v}}, \quad \boldsymbol{\sigma} = \boldsymbol{\sigma}^{\mathsf{T}}, \tag{67}$$

$$\rho \dot{u} = \boldsymbol{\sigma} : \nabla \boldsymbol{v} + \nabla \cdot (\{\boldsymbol{\zeta}\} \cdot \{\boldsymbol{\xi}'\}) - \nabla \cdot \mathbf{q} + \rho r + \sum_\alpha \rho^\alpha \mathbf{b}^\alpha \cdot \boldsymbol{\mu}^\alpha, \tag{68}$$

$$\{\boldsymbol{\xi}'\} = \{\dot{\boldsymbol{\xi}}\} + \sum_\alpha \{\nabla \boldsymbol{\xi}^\alpha \cdot \boldsymbol{\mu}^\alpha\}, \tag{69}$$

$$\rho \dot{\eta} + \nabla \cdot \sum_\alpha \left(\frac{\mathbf{q}^\alpha}{\theta^\alpha} + \rho^\alpha \eta^\alpha \boldsymbol{\mu}^\alpha\right) - \sum_\alpha \frac{\rho^\alpha r^\alpha}{\theta^\alpha} \geq 0. \tag{70}$$

For the particular case when $\theta^\alpha = \theta$ is uniform among constituents at $(\mathbf{x}, t)$, then Eq. 70 simplifies to

$$\rho \dot{\eta} + \nabla \cdot (\hat{\mathbf{q}}/\theta) - \rho r/\theta \geq 0, \quad \hat{\mathbf{q}} = \sum_\alpha (\mathbf{q}^\alpha + \theta \rho^\alpha \eta^\alpha \boldsymbol{\mu}^\alpha). \tag{71}$$

The quantity $\{\boldsymbol{\zeta}\} \cdot \{\boldsymbol{\xi}'\}$ in Eq. 69 can be identified with an interstitial flux vector from Dunn and Serrin[161] in a broad sense, but the present theory does not later incorporate higher-order deformation or density gradients in energy potentials as in that work. Notice that the entropy fluxes in the divergence terms of Eqs. 70 and 71 are generally different than what would be obtained from the mixture heat flux $\mathbf{q}$ of Eq. 63 entering Eq. 68. The difference is well-known[143,144] and consistent with Bowen and Truesdell.[67,140] It emerges naturally if the spatial form of the second law in Eq. 20 is accepted as fundamental. If a global form of Eq. 70 is instead used as a

starting point, then different energy/entropy fluxes in first and second laws must be prescribed a priori.[67]

2.4.2 Singular Surfaces

Jump conditions across singular surfaces can be derived from Eqs. 67, 68, and 71 using the methods already discussed for constituent α. Let $\mathcal{U}$ now be the Eulerian shock speed for the mixture as a whole. Analogs of Eqs. 27–30 are, with an obvious change of notation,

$$[\![\rho(\upsilon_n - \mathcal{U})]\!] = 0, \qquad [\![\rho\boldsymbol{\upsilon}(\upsilon_n - \mathcal{U})]\!] = [\![\mathbf{t}]\!], \tag{72}$$

$$[\![\rho(u + \tfrac{1}{2}|\boldsymbol{\upsilon}|^2)(\upsilon_n - \mathcal{U})]\!] = [\![\mathbf{t}\cdot\boldsymbol{\upsilon} + \{\mathbf{z}\}\cdot\{\boldsymbol{\xi}'\} - \hat{q}_n]\!], \tag{73}$$

$$[\![\rho\eta(\mathcal{U} - \upsilon_n) - \hat{q}_n/\theta]\!] \geq 0. \tag{74}$$

Eulerian equations for the 1-D case follow trivially.

Lagrangian equations for the 1-D case are obtained by defining a Lagrangian speed $\mathcal{U}_0$, deformation mapping F, and space–time continuous reference mass density ρ_0 to obey

$$\mathcal{U}_0 = F^{-1}(\mathcal{U} - \upsilon), \qquad F = \rho_0/\rho. \tag{75}$$

With ρ_0, υ, and $\mathcal{U}$ given, F and $\mathcal{U}_0$ are uniquely defined. Analogs of Eqs. 38–41 are then derived as, with $t_k \to t_1 = \sigma$,

$$\rho_0\mathcal{U}_0[\![1/\rho]\!] = -[\![\upsilon]\!], \qquad \rho_0\mathcal{U}_0[\![\upsilon]\!] = -[\![\sigma]\!], \tag{76}$$

$$\rho_0\mathcal{U}_0[\![u + \tfrac{1}{2}\upsilon^2]\!] = -[\![\sigma\upsilon + \{z\}\{\xi'\} - \hat{q}]\!], \tag{77}$$

$$\rho_0\mathcal{U}_0[\![\eta]\!] - [\![\hat{q}/\theta]\!] \geq 0. \tag{78}$$

Equations fully analogous to Eqs. 42–44 can be derived summarily with the obvious substitutions.

Presuming invertibility and integrability of the second of Eq. 75, a 1-D deformation gradient $F = \partial x/\partial X$ and Lagrangian coordinate X for the mixture exist, whereby

$$\dot{F} = (\partial\upsilon/\partial x)F = \partial\upsilon/\partial X, \tag{79}$$

$$X(x,t) = \chi^{-1}(x,t) = \int_{x_0}^{x} F^{-1}(\tilde{x},t)\mathrm{d}\tilde{x}. \tag{80}$$

The analog of the displacement derivative in Eq. 45 for the mixture is then defined

as

$$\delta_t(\square) = \partial_t(\square) + \mathcal{U}\partial(\square)/\partial x = (\dot{\square}) + \mathcal{U}_0\partial(\square)/\partial X. \tag{81}$$

2.4.3 Steady Wave Forms

Given Eqs. 67, 68, 71, 79, and 80, the treatment of steady Lagrangian waves can be applied to the mixture as a whole. Let $f(X,t) = f(X - \mathcal{D}t) = f(Y)$ in a steady wave, with $\mathcal{D}$ its constant speed. Using relations akin to Eqs. 46 and 47, the local compatibility and linear momentum laws, respective Eqs. 79 and 67 in 1-D, are

$$\mathrm{d}\upsilon/\mathrm{d}Y = -\mathcal{D}\,\mathrm{d}F^\alpha/\mathrm{d}Y, \tag{82}$$

$$\mathrm{d}\sigma/\mathrm{d}Y = -\rho_0\mathcal{D}\,\mathrm{d}\upsilon/\mathrm{d}Y - \rho_0 b. \tag{83}$$

Integrating from $Y^+ \to Y^-$ gives conditions like Eq. 76:

$$[\![\upsilon]\!] = -\mathcal{D}[\![F]\!] = -\mathcal{D}\rho_0[\![1/\rho]\!], \tag{84}$$

$$[\![\sigma]\!] = -\rho_0\mathcal{D}[\![\upsilon]\!] + \int_-^+ \rho_0 b\,\mathrm{d}Y. \tag{85}$$

Energy conservation and entropy production in Eqs. 68 and 70, omitted here for brevity, can be addressed similarly.[121,127]

2.4.4 Volume Fractions and Mass Concentrations

Returning to the general, 3-D spatial formulation, diffusion problems are often analyzed using dimensionless measures of local amounts of each constituent. Recall ρ^α is the local mass of α per unit total spatial volume of mixture. The spatial volume fraction n^α is the ratio of volume occupied by α to that of the mixture, while the real mass density ρ^α_{R} is the local mass of α per unit spatial volume occupied by α (i.e., ρ^α_{R} is mass density of the isolated, fully dense constituent). The spatial mass concentration m^α is the mass of α per total mass of the mixture. Equations for volume fractions and mass concentrations are

$$n^\alpha(\mathbf{x},t) = \frac{\rho^\alpha(\mathbf{x},t)}{\rho^\alpha_{\mathrm{R}}(\mathbf{x},t)}, \qquad \sum_\alpha n^\alpha = 1, \tag{86}$$

$$m^\alpha(\mathbf{x},t) = \frac{\rho^\alpha(\mathbf{x},t)}{\rho(\mathbf{x},t)}, \qquad \sum_\alpha m^\alpha = 1. \tag{87}$$

At a reference time denoted by $t = t_0$, when all particles occupy positions $\mathbf{X}^\alpha$,

$$n_0^\alpha(\mathbf{X}^\alpha) = \rho_0^\alpha(\mathbf{X}^\alpha)/\rho_{\mathrm{R}0}^\alpha(\mathbf{X}^\alpha), \qquad m_0^\alpha(\mathbf{X}^\alpha) = \rho_0^\alpha(\mathbf{X}^\alpha)/\rho_0(\mathbf{X}^\alpha). \tag{88}$$

3. Constitutive Theory

Thermodynamic identities are derived in Section 3.1 by appealing to the local balance of energy and the entropy inequality. Pragmatic and thermodynamically admissible energy functions and kinetic relations are posited, respectively, in Sections 3.2 and 3.3. Metric tensors are discussed in Section 3.4, and a summary of the constitutive theory follows in Section 3.5.

3.1 Thermodynamics

3.1.1 Generic Energy Potentials and Kinetic Forms

Helmholtz free energy per unit mass and entropy density are of the following functional forms, each depending only on state variables for its particular constituent α and not others β when $\beta \neq \alpha$:

$$\psi^\alpha = \psi^\alpha(\mathbf{F}^\alpha, \theta^\alpha, \{\boldsymbol{\xi}^\alpha\}, \{\nabla_0^\alpha \boldsymbol{\xi}^\alpha\}, \mathbf{X}^\alpha), \tag{89}$$

$$\eta^\alpha = \eta^\alpha(\mathbf{F}^\alpha, \theta^\alpha, \{\boldsymbol{\xi}^\alpha\}, \{\nabla_0^\alpha \boldsymbol{\xi}^\alpha\}, \mathbf{X}^\alpha). \tag{90}$$

Partial stress consists of elastic $\bar{\boldsymbol{\sigma}}^\alpha$ and viscous $\hat{\boldsymbol{\sigma}}^\alpha$ parts:

$$\begin{aligned} \boldsymbol{\sigma}^\alpha = \bar{\boldsymbol{\sigma}}^\alpha(\mathbf{F}^\alpha, \theta^\alpha, \{\boldsymbol{\xi}^\alpha\}, \{\nabla_0^\alpha \boldsymbol{\xi}^\alpha\}, \mathbf{X}^\alpha) \\ + \hat{\boldsymbol{\sigma}}^\alpha(\mathbf{F}^\alpha, \theta^\alpha, \{\boldsymbol{\xi}^\alpha\}, \{\nabla_0^\alpha \boldsymbol{\xi}^\alpha\}, D_t^\alpha \mathbf{F}^\alpha, \mathbf{X}^\alpha). \end{aligned} \tag{91}$$

Equations 89–91 are justified as the standard for ideal thermoelastic mixtures[67,87,162] with three additions. First, internal state variables are added to represent dissipative processes such as viscoelasticity and damage[163–165] and growth and remodeling.[166,167] Second, state variable gradients are added to represent surface energies or phase boundaries[50,51] and support derivation of Ginzburg–Landau kinetics for these variables.[86,148,151] Lastly, viscous stress[168] is added to address (e.g., Newtonian) viscosity, especially in biologic fluids.[3]

Arguments in Eqs. 2 and 3 are linked at time t via[94,97]

$$\{\boldsymbol{\Xi}^\alpha\}(t) = \{\boldsymbol{\Xi}^\alpha(\{\boldsymbol{\xi}^\alpha\}, \mathbf{X}^\alpha, \mathbf{x})\}(t). \tag{92}$$

Thus, all dependence of response functions on metrics $(\mathbf{g}, \mathbf{G}^\alpha)$ and states $\{\boldsymbol{\Xi}^\alpha\}$ is implicitly included via arguments $\{\boldsymbol{\xi}^\alpha\}$. Kinetic equations for heat flux, internal state, and interphase mass, momentum, and energy exchange are more general, allowing for dependence on all constituents $\beta = 1, \ldots, N$ including $\alpha = \beta$ and $\alpha \neq \beta$:

$$\mathbf{q}^\alpha = \mathbf{q}^\alpha(\mathbf{F}^\beta, \nabla\mathbf{F}^\beta, \theta^\beta, \nabla\theta^\beta, \boldsymbol{\xi}^\beta, \nabla_0^\beta\boldsymbol{\xi}^\beta, \boldsymbol{\upsilon}^\beta, \rho^\beta), \tag{93}$$

$$\mathbf{h}^\alpha = \mathbf{h}^\alpha(\mathbf{F}^\beta, \nabla\mathbf{F}^\beta, \theta^\beta, \nabla\theta^\beta, \boldsymbol{\xi}^\beta, \nabla_0^\beta\boldsymbol{\xi}^\beta, \boldsymbol{\upsilon}^\beta, \rho^\beta), \tag{94}$$

$$c^\alpha = c^\alpha(\mathbf{F}^\beta, \nabla\mathbf{F}^\beta, \theta^\beta, \nabla\theta^\beta, \boldsymbol{\xi}^\beta, \nabla_0^\beta\boldsymbol{\xi}^\beta, \boldsymbol{\upsilon}^\beta, \rho^\beta), \tag{95}$$

$$\epsilon^\alpha = \epsilon^\alpha(\mathbf{F}^\beta, \nabla\mathbf{F}^\beta, \theta^\beta, \nabla\theta^\beta, \boldsymbol{\xi}^\beta, \nabla_0^\beta\boldsymbol{\xi}^\beta, \boldsymbol{\upsilon}^\beta, \rho^\beta), \tag{96}$$

$$D_t^\alpha\{\boldsymbol{\xi}^\alpha\} = D_t^\alpha\{\boldsymbol{\xi}^\alpha\}(\mathbf{F}^\beta, \nabla\mathbf{F}^\beta, \theta^\beta, \nabla\theta^\beta, \boldsymbol{\xi}^\beta, \nabla_0^\beta\boldsymbol{\xi}^\beta, \boldsymbol{\upsilon}^\beta, \rho^\beta). \tag{97}$$

Notation $\{\cdot\}$ on $\boldsymbol{\xi}^\alpha$ and admissible explicit dependence on $\mathbf{X}^\alpha$ for heterogeneous properties of constituents α are omitted in arguments of Eqs. 93–97 for brevity.

Particular forms of Eqs. 93–96 must satisfy principles of spatial invariance for objective spatial vectors $\mathbf{q}^\alpha$ and $\mathbf{h}^\alpha$ and scalars c^α and ϵ^α. Evolution equations in Eq. 97 must also be objective. Invariance under rigid translation of the mixture as a whole necessitates that dependence on velocities $\boldsymbol{\upsilon}^\alpha$ is at most only on the $N-1$ velocity differences $\boldsymbol{\upsilon}^1 - \boldsymbol{\upsilon}^N, \ldots, \boldsymbol{\upsilon}^{N-1} - \boldsymbol{\upsilon}^N$. See the treatise of Bowen.[67] Diffusion velocities $\boldsymbol{\mu}^\alpha = \boldsymbol{\mu}^\alpha(\boldsymbol{\upsilon}^\beta, \rho^\beta)$ of Eq. 57 fulfill this requirement.

Spatial invariance of Eqs. 89 and 90 is obtained via dependence on $\mathbf{F}^\alpha$ through symmetric deformation tensor $\mathbf{C}^\alpha$:

$$\mathbf{C}^\alpha = (\mathbf{F}^\alpha)^\mathsf{T}\mathbf{F}^\alpha, \qquad (C^\alpha)_J^K = (G^\alpha)^{KI}(F^\alpha)_I^i g_{ij}(F^\alpha)_J^j; \tag{98}$$

$$\partial\psi^\alpha/\partial\mathbf{F}^\alpha = 2\mathbf{F}^\alpha\partial\psi^\alpha/\partial\mathbf{C}^\alpha, \quad J^\alpha = \sqrt{\det\mathbf{C}^\alpha}; \tag{99}$$

$$D_t^\alpha\mathbf{C}^\alpha = 2(\mathbf{F}^\alpha)^\mathsf{T}\mathbf{d}^\alpha\mathbf{F}^\alpha, \qquad 2\mathbf{d}^\alpha = \mathbf{l}^\alpha + (\mathbf{l}^\alpha)^\mathsf{T}. \tag{100}$$

The spatial deformation rate is $\mathbf{d}^\alpha$, and $D_t^\alpha\mathbf{C}^\alpha$ is taken with metric components $(G^\alpha)^{IJ}$ and g_{ij} held fixed with respect to t in Eq. 100.

3.1.2 Thermodynamic Restrictions and Constitutive Identities

Expanding $D_t^\alpha \psi^\alpha$ using the chain rule on Eq. 89 and inserting the result and Eq. 91 into Eq. 23 gives

$$\begin{aligned}\sum_\alpha \frac{1}{\theta^\alpha}\{&[\bar{\boldsymbol{\sigma}}^\alpha (\mathbf{F}^\alpha)^{-\mathsf{T}} - 2\rho^\alpha \mathbf{F}^\alpha \frac{\partial \psi^\alpha}{\partial \mathbf{C}^\alpha}] : D_t^\alpha \mathbf{F}^\alpha \\ &- \rho^\alpha [\eta^\alpha + \partial \psi^\alpha / \partial \theta^\alpha] D_t^\alpha \theta^\alpha \\ &+ [\{(\mathbf{F}^\alpha)^{-1} \boldsymbol{\zeta}^\alpha\} - \rho^\alpha \frac{\partial \psi^\alpha}{\partial \{\nabla_0 \boldsymbol{\xi}^\alpha\}}] : \{D_t^\alpha (\nabla_0 \boldsymbol{\xi}^\alpha)\} \\ &+ [\{(\mathbf{F}^\alpha)^{-1} : \nabla_0^\alpha \boldsymbol{\zeta}^\alpha\} - \rho^\alpha \frac{\partial \psi^\alpha}{\partial \{\boldsymbol{\xi}^\alpha\}}] \cdot \{D_t^\alpha \boldsymbol{\xi}^\alpha\} \\ &+ \hat{\boldsymbol{\sigma}}^\alpha : \mathbf{d}^\alpha - (\mathbf{q}^\alpha \cdot \nabla \theta^\alpha)/\theta^\alpha + \epsilon^\alpha + c^\alpha \theta^\alpha \eta^\alpha\} \geq 0. \end{aligned} \tag{101}$$

Identities from Eqs. 6 and 8 have been used to obtain

$$\begin{aligned}\nabla \cdot (\{\boldsymbol{\zeta}^\alpha\} \cdot \{D_t^\alpha \boldsymbol{\xi}^\alpha\}) = (\nabla \cdot \{\boldsymbol{\zeta}^\alpha\}) \cdot \{D_t^\alpha \boldsymbol{\xi}^\alpha\} \\ + \{(\mathbf{F}^\alpha)^{-1} \boldsymbol{\zeta}^\alpha\} : \{D_t^\alpha (\nabla_0^\alpha \boldsymbol{\xi}^\alpha)\}. \end{aligned} \tag{102}$$

From standard arguments[51,148,168,169] and Eqs. 89–97, the first three sets of terms in Eq. 101 should vanish for admissibility under general thermodynamic processes, leading to the following constitutive equalities:

$$\bar{\boldsymbol{\sigma}}^\alpha = 2\rho^\alpha \mathbf{F}^\alpha \frac{\partial \psi^\alpha}{\partial \mathbf{C}^\alpha} (\mathbf{F}^\alpha)^{\mathsf{T}}, \qquad \eta^\alpha = -\frac{\partial \psi^\alpha}{\partial \theta^\alpha}, \tag{103}$$

$$\{\boldsymbol{\zeta}^\alpha\} = \rho^\alpha \{\mathbf{F}^\alpha \partial \psi^\alpha / \partial \nabla_0^\alpha \boldsymbol{\xi}^\alpha\} = \rho^\alpha \frac{\partial \psi^\alpha}{\partial \{\nabla \boldsymbol{\xi}^\alpha\}}, \tag{104}$$

$$\{\boldsymbol{\pi}^\alpha\} = \rho^\alpha \partial \psi^\alpha / \partial \{\boldsymbol{\xi}^\alpha\}, \tag{105}$$

where Eq. 105 defines a conjugate force to internal state variables or order parameters. Then Eq. 101 reduces to

$$\begin{aligned}\sum_\alpha \frac{1}{\theta^\alpha}[&(\{\nabla \cdot \boldsymbol{\zeta}^\alpha\} - \{\boldsymbol{\pi}^\alpha\}) \cdot \{D_t^\alpha \boldsymbol{\xi}^\alpha\} \\ &+ \hat{\boldsymbol{\sigma}}^\alpha : \mathbf{d}^\alpha - (\mathbf{q}^\alpha \cdot \nabla \theta^\alpha)/\theta^\alpha + \epsilon^\alpha + c^\alpha \theta^\alpha \eta^\alpha] \geq 0. \end{aligned} \tag{106}$$

Applying the Legendre transformation from Eq. 22 with

$$u^\alpha = u^\alpha(\mathbf{F}^\alpha, \eta^\alpha, \{\boldsymbol{\xi}^\alpha\}, \{\nabla_0^\alpha \boldsymbol{\xi}^\alpha\}, \mathbf{X}^\alpha), \tag{107}$$

$$\theta^\alpha = \theta^\alpha(\mathbf{F}^\alpha, \eta^\alpha, \{\boldsymbol{\xi}^\alpha\}, \{\nabla_0^\alpha \boldsymbol{\xi}^\alpha\}, \mathbf{X}^\alpha), \tag{108}$$

in conjunction with Eqs. 103 and 104 gives

$$\bar{\boldsymbol{\sigma}}^\alpha = 2\rho^\alpha \mathbf{F}^\alpha \frac{\partial u^\alpha}{\partial \mathbf{C}^\alpha}(\mathbf{F}^\alpha)^\mathsf{T}, \qquad \theta^\alpha = \frac{\partial u^\alpha}{\partial \eta^\alpha}, \tag{109}$$

$$\{\boldsymbol{\pi}^\alpha\} = \rho^\alpha \frac{\partial u^\alpha}{\partial \{\boldsymbol{\xi}^\alpha\}}, \quad \{\boldsymbol{\zeta}^\alpha\} = \rho^\alpha \frac{\partial u^\alpha}{\partial \{\nabla \boldsymbol{\xi}^\alpha\}}. \tag{110}$$

Define specific heat per unit mass at constant strain c_ϵ^α, thermal stress coefficients $\boldsymbol{\beta}^\alpha$, and Grüneisen tensor $\boldsymbol{\gamma}^\alpha$:

$$c_\epsilon^\alpha = \theta^\alpha \partial \eta^\alpha / \partial \theta^\alpha = -\theta^\alpha \, \partial^2 \psi^\alpha / \partial (\theta^\alpha)^2, \tag{111}$$

$$\boldsymbol{\beta}^\alpha = \rho^\alpha c_\epsilon^\alpha \boldsymbol{\gamma}^\alpha = -2\rho^\alpha \, \partial^2 \psi^\alpha / \partial \theta^\alpha \partial \mathbf{C}^\alpha. \tag{112}$$

Define the intrinsic dissipation for constituent α:

$$\mathfrak{D}^\alpha = (\{\nabla \cdot \boldsymbol{\zeta}^\alpha\} - \{\boldsymbol{\pi}^\alpha\}) \cdot \{D_t^\alpha \boldsymbol{\xi}^\alpha\} + \hat{\boldsymbol{\sigma}}^\alpha : \mathbf{d}^\alpha. \tag{113}$$

Expand the rate of η^α using Eqs. 90, 103, 111, and 112:

$$\begin{aligned} \rho^\alpha \theta^\alpha D_t^\alpha \eta^\alpha = \rho^\alpha c_\epsilon^\alpha D_t^\alpha \theta^\alpha + \tfrac{1}{2}\theta^\alpha \boldsymbol{\beta}^\alpha : D_t^\alpha \mathbf{C}^\alpha \\ - \rho^\alpha \theta^\alpha [(\partial^2 \psi / \partial \theta^\alpha \partial \{\boldsymbol{\xi}^\alpha\}) \cdot \{D_t^\alpha \boldsymbol{\xi}^\alpha\} \\ + (\partial^2 \psi / \partial \theta^\alpha \partial \{\nabla \boldsymbol{\xi}^\alpha\}) : \{\nabla (D_t^\alpha \boldsymbol{\xi}^\alpha)\}]. \end{aligned} \tag{114}$$

From Eq. 18, time differentiation of Eq. 22, and Eqs. 103 and 104:

$$\rho^\alpha \theta^\alpha D_t^\alpha \eta^\alpha = \mathfrak{D}^\alpha - \nabla \cdot \mathbf{q}^\alpha + \rho^\alpha r^\alpha + \epsilon^\alpha. \tag{115}$$

Temperature rates then are, combining Eqs. 114 and 115,

$$\begin{aligned} \rho^\alpha c_\epsilon^\alpha D_t^\alpha \theta^\alpha = \; & \mathfrak{D}^\alpha - \tfrac{1}{2}\theta^\alpha \boldsymbol{\beta}^\alpha : D_t^\alpha \mathbf{C}^\alpha \\ & + \rho^\alpha \theta^\alpha [(\partial^2 \psi / \partial \theta^\alpha \partial \{\boldsymbol{\xi}^\alpha\}) \cdot \{D_t^\alpha \boldsymbol{\xi}^\alpha\} \\ & + (\partial^2 \psi / \partial \theta^\alpha \partial \{\nabla \boldsymbol{\xi}^\alpha\}) : \{\nabla (D_t^\alpha \boldsymbol{\xi}^\alpha)\}] \\ & - \nabla \cdot \mathbf{q}^\alpha + \rho^\alpha r^\alpha + \epsilon^\alpha. \end{aligned} \tag{116}$$

3.1.3 Alternative Formulation with Partitioned Metric Tensors

Decompositions of generalized Finsler-type metrics in Eqs. 2 and 3 into symmetric position-dependent (i.e., classical) and dimensionless, invertible, space–time dependent parts are[94,97,99]

$$\mathbf{g}(\mathbf{x},t) = \bar{\mathbf{g}}(\mathbf{x})\,\hat{\mathbf{g}}(\{\boldsymbol{\xi}^\alpha(\mathbf{x},t)\}), \tag{117}$$

$$\mathbf{G}^\alpha(\mathbf{X}^\alpha,t) = \bar{\mathbf{G}}^\alpha(\mathbf{X}^\alpha)\,\hat{\mathbf{G}}^\alpha(\{\boldsymbol{\Xi}^\alpha(\mathbf{X}^\alpha,t)\}). \tag{118}$$

A deformation $\bar{\mathbf{C}}^\alpha$ and Jacobian $\bar{J}^\alpha$ based on $(\bar{\mathbf{g}}, \bar{\mathbf{G}}^\alpha)$ are

$$(\bar{C}^\alpha)^K_J = \bar{G}^{KI}(F^\alpha)^i_I \bar{g}_{ij}(F^\alpha)^j_J(\mathbf{G}^\alpha)_K \otimes (\mathbf{G}^\alpha)^J, \tag{119}$$

$$\bar{J}^\alpha = \sqrt{\det \bar{\mathbf{C}}^\alpha} = J^\alpha\sqrt{\hat{G}^\alpha/\hat{g}}, \tag{120}$$

with dimensionless Finsler scaling factors $\hat{g} = \det \hat{\mathbf{g}}$ and $\hat{G}^\alpha = \det \hat{\mathbf{G}}^\alpha$.

Alternative constitutive equations,[97] also energetically objective, are obtained by positing dependence of ψ^α, η^α, u^α, and θ^α through $\bar{\mathbf{C}}^\alpha(\mathbf{F}^\alpha)$ rather than $\mathbf{C}^\alpha$, whereby

$$\begin{aligned} &\partial\psi^\alpha/\partial\mathbf{F}^\alpha = 2\mathbf{F}^\alpha\partial\psi^\alpha/\partial\bar{\mathbf{C}}^\alpha \\ &\quad\leftrightarrow\ \partial\psi^\alpha/\partial(F^\alpha)^i_J = 2\bar{g}_{ik}(F^\alpha)^k_L\partial\psi^\alpha/\partial(\bar{C}^\alpha)_{JL}. \end{aligned} \tag{121}$$

Derivations in Eqs. 101–116 continue to apply for $\psi^\alpha(\bar{\mathbf{C}}^\alpha,\cdot)$, $\eta^\alpha(\bar{\mathbf{C}}^\alpha,\cdot)$, and so on, with several changes manifested by Eq. 121:

$$\begin{aligned} (\bar{\sigma}^\alpha)^j_i &= 2\rho^\alpha\bar{g}_{ik}(F^\alpha)^k_L(F^\alpha)^j_J\partial\psi^\alpha/\partial(\bar{C}^\alpha)_{JL} \\ &= 2\rho^\alpha\bar{g}_{ik}(F^\alpha)^k_L(F^\alpha)^j_J\partial u^\alpha/\partial(\bar{C}^\alpha)_{JL}, \end{aligned} \tag{122}$$

$$\bar{\boldsymbol{\beta}}^\alpha = \rho^\alpha c^\alpha_\epsilon\bar{\boldsymbol{\gamma}}^\alpha = -2\rho^\alpha\,\partial^2\psi^\alpha/\partial\theta^\alpha\partial\bar{\mathbf{C}}^\alpha, \tag{123}$$

$$\begin{aligned} \rho^\alpha c^\alpha_\epsilon D^\alpha_t\theta^\alpha = \ &\mathfrak{D}^\alpha - \tfrac{1}{2}\theta^\alpha\bar{\boldsymbol{\beta}}^\alpha : D^\alpha_t\bar{\mathbf{C}}^\alpha \\ &+ \rho^\alpha\theta^\alpha[(\partial^2\psi/\partial\theta^\alpha\partial\{\boldsymbol{\xi}^\alpha\})\cdot\{D^\alpha_t\boldsymbol{\xi}^\alpha\} \\ &+ (\partial^2\psi/\partial\theta^\alpha\partial\{\nabla\boldsymbol{\xi}^\alpha\}) : \{\nabla(D^\alpha_t\boldsymbol{\xi}^\alpha)\}] \\ &- \nabla\cdot\mathbf{q}^\alpha + \rho^\alpha r^\alpha + \epsilon^\alpha. \end{aligned} \tag{124}$$

Mixed-variant stress $\bar{\boldsymbol{\sigma}}^\alpha$ in Eq. 122 excludes $\hat{\mathbf{g}}(\mathbf{x},t)$. The contravariant stress components defined as $(\bar{\sigma}^\alpha)^{ij} = \frac{1}{2}[g^{ik}(\bar{\sigma}^\alpha)^j_k + g^{jk}(\bar{\sigma}^\alpha)^i_k]$ or $(\bar{\sigma}^\alpha)^{ij} = \bar{g}^{ik}(\bar{\sigma}^\alpha)^j_k$ must

be symmetric. The former definition depends on $\hat{\mathbf{g}}(\mathbf{x},t)$ implicitly from g^{ik}. This choice presumes, a priori, that skew contributions from Eq. 122 perform no work in the energy balance and thus can be redefined as zero. The latter prescription either redefines raising/lowering indices on Cauchy stress or presumes that $\mathbf{d}^\alpha$ is defined in covariant form by lowering of $\mathbf{l}^\alpha$ with $\bar{g}_{ij}$, rather than the typical g_{ij} prior to symmetrization.

3.2 Energy Functions for Soft-Tissue Biomechanics

3.2.1 Free and Internal Energy Contributions

Internal state variables $\{\boldsymbol{\xi}^\alpha\}$ consist of three sets: configurational variables associated with viscoelastic processes $\{\boldsymbol{\Gamma}^\alpha\}$, damage variables associated with degradation processes $\{\mathbf{D}^\alpha\}$, and electrochemical activation (e.g., muscle contraction) variables $\{\boldsymbol{\Delta}^\alpha\}$[27,31,38,97]:

$$\{\boldsymbol{\xi}^\alpha\}(\mathbf{x},t) = (\{\boldsymbol{\Gamma}^\alpha\},\{\mathbf{D}^\alpha\},\{\boldsymbol{\Delta}^\alpha\})(\mathbf{x},t). \tag{125}$$

In the present work, as in phase-field and related theories,[38,97] free and internal energy functions can depend on spatial gradients of damage variables, which are viewed as order parameters, but not on spatial gradients of viscoelastic and tissue activation variables. The $(\{\boldsymbol{\Gamma}^\alpha\},\{\boldsymbol{\Delta}^\alpha\})$ are conventional, rather than gradient-type, internal state variables.

A novelty of the present formulation is separate order parameters for degradation of matrix and each fiber family. Prior models[37,38] used but a single order parameter for the whole solid. Here, since strain energies of matrix and fibers are separately resolved, and since strain energies are driving forces for fracture, physics suggest distinct order parameters be assigned for degradation of matrix and fibers. This enables delineation of mechanisms that can be compared with experimental observations. In addition, the current approach is realistic in the sense that unstretched and unsheared fibers should not witness any ruptures. Use of distinct order parameters for fiber families is similar to assigning separate parameters for fractures on discrete cleavage planes in phase-field crystal models.[151]

Denote by $\varsigma_{\mathrm{V}}^\alpha$ and $\varsigma_{\mathrm{S}}^\alpha$ degradation functions associated with loss of strength due to changes in bulk and deviatoric strain energies, respectively. These scalar functions

obey

$$\varsigma_{\mathrm{V}}^{\alpha} = \varsigma_{\mathrm{V}}^{\alpha}(\{\mathbf{D}^{\alpha}\}, \mathbf{C}^{\alpha}) \in [0,1], \qquad \varsigma_{\mathrm{S}}^{\alpha} = \varsigma_{\mathrm{S}}^{\alpha}(\{\mathbf{D}^{\alpha}\}) \in [0,1], \tag{126}$$

$$\partial \varsigma_{\mathrm{V}}^{\alpha} / \partial \mathbf{C}^{\alpha}(\{\mathbf{D}^{\alpha}\}, \mathbf{C}^{\alpha}) = \mathbf{0} \,\forall\, \mathbf{C}^{\alpha} \neq \mathbf{1}. \tag{127}$$

A degradation operator for fibrous energy contributions with similar properties is $\varsigma_{\mathrm{F}}^{\alpha}(\{\mathbf{D}^{\alpha}\})$. Let $\Psi^{\alpha} = \rho_{\mathrm{R}0}^{\alpha}\psi^{\alpha}$ and $U^{\alpha} = \rho_{\mathrm{R}0}^{\alpha}u^{\alpha}$ be free and internal energies per unit reference volume of individual phases. Pragmatic functional forms consist of the following sums:

$$\begin{aligned}
\Psi^{\alpha}(\mathbf{C}^{\alpha}, \theta^{\alpha}, \{\boldsymbol{\xi}^{\alpha}\}, \{\nabla_0^{\alpha}\mathbf{D}^{\alpha}\}) =& \varsigma_{\mathrm{V}}^{\alpha}(\{\mathbf{D}^{\alpha}\}, \mathbf{C}^{\alpha})\Psi_{\mathrm{V}}^{\alpha}(J^{\alpha}, \theta^{\alpha}) \\
&+ \varsigma_{\mathrm{S}}^{\alpha}(\{\mathbf{D}^{\alpha}\})[\Psi_{\mathrm{S}}^{\alpha}(\mathbf{C}^{\alpha}) + \Psi_{\Gamma}^{\alpha}(\mathbf{C}^{\alpha}, \{\boldsymbol{\Gamma}^{\alpha}\})] \\
&+ \varsigma_{\mathrm{F}}^{\alpha}(\{\mathbf{D}^{\alpha}\}) \circ [\Psi_{\mathrm{F}}^{\alpha}(\mathbf{C}^{\alpha}) + \Psi_{\Phi}^{\alpha}(\mathbf{C}^{\alpha}, \{\boldsymbol{\Gamma}^{\alpha}\})] \\
&+ \Psi_{\mathrm{A}}^{\alpha}(\mathbf{C}^{\alpha}, \{\boldsymbol{\Delta}^{\alpha}\}) + \Psi_{\theta}^{\alpha}(\theta^{\alpha}) \\
&+ \Psi_{\sigma}^{\alpha}(J^{\alpha}) + \Psi_{\mathrm{D}}^{\alpha}(\{\boldsymbol{\xi}^{\alpha}\}, \{\nabla_0^{\alpha}\mathbf{D}^{\alpha}\}),
\end{aligned} \tag{128}$$

$$\begin{aligned}
U^{\alpha}(\mathbf{C}^{\alpha}, \eta^{\alpha}, \{\boldsymbol{\xi}^{\alpha}\}, \{\nabla_0^{\alpha}\mathbf{D}^{\alpha}\}) =& \varsigma_{\mathrm{V}}^{\alpha}(\{\mathbf{D}^{\alpha}\}, \mathbf{C}^{\alpha})U_{\mathrm{V}}^{\alpha}(J^{\alpha}, \eta^{\alpha}) \\
&+ \varsigma_{\mathrm{S}}^{\alpha}(\{\mathbf{D}^{\alpha}\})[U_{\mathrm{S}}^{\alpha}(\mathbf{C}^{\alpha}) + U_{\Gamma}^{\alpha}(\mathbf{C}^{\alpha}, \{\boldsymbol{\Gamma}^{\alpha}\})] \\
&+ \varsigma_{\mathrm{F}}^{\alpha}(\{\mathbf{D}^{\alpha}\}) \circ [U_{\mathrm{F}}^{\alpha}(\mathbf{C}^{\alpha}) + U_{\Phi}^{\alpha}(\mathbf{C}^{\alpha}, \{\boldsymbol{\Gamma}^{\alpha}\})] \\
&+ U_{\mathrm{A}}^{\alpha}(\mathbf{C}^{\alpha}, \{\boldsymbol{\Delta}^{\alpha}\}) + U_{\theta}^{\alpha}(\eta^{\alpha}) \\
&+ U_{\sigma}^{\alpha}(J^{\alpha}) + U_{\mathrm{D}}^{\alpha}(\{\boldsymbol{\xi}^{\alpha}\}, \{\nabla_0^{\alpha}\mathbf{D}^{\alpha}\}).
\end{aligned} \tag{129}$$

In Ψ^{α}, volumetric equilibrium free energy for the entire constituent α is $\Psi_{\mathrm{V}}^{\alpha}$, including isotropic thermoelastic coupling. Deviatoric equilibrium energy of the isotropic matrix is $\Psi_{\mathrm{S}}^{\alpha}$. Viscoelastic configurational energy of the isotropic matrix is Ψ_{Γ}^{α}. Anisotropic deviatoric equilibrium free energy from fibrous microstructures is $\Psi_{\mathrm{F}}^{\alpha}$. Configurational energy, often but not always anisotropic, from fibers is Ψ_{Φ}^{α}. Energy from fiber activation is $\Psi_{\mathrm{A}}^{\alpha}$. Thermal energy of specific heat is Ψ_{θ}^{α}. Energy from a nonzero reference pressure is Ψ_{σ}^{α}. Surface energy from fractures, tears, and other damage is contained in $\Psi_{\mathrm{D}}^{\alpha}$.

Fully analogous descriptors apply to internal energy contributions in U^{α}. Forms for free energy and internal energy in Eqs. 128 and 129 are not the most mathematically and physically general, but they are sufficient for soft tissue materials of

present interest given the scope of available data on their properties and response. A few, or even most, terms vanish for certain classes of materials (isotropic solids, viscoelastic fluids, gas phases, etc.). All functions in Eqs. 128 and 129 in materials with heterogeneous properties can further depend explicitly on $\mathbf{X}^\alpha$, omitted in the arguments for brevity. Dependence of state-dependent metric tensors is implicit, for example in J^α and scalar functions of certain vectors and tensors.

3.2.2 Ideal Gas EOS

For gaseous fluids such as air in the lung, an ideal gas model[87] is sufficient. For the ideal gas, $\psi^\alpha = (\Psi_{\rm V}^\alpha + \Psi_\theta^\alpha)/\rho_{\rm R0}^\alpha$ and $u^\alpha = (U_{\rm V}^\alpha + U_\theta^\alpha)/\rho_{\rm R0}^\alpha$. At a reference state, the following conditions hold: $J^\alpha = 1$, $\theta^\alpha = \theta_0^\alpha$, $\eta^\alpha = \eta_0^\alpha$, $\rho_0^\alpha = n_0^\alpha \rho_{\rm R0}^\alpha$, $p_{\rm V}^\alpha = p_0^\alpha = n_0^\alpha p_{\rm R0}^\alpha$, and $c_\epsilon^\alpha = c_{\epsilon 0}^\alpha$. Quantities with zero subscripts are constants, and $p_{\rm V}^\alpha = -\frac{1}{3}{\rm tr}\bar{\boldsymbol{\sigma}}^\alpha$ is the partial inviscid pressure. From the identity $\partial J^\alpha/\partial \mathbf{C}^\alpha = \frac{1}{2}J^\alpha(\mathbf{C}^\alpha)^{-1}$, the stress contribution is spherical: $\bar{\boldsymbol{\sigma}}^\alpha = -p_{\rm V}^\alpha \mathbf{1}$. The ideal gas constant is $\mathfrak{R}^\alpha$. The pressure-density-temperature EOS and internal energy function are

$$p_{\rm V}^\alpha = \rho^\alpha \mathfrak{R}^\alpha \theta^\alpha, \qquad u^\alpha = c_{\epsilon 0}^\alpha \theta^\alpha. \tag{130}$$

From Eq. 130 and $\psi^\alpha = u^\alpha + \theta^\alpha(\partial\psi^\alpha/\partial\theta^\alpha)$, it follows that

$$\psi^\alpha(J^\alpha, \theta^\alpha) = -\mathfrak{R}^\alpha \theta^\alpha \ln J^\alpha - c_{\epsilon 0}^\alpha \theta^\alpha[\ln(\theta^\alpha/\theta_0^\alpha) - 1], \tag{131}$$

$$u^\alpha(J^\alpha, \eta^\alpha) = c_{\epsilon 0}^\alpha \theta_0^\alpha (J^\alpha)^{-\gamma_0^\alpha} \exp(\eta^\alpha/c_{\epsilon 0}^\alpha), \tag{132}$$

noting $\eta_0^\alpha = 0$ and $\gamma_0^\alpha = \mathfrak{R}^\alpha/c_{\epsilon 0}^\alpha$. The thermal stress tensor is $\boldsymbol{\beta}^\alpha = \rho^\alpha \mathfrak{R}^\alpha (\mathbf{C}^\alpha)^{-1}$ in Eq. 112, and $c_\epsilon^\alpha = c_{\epsilon 0}^\alpha$ in Eq. 111. The ideal gas model is justified as standard for shock compression of air.[127] Other models[72,74] could be substituted if consistent with Eqs. 128 and 129.

3.2.3 Condensed Matter EOS

For solid and liquid tissue phases, an EOS combining the third-order logarithmic form used for high-pressure physics[170–172] with an exponential form for tissue mechanics[36] is sufficiently general for the present applications. This model is chosen for its ability to capture bulk stiffening at high pressure as well as tensile stiffening observed in dilatation of some soft tissues.[3,36] It requires relatively few parameters, and its accuracy for depicting shock Hugoniot data for water, blood, and muscle is

demonstrated in Section 4.1.

Thermoelastic coupling is linear and isotropic with constant volumetric expansion coefficient A^α, and specific heat c_ϵ^α is constant. Reference temperature is θ_0^α, and reference pressure is $p_{\mathrm{R}0}^\alpha$. The reference isothermal bulk modulus is B_θ^α, and the pressure derivative of the isothermal bulk modulus in the reference state is $B_{\theta\mathrm{p}}^\alpha$. Analogously, the isentropic bulk modulus and pressure derivative are B_η^α and $B_{\eta\mathrm{p}}^\alpha$. Denote a constant controlling exponential stiffening by k_{V}^α.

Free energies per unit initial volume of constituent α are

$$\Psi_{\mathrm{V}}^\alpha = \frac{B_\theta^\alpha}{2}\left[\frac{\exp\{k_{\mathrm{V}}^\alpha(\ln J^\alpha)^2\}-1}{k_{\mathrm{V}}^\alpha} - \frac{(B_{\theta\mathrm{p}}^\alpha-2)(\ln J^\alpha)^3}{3}\right] - A^\alpha B_\theta^\alpha(\theta^\alpha-\theta_0^\alpha)\ln J^\alpha,$$

$$\Psi_\sigma^\alpha = -p_{\mathrm{R}0}^\alpha \ln J^\alpha, \tag{133}$$

$$\Psi_\theta^\alpha = -\rho_{\mathrm{R}0}^\alpha c_\epsilon^\alpha[\theta^\alpha\ln(\theta^\alpha/\theta_0^\alpha) - (\theta^\alpha-\theta_0^\alpha)]. \tag{134}$$

The contribution to stress $\bar{\boldsymbol{\sigma}}^\alpha$ from Ψ_{V}^α and Ψ_σ^α is spherical, with Cauchy pressure

$$\begin{aligned} p_{\mathrm{V}}^\alpha &= -\frac{\rho^\alpha}{\rho_{\mathrm{R}0}^\alpha}\frac{\partial(\Psi_{\mathrm{V}}^\alpha+\Psi_\sigma^\alpha)}{\partial\ln J^\alpha} \\ &= -\frac{\rho^\alpha}{\rho_{\mathrm{R}0}^\alpha}B_\theta^\alpha\ln J^\alpha[\exp\{k_{\mathrm{V}}^\alpha(\ln J^\alpha)^2\} - \tfrac{1}{2}(B_{\theta\mathrm{p}}^\alpha-2)\ln J^\alpha] \\ &\quad + \frac{\rho^\alpha}{\rho_{\mathrm{R}0}^\alpha}A^\alpha B_\theta^\alpha(\theta^\alpha-\theta_0^\alpha) + \frac{\rho^\alpha}{\rho_{\mathrm{R}0}^\alpha}p_{\mathrm{R}0}^\alpha. \end{aligned} \tag{135}$$

From Eq. 16, if $c^\alpha = \rho^\alpha\partial_t\ln\sqrt{g}$, $\partial_t\ln\sqrt{g} = D_t^\alpha\ln\sqrt{G^\alpha}$, and $\rho_0^\alpha = \rho_0^\alpha(\mathbf{X}^\alpha)$, then

$$\rho_0^\alpha = \rho^\alpha J^\alpha \Rightarrow \rho^\alpha/\rho_{\mathrm{R}0}^\alpha = n_0^\alpha/J^\alpha. \tag{136}$$

Recall n_0^α is the initial volume fraction of constituent α defined in Eq. 88. The thermal stress tensor and Grüneisen tensor are, respectively,

$$\boldsymbol{\beta}^\alpha = \frac{\rho^\alpha}{\rho_{\mathrm{R}0}^\alpha}A^\alpha B_\theta^\alpha(\mathbf{C}^\alpha)^{-1}, \quad \boldsymbol{\gamma}^\alpha = \frac{A^\alpha B_\theta^\alpha}{\rho_{\mathrm{R}0}^\alpha c_\epsilon^\alpha}(\mathbf{C}^\alpha)^{-1}. \tag{137}$$

The scalar Grüneisen constant is

$$\gamma_0^\alpha = \frac{A^\alpha B_\theta^\alpha}{\rho_{\mathrm{R}0}^\alpha c_\epsilon^\alpha}. \tag{138}$$

The internal energy function complementary to Eqs. 133 and 134 is

$$U_{\rm V}^\alpha = \frac{B_\eta^\alpha}{2}\left[\frac{\exp\{k_{\rm V}^\alpha(\ln J^\alpha)^2\}-1}{k_{\rm V}^\alpha} - \frac{(B_{\eta{\rm p}}^\alpha-2)(\ln J^\alpha)^3}{3}\right] - \rho_{\rm R0}^\alpha\theta_0^\alpha\gamma_0^\alpha\eta^\alpha\ln J^\alpha,$$

$$U_\sigma^\alpha = -p_{\rm R0}^\alpha \ln J^\alpha, \tag{139}$$

$$U_\theta^\alpha = \rho_{\rm R0}^\alpha\theta_0^\alpha\eta^\alpha[1+\eta^\alpha/(2c_\epsilon^\alpha)]. \tag{140}$$

Pressure and temperature from Eqs. 139 and 140 are, respectively,

$$\begin{aligned} p_{\rm V}^\alpha &= -\frac{\rho^\alpha}{\rho_{\rm R0}^\alpha}\frac{\partial(U_{\rm V}^\alpha+U_\sigma^\alpha)}{\partial\ln J^\alpha} \\ &= -\frac{\rho^\alpha}{\rho_{\rm R0}^\alpha}B_\eta^\alpha\ln J^\alpha[\exp\{k_{\rm V}^\alpha(\ln J^\alpha)^2\} - \tfrac{1}{2}(B_{\eta{\rm p}}^\alpha-2)\ln J^\alpha] \\ &\qquad + \rho^\alpha\theta_0^\alpha\gamma_0^\alpha\eta^\alpha + \rho^\alpha p_{\rm R0}^\alpha/\rho_{\rm R0}^\alpha, \end{aligned} \tag{141}$$

$$\theta^\alpha = \frac{1}{\rho_{\rm R0}^\alpha}\frac{\partial(U_{\rm V}^\alpha+U_\theta^\alpha)}{\partial\eta^\alpha} = \theta_0^\alpha[1+\frac{\eta^\alpha}{c_\epsilon^\alpha}-\gamma_0^\alpha\ln J^\alpha]. \tag{142}$$

Bulk moduli B_θ^α and B_η^α are nonnegative, and $k_{\rm V}^\alpha$ should be nonnegative for stiffening under large strain typical of soft tissues, whether volumetric strain is compressive or tensile. If $B_{\theta{\rm p}}^\alpha > 2$, the pressure contribution is that the material stiffens in compression and softens in tension, and vice versa for $B_{\theta{\rm p}}^\alpha < 2$. Similar statements hold for $B_{\eta{\rm p}}^\alpha$.

Energy functions in Eqs. 133 and 139 are not (poly)convex in J^α. Polyconvexity is appealing for existence of unique solutions to boundary value problems[173] but is not essential. From Eqs. 128 and 129, if $\varsigma_{\rm V}^\alpha < 1$, then the $p_{\rm V}^\alpha$ contributions from $\Psi_{\rm V}^\alpha$ and $U_{\rm V}^\alpha$ (i.e., all terms except the rightmost terms in Eqs. 135 and 141 containing $p_{\rm R0}^\alpha$) require multiplication by $\varsigma_{\rm V}^\alpha$, as do $\boldsymbol{\beta}^\alpha$, $\boldsymbol{\gamma}^\alpha$, and γ_0^α.

3.2.4 Deviatoric Matrix Equilibrium

The deviatoric deformation gradient and deviatoric deformation tensor are, with $f = f(\tilde{\mathbf{C}}^\alpha)$ a generic differentiable function of its argument,

$$\tilde{\mathbf{F}}^\alpha = (J^\alpha)^{-1/3}\mathbf{F}^\alpha, \qquad \tilde{\mathbf{C}}^\alpha = (J^\alpha)^{-2/3}\mathbf{C}^\alpha, \tag{143}$$

$$\frac{\partial f}{\partial\mathbf{C}^\alpha} = (J^\alpha)^{-2/3}\left[\frac{\partial f}{\partial\tilde{\mathbf{C}}^\alpha} - \frac{1}{3}\left(\frac{\partial f}{\partial\tilde{\mathbf{C}}^\alpha}:\mathbf{C}^\alpha\right)(\mathbf{C}^\alpha)^{-1}\right]. \tag{144}$$

Let $\mu_{\mathrm{S}}^{\alpha} \geq 0$ be a shear modulus, herein a material constant. The strain energy is[173]

$$\Psi_{\mathrm{S}}^{\alpha} = U_{\mathrm{S}}^{\alpha} = \tfrac{1}{2}\mu_{\mathrm{S}}^{\alpha}(\mathrm{tr}\,\tilde{\mathbf{C}}^{\alpha} - 3). \tag{145}$$

From Eq. 144, the contribution of Eq. 145 to Cauchy stress is

$$\begin{aligned}\boldsymbol{\sigma}_{\mathrm{S}}^{\alpha} &= 2\frac{\rho^{\alpha}}{\rho_{\mathrm{R0}}^{\alpha}}\mathbf{F}^{\alpha}\frac{\partial\Psi_{\mathrm{S}}^{\alpha}}{\partial\mathbf{C}^{\alpha}}(\mathbf{F}^{\alpha})^{\mathsf{T}} = 2\frac{\rho^{\alpha}}{\rho_{\mathrm{R0}}^{\alpha}}\mathbf{F}^{\alpha}\frac{\partial U_{\mathrm{S}}^{\alpha}}{\partial\mathbf{C}^{\alpha}}(\mathbf{F}^{\alpha})^{\mathsf{T}} \\ &= \frac{\rho^{\alpha}}{\rho_{\mathrm{R0}}^{\alpha}}\mu_{\mathrm{S}}^{\alpha}[\tilde{\mathbf{B}}^{\alpha} - \tfrac{1}{3}(\mathrm{tr}\tilde{\mathbf{B}}^{\alpha})\mathbf{1}], \qquad \tilde{\mathbf{B}}^{\alpha} = \tilde{\mathbf{F}}^{\alpha}(\tilde{\mathbf{F}}^{\alpha})^{\mathsf{T}}.\end{aligned} \tag{146}$$

This contribution is linear in spatial deformation tensor $\tilde{\mathbf{B}}^{\alpha}$, traceless, and ultimately scaled by $\varsigma_{\mathrm{S}}^{\alpha}$. Further nonlinearity can be furnished by $\Psi_{\mathrm{F}}^{\alpha}$ and U_{F}^{α}. The function in Eq. 145 is polyconvex[173] and isotropic. Many strain energy functions have been proposed for soft-tissue elasticity.[24] The present form in Eq. 145 is used because it requires only one parameter $\mu_{\mathrm{S}}^{\alpha}$, is simple to implement, and is widely used.[128,173] It is also compatible with Eqs. 89, 128, and the fiber elasticity model that follows next.

3.2.5 Fiber Equilibrium

Let index k denote a fiber family of reference alignment by unit vector $\boldsymbol{\iota}_{k}^{\alpha}$. Let $\kappa_{k}^{\alpha} \in [0, \frac{1}{3}]$ be dispersion constants. Structure tensors[28] are

$$\mathbf{H}_{k}^{\alpha} = \kappa_{k}^{\alpha}\mathbf{1} + (1 - 3\kappa_{k}^{\alpha})\boldsymbol{\iota}_{k}^{\alpha} \otimes \boldsymbol{\iota}_{k}^{\alpha}. \tag{147}$$

Strain energy contributions are of functional forms

$$\Psi_{\mathrm{F}}^{\alpha} = \Psi_{\mathrm{F}}^{\alpha}(\tilde{\mathbf{C}}^{\alpha}, \mathbf{H}_{k}^{\alpha}(\mathbf{X}^{\alpha})) = U_{\mathrm{F}}^{\alpha}(\tilde{\mathbf{C}}^{\alpha}, \mathbf{H}_{k}^{\alpha}(\mathbf{X}^{\alpha})), \tag{148}$$

with $\mathbf{H}_{k}^{\alpha}$ time-independent at $\mathbf{X}^{\alpha}$ (i.e., not transient-state variables). Depending on the number of fiber families k and their orientations, different scalar invariants entering Eq. 148 are possible. For the current presentation, one invariant per fiber family is sufficient: $I_{k}^{\alpha} = \tilde{\mathbf{C}}^{\alpha} : \mathbf{H}_{k}^{\alpha}$. The following particular form of Eq. 148 is polyconvex[16,23,97,173]:

$$\Psi_{\mathrm{F}}^{\alpha} = \sum_{k} \Psi_{\mathrm{F}k}^{\alpha} = \sum_{k} \frac{\mu_{k}^{\alpha}}{4k_{k}^{\alpha}}\{\exp[k_{k}^{\alpha}(I_{k}^{\alpha} - 1)^{2}] - 1\}\mathrm{H}(I_{k}^{\alpha} - 1). \tag{149}$$

A fiber modulus and stiffening coefficient are the respective material constants $\mu_k^\alpha \geq 0$ and $k_k^\alpha > 0$. Optional right-continuous Heaviside function is $\mathrm{H}(\cdot)$; this disables fiber stiffness for buckling in compression along $\boldsymbol{\iota}_k^\alpha$. Contributions to stress are traceless:

$$\begin{aligned}\boldsymbol{\sigma}_{\mathrm{F}}^\alpha &= 2\frac{\rho^\alpha}{\rho_{\mathrm{R}0}^\alpha}\mathbf{F}^\alpha\frac{\partial\Psi_{\mathrm{F}}^\alpha}{\partial\mathbf{C}^\alpha}(\mathbf{F}^\alpha)^{\mathsf{T}} = 2\frac{\rho^\alpha}{\rho_{\mathrm{R}0}^\alpha}\mathbf{F}^\alpha\frac{\partial U_{\mathrm{F}}^\alpha}{\partial\mathbf{C}^\alpha}(\mathbf{F}^\alpha)^{\mathsf{T}} \\ &= \frac{\rho^\alpha}{\rho_{\mathrm{R}0}^\alpha}\sum_k \mu_k^\alpha(I_k^\alpha - 1)\exp[k_k^\alpha(I_k^\alpha-1)^2]\mathrm{H}(I_k^\alpha-1)\tilde{\mathbf{h}}_k^\alpha, \\ \tilde{\mathbf{h}}_k^\alpha &= \tilde{\mathbf{F}}^\alpha\mathbf{H}_k^\alpha(\tilde{\mathbf{F}}^\alpha)^{\mathsf{T}} - \tfrac{1}{3}\mathrm{tr}[\tilde{\mathbf{F}}^\alpha\mathbf{H}_k^\alpha(\tilde{\mathbf{F}}^\alpha)^{\mathsf{T}}]\mathbf{1}. \end{aligned} \tag{150}$$

Family k is isotropic as $\kappa_k^\alpha \to \frac{1}{3}$. Fiber compressibility is implicitly encompassed by the condensed matter EOS for phase α rather than distinct energetic terms. Stress contributions from Eq. 150 are affected by $\varsigma_{\mathrm{F}}^\alpha$ if fibers are damaged.

Many other anisotropic elasticity models for soft tissues exist.[24] The framework of Eqs. 147–150 is implemented here because it is widely used (e.g., based on seminal works of Holzapfel et al.,[23] Holzapfel and Ogden,[16] and Gasser et al.[28]) and can account for energies and anisotropies induced by any number of fiber families of arbitrary orientations.

3.2.6 Matrix Viscoelasticity

The viscoelastic formulation combines features from prior works[36,164,165,174,175] in a thermodynamically consistent manner. Let $\{\boldsymbol{\Gamma}^\alpha\} \to \{\boldsymbol{\Gamma}_{\mathrm{V}l}^\alpha, \boldsymbol{\Gamma}_{\mathrm{S}m}^\alpha, \boldsymbol{\Gamma}_{\Phi k,n}^\alpha\}$ be internal strain-like configurational variables for constituent α. Index l spans a set of discrete relaxation time constants $\tau_{\mathrm{V}l}^\alpha = \tau_{\mathrm{V}1}^\alpha, \ldots$ for viscoelastic relaxation processes associated with volumetric deformation of the matrix. Index m spans times $\tau_{\mathrm{S}m}^\alpha$ associated with deviatoric (shear) deformation of the matrix. Index n spans times $\tau_{\Phi k,n}^\alpha$ associated with fiber family k, as discussed in Section 3.2.7.

Internal stresses $\{\mathbf{Q}_{\mathrm{V}l}^\alpha, \mathbf{Q}_{\mathrm{S}m}^\alpha\}$ conjugate to the matrix internal strains, in coordinates referred to $\mathfrak{M}^\alpha$, obey[165,174]

$$\mathbf{Q}_{\mathrm{V}l}^\alpha = -\frac{\partial\Psi_\Gamma^\alpha}{\partial\boldsymbol{\Gamma}_{\mathrm{V}l}^\alpha} = 2\frac{\partial\Psi_{\mathrm{V}l}^\alpha}{\partial\mathbf{C}^\alpha}, \qquad \mathbf{Q}_{\mathrm{S}m}^\alpha = -\frac{\partial\Psi_\Gamma^\alpha}{\partial\boldsymbol{\Gamma}_{\mathrm{S}m}^\alpha} = 2\frac{\partial\Psi_{\mathrm{S}m}^\alpha}{\partial\mathbf{C}^\alpha}, \tag{151}$$

$$\Psi_\Gamma^\alpha = U_\Gamma^\alpha = \sum_l \Psi_{\mathrm{V}l}^\alpha(\mathbf{\Gamma}_{\mathrm{V}l}^\alpha, \mathbf{C}^\alpha) + \sum_m \Psi_{\mathrm{S}m}^\alpha(\mathbf{\Gamma}_{\mathrm{S}m}^\alpha, \mathbf{C}^\alpha)$$
$$= \sum_l \int \tfrac{1}{2}\mathbf{Q}_{\mathrm{V}l}^\alpha : \mathrm{d}\mathbf{C}^\alpha + \sum_m \int \tfrac{1}{2}\mathbf{Q}_{\mathrm{S}m}^\alpha : \mathrm{d}\mathbf{C}^\alpha. \tag{152}$$

Indefinite integrals in Eq. 152 are not needed explicitly. Evolution equations for internal stresses are

$$D_t^\alpha \mathbf{Q}_{\mathrm{V}l}^\alpha + \mathbf{Q}_{\mathrm{V}l}^\alpha/\tau_{\mathrm{V}l}^\alpha = 2D_t^\alpha(\partial\hat{\Psi}_{\mathrm{V}l}^\alpha/\partial\mathbf{C}^\alpha), \tag{153}$$
$$D_t^\alpha \mathbf{Q}_{\mathrm{S}m}^\alpha + \mathbf{Q}_{\mathrm{S}m}^\alpha/\tau_{\mathrm{S}m}^\alpha = 2D_t^\alpha(\partial\hat{\Psi}_{\mathrm{S}m}^\alpha/\partial\mathbf{C}^\alpha), \tag{154}$$
$$\hat{\Psi}_{\mathrm{V}l}^\alpha = \tfrac{1}{2}\beta_{\mathrm{V}l}^\alpha B_\theta^\alpha(\ln J^\alpha)^2, \tag{155}$$
$$\hat{\Psi}_{\mathrm{S}m}^\alpha = \tfrac{1}{2}\beta_{\mathrm{S}m}^\alpha \mu_{\mathrm{S}}^\alpha(\mathrm{tr}\,\tilde{\mathbf{C}}^\alpha - 3). \tag{156}$$

Dimensionless factors are $\beta_{\mathrm{V}l}^\alpha \geq 0$ and $\beta_{\mathrm{S}m}^\alpha \geq 0$. Initial conditions and convolution solutions to the volumetric component of Eq. 153 and shear component of Eq. 154 are, respectively, as follows:

$$\mathbf{Q}_{\mathrm{V}l0}^\alpha = 2\partial\hat{\Psi}_{\mathrm{V}l}^\alpha/\partial\mathbf{C}^\alpha, \quad \mathbf{Q}_{\mathrm{S}m0}^\alpha = 2\partial\hat{\Psi}_{\mathrm{S}m}^\alpha/\partial\mathbf{C}^\alpha, \tag{157}$$
$$\mathbf{Q}_{\mathrm{V}l}^\alpha(t) = \mathbf{Q}_{\mathrm{V}l0}^\alpha \exp[-t/\tau_{\mathrm{V}l}^\alpha] + \int_{0+}^t \exp[-(t-s)/\tau_{\mathrm{V}l}^\alpha] D_s^\alpha(2\partial\hat{\Psi}_{\mathrm{V}l}^\alpha/\partial\mathbf{C}^\alpha)\mathrm{d}s, \tag{158}$$
$$\mathbf{Q}_{\mathrm{S}m}^\alpha(t) = \mathbf{Q}_{\mathrm{S}m0}^\alpha \exp[-t/\tau_{\mathrm{S}m}^\alpha] + \int_{0+}^t \exp[-(t-s)/\tau_{\mathrm{S}m}^\alpha] D_s^\alpha(2\partial\hat{\Psi}_{\mathrm{S}m}^\alpha/\partial\mathbf{C}^\alpha)\mathrm{d}s. \tag{159}$$

Cauchy stress contributions are sums over l, m:

$$\boldsymbol{\sigma}_\Gamma^\alpha = 2\frac{\rho^\alpha}{\rho_{\mathrm{R}0}^\alpha}\mathbf{F}^\alpha\frac{\partial\Psi_\Gamma^\alpha}{\partial\mathbf{C}^\alpha}(\mathbf{F}^\alpha)^\mathsf{T} = 2\frac{\rho^\alpha}{\rho_{\mathrm{R}0}^\alpha}\mathbf{F}^\alpha\frac{\partial U_\Gamma^\alpha}{\partial\mathbf{C}^\alpha}(\mathbf{F}^\alpha)^\mathsf{T}$$
$$= \frac{\rho^\alpha}{\rho_{\mathrm{R}0}^\alpha}\sum_l \mathbf{F}^\alpha\mathbf{Q}_{\mathrm{V}l}^\alpha(\mathbf{F}^\alpha)^\mathsf{T} + \frac{\rho^\alpha}{\rho_{\mathrm{R}0}^\alpha}\sum_m \mathbf{F}^\alpha\mathbf{Q}_{\mathrm{S}m}^\alpha(\mathbf{F}^\alpha)^\mathsf{T}. \tag{160}$$

As $t/\tau_{\mathrm{V}l}^\alpha \to 0$ and $t/\tau_{\mathrm{S}m}^\alpha \to 0$, $\boldsymbol{\sigma}_\Gamma^\alpha$ in Eq. 160 sums to the instantaneous (i.e., glassy)

viscoelastic stresses

$$2\frac{\rho^\alpha}{\rho^\alpha_{\mathrm{R}0}}\sum_l \mathbf{F}^\alpha\frac{\partial\hat{\Psi}^\alpha_{\mathrm{V}l}}{\partial\mathbf{C}^\alpha}(\mathbf{F}^\alpha)^{\mathsf{T}} + 2\frac{\rho^\alpha}{\rho^\alpha_{\mathrm{R}0}}\sum_m \mathbf{F}^\alpha\frac{\partial\hat{\Psi}^\alpha_{\mathrm{S}m}}{\partial\mathbf{C}^\alpha}(\mathbf{F}^\alpha)^{\mathsf{T}}$$
$$= \frac{\rho^\alpha}{\rho^\alpha_{\mathrm{R}0}}\sum_l \beta^\alpha_{\mathrm{V}l}B^\alpha_\theta(\ln J^\alpha)\mathbf{1} + \frac{\rho^\alpha}{\rho^\alpha_{\mathrm{R}0}}\sum_m \beta^\alpha_{\mathrm{S}m}\mu^\alpha_{\mathrm{S}}[\tilde{\mathbf{B}}^\alpha - \frac{1}{3}(\mathrm{tr}\tilde{\mathbf{B}}^\alpha)\mathbf{1}]. \tag{161}$$

As $t/\tau^\alpha_{\mathrm{V}l} \to \infty$ and $t/\tau^\alpha_{\mathrm{S}m} \to \infty$, $\mathbf{Q}^\alpha_{\mathrm{V}l} \to \mathbf{0}$ and $\mathbf{Q}^\alpha_{\mathrm{S}m} \to \mathbf{0}$ so that $\boldsymbol{\sigma}^\alpha_\Gamma \to \mathbf{0}$ in Eq. 160 for relaxed equilibrium response.

Numerous viscoelastic theories for soft materials exist.[3,176] The framework of constitutive Eqs. 151–161 is used here because its internal variable formalism is compatible with Eqs. 89, 97, 128, and 145. Algorithms for updating viscoelastic stress contributions are robust and efficient[165] and have been used elsewhere for soft tissues.[27]

3.2.7 Fiber Viscoelasticity

Dissipative response of fiber families $k = 1, \ldots$ is dictated by internal variables $\mathbf{\Gamma}^\alpha_{\Phi k,n}$ each with $n = 1, \ldots$ relaxation times $\tau^\alpha_{\Phi k,n}$ and conjugate internal stresses $\mathbf{Q}^\alpha_{\Phi k,n}$. Internal stresses and energies are

$$\mathbf{Q}^\alpha_{\Phi k,n} = -\partial\Psi^\alpha_\Phi/\partial\mathbf{\Gamma}^\alpha_{\Phi k,n} = 2\partial\Psi^\alpha_{\Phi k,n}/\partial\mathbf{C}^\alpha, \tag{162}$$

$$\Psi^\alpha_\Phi = U^\alpha_\Phi = \sum_k \Psi^\alpha_{\Phi k} = \sum_k\sum_n \Psi^\alpha_{\Phi k,n}(\mathbf{\Gamma}^\alpha_{\Phi k,n}, \mathbf{C}^\alpha)$$
$$= \sum_k\sum_n \int \tfrac{1}{2}\mathbf{Q}^\alpha_{\Phi k,n} : \mathrm{d}\mathbf{C}^\alpha. \tag{163}$$

Evolution equations and stored viscoelastic energies are

$$D^\alpha_t\mathbf{Q}^\alpha_{\Phi k,n} + \mathbf{Q}^\alpha_{\Phi k,n}/\tau^\alpha_{\Phi k,n} = 2D^\alpha_t(\partial\hat{\Psi}^\alpha_{\Phi k,n}/\partial\mathbf{C}^\alpha), \tag{164}$$

$$\hat{\Psi}^\alpha_{\Phi k,n} = \frac{\beta^\alpha_{\Phi k,n}\mu^\alpha_k}{4k^\alpha_k}\{\exp[k^\alpha_k(I^\alpha_k - 1)^2] - 1\}\mathrm{H}(I^\alpha_k - 1), \tag{165}$$

with $\beta^{\alpha}_{\Phi k,n} \geq 0$. Initial conditions and solutions (i.e., convolution integrals), followed by Cauchy stress terms, are

$$\mathbf{Q}^{\alpha}_{\Phi k,n0} = 2\partial\hat{\Psi}^{\alpha}_{\Phi k,n}/\partial\mathbf{C}^{\alpha}, \tag{166}$$

$$\mathbf{Q}^{\alpha}_{\Phi k,n}(t) = \mathbf{Q}^{\alpha}_{\Phi k,n0}\exp[-t/\tau^{\alpha}_{\Phi k,n}] + \int_{0+}^{t}\exp[-(t-s)/\tau^{\alpha}_{\Phi k,n}]D^{\alpha}_{s}(2\partial\hat{\Psi}^{\alpha}_{\Phi k,n}/\partial\mathbf{C}^{\alpha})\mathrm{d}s, \tag{167}$$

$$\boldsymbol{\sigma}^{\alpha}_{\Phi} = 2\frac{\rho^{\alpha}}{\rho^{\alpha}_{\mathrm{R}0}}\mathbf{F}^{\alpha}\frac{\partial\Psi^{\alpha}_{\Phi}}{\partial\mathbf{C}^{\alpha}}(\mathbf{F}^{\alpha})^{\mathsf{T}} = 2\frac{\rho^{\alpha}}{\rho^{\alpha}_{\mathrm{R}0}}\mathbf{F}^{\alpha}\frac{\partial U^{\alpha}_{\Phi}}{\partial\mathbf{C}^{\alpha}}(\mathbf{F}^{\alpha})^{\mathsf{T}} = \frac{\rho^{\alpha}}{\rho^{\alpha}_{\mathrm{R}0}}\sum_{k}\sum_{n}\mathbf{F}^{\alpha}\mathbf{Q}^{\alpha}_{\Phi k,n}(\mathbf{F}^{\alpha})^{\mathsf{T}}. \tag{168}$$

As $t/\tau^{\alpha}_{\Phi k,n} \to 0$, $\boldsymbol{\sigma}^{\alpha}_{\Phi}$ in Eq. 168 becomes the glassy stress

$$2\frac{\rho^{\alpha}}{\rho^{\alpha}_{\mathrm{R}0}}\sum_{k}\sum_{n}\mathbf{F}^{\alpha}\frac{\partial\hat{\Psi}^{\alpha}_{\Phi k,n}}{\partial\mathbf{C}^{\alpha}}(\mathbf{F}^{\alpha})^{\mathsf{T}} = \frac{\rho^{\alpha}}{\rho^{\alpha}_{\mathrm{R}0}}\sum_{k}\sum_{n}\{\beta^{\alpha}_{\Phi k,n}\mu^{\alpha}_{k}(I^{\alpha}_{k}-1) \times \exp[k^{\alpha}_{k}(I^{\alpha}_{k}-1)^{2}]\mathrm{H}(I^{\alpha}_{k}-1)\tilde{\mathbf{h}}^{\alpha}_{k}\}. \tag{169}$$

As $t/\tau^{\alpha}_{\Phi k,n} \to \infty$, $\mathbf{Q}^{\alpha}_{\Phi k,n} \to \mathbf{0}$ leading to $\boldsymbol{\sigma}^{\alpha}_{\Phi} \to \mathbf{0}$ in Eq. 168. This viscoelastic fiber model of Holzapfel,[165] Holzapfel et al.,[174] and Gultekin et al.[27] is used for like reasons as, and consistency with, the framework for soft-tissue matrix viscoelasticity in Section 3.2.6.

3.2.8 Active Tension

Electrochemistry of soft tissue cellular activation[177] is beyond the present scope. A phenomenological approach is implemented instead, generalizing other continuum models.[31,178,179] Let $\{\boldsymbol{\Delta}^{\alpha}\} \to \{\Delta^{\alpha}_{k}\}(\mathbf{X}^{\alpha}, t)$ be a set of scalar internal variables associated with potentially active fiber families k in phase α. These variables can include internal strains in contractile elements and time-dependent switching functions. Define the fiber orientation tensors $\mathbf{H}^{\alpha}_{k}$ as in Eq. 147. In many models, cells are fully aligned such that $k = 1$ and $\kappa^{\alpha}_{1} = 0$,[31,178] but this is inessential.[179] Stretch in the fiber direction is defined as $\lambda^{\alpha}_{k} = \sqrt{I^{\alpha}_{k}}$. A generic energy function is

$$\Psi^{\alpha}_{\mathrm{A}} = U^{\alpha}_{\mathrm{A}} = \sum_{k}\Psi^{\alpha}_{\mathrm{A}k} = \sum_{k}[\Lambda^{\alpha}_{k}(\lambda^{\alpha}_{k}, \{\Delta^{\alpha}_{k}\}) + \chi^{\alpha}_{k}(\{\Delta^{\alpha}_{k}\})]. \tag{170}$$

Strain energy functions Λ_k^α furnish active stress terms

$$\boldsymbol{\sigma}_{\mathrm{A}}^\alpha = 2\frac{\rho^\alpha}{\rho_{\mathrm{R}0}^\alpha}\mathbf{F}^\alpha\frac{\partial\Psi_{\mathrm{A}}^\alpha}{\partial\mathbf{C}^\alpha}(\mathbf{F}^\alpha)^{\mathsf{T}} = 2\frac{\rho^\alpha}{\rho_{\mathrm{R}0}^\alpha}\mathbf{F}^\alpha\frac{\partial U_{\mathrm{A}}^\alpha}{\partial\mathbf{C}^\alpha}(\mathbf{F}^\alpha)^{\mathsf{T}} = \frac{\rho^\alpha}{\rho_{\mathrm{R}0}^\alpha}\sum_k\frac{1}{\lambda_k^\alpha}\frac{\partial\Lambda_k^\alpha}{\partial\lambda_k^\alpha}\tilde{\mathbf{h}}_k^\alpha. \quad (171)$$

Energy functions χ_k^α ensure nonnegative net dissipation. Stresses $\boldsymbol{\sigma}_{\mathrm{A}}^\alpha$ should vanish for passive conditions.

The general form in Eq. 170 is sufficient to embody successful models of muscle contraction.[31,178,179] It is physically justified by coupling of (muscle) fiber stretch to activation energy and active stress. For example, Eqs. 170 and 171 do not involve deformation of the matrix since the matrix is deemed a passive element of muscle.[178,179]

3.2.9 Damage: Fracture, Tearing, or Cavitation

Internal variables $\{\mathbf{D}^\alpha\} \to \{\bar{D}^\alpha, D_k^\alpha\}$. For each constituent α, scalar damage measures in the isotropic matrix or fluid are $\bar{D}^\alpha \in [0,1]$, and $D_k^\alpha \in [0,1]$ are scalar functions for each fiber family k. All are akin to order parameters in phase-field fracture theory.[38,50,180]

Degradation functions in Eqs. 126–129 are, with $\bar{\vartheta}^\alpha \in [0,\infty), \vartheta_k^\alpha \in [0,\infty)$ constants,

$$\varsigma_{\mathrm{V}}^\alpha = [1-\bar{D}^\alpha\mathrm{H}(\ln J^\alpha)]^{\bar{\vartheta}^\alpha}, \qquad \varsigma_{\mathrm{S}}^\alpha = (1-\bar{D}^\alpha)^{\bar{\vartheta}^\alpha}, \quad (172)$$

$$\varsigma_{\mathrm{F}}^\alpha\circ(\cdot) = \varsigma_{\mathrm{F}}^\alpha\circ\sum_k(\cdot)_k = \sum_k\varsigma_{\mathrm{F}k}^\alpha(\cdot)_k = \sum_k(1-D_k^\alpha)^{\vartheta_k^\alpha}(\cdot)_k,$$

$$\varsigma_{\mathrm{F}k}^\alpha = (1-D_k^\alpha)^{\vartheta_k^\alpha}. \quad (173)$$

The Heaviside function in $\varsigma_{\mathrm{V}}^\alpha$ prevents degradation in compression so that the bulk modulus is preserved,[50,151] as in a compressible elastic fluid. Operator $\varsigma_{\mathrm{F}}^\alpha$ in Eqs. 128 and 129 is applied to a sum of energetic contributions (i.e., hyperelastic and viscoelastic) over all families k via Eq. 173.

Partial stress less viscous stress of constituent α is $\bar{\boldsymbol{\sigma}}^\alpha = \boldsymbol{\sigma}^\alpha - \hat{\boldsymbol{\sigma}}^\alpha$. For an ideal gas, $\bar{D}^\alpha = \bar{\vartheta}^\alpha = 0 \to \varsigma_{\mathrm{V}}^\alpha = 1$, so $\bar{\boldsymbol{\sigma}}^\alpha = -\rho^\alpha\mathfrak{R}^\alpha\theta^\alpha\mathbf{1}$ by Eq. 130. For solid and liquid constituents α, applying Eq. 128, this stress is the sum of Eqs. 135, 146, 150, 160,

168, and 171, scaled by one or more functions in Eqs. 172 and 173:

$$\begin{aligned}\bar{\boldsymbol{\sigma}}^{\alpha} = &\frac{\rho^{\alpha}}{\rho^{\alpha}_{\mathrm{R}0}}[1-\bar{D}^{\alpha}\mathrm{H}(\ln J^{\alpha})]^{\bar{\vartheta}^{\alpha}}B^{\alpha}_{\theta}\\ &\times\{\ln J^{\alpha}[\exp\{k^{\alpha}_{\mathrm{V}}(\ln J^{\alpha})^2\}-\tfrac{1}{2}(B^{\alpha}_{\theta\mathrm{p}}-2)\ln J^{\alpha}]\\ &\quad -A^{\alpha}(\theta^{\alpha}-\theta^{\alpha}_{0})\}\mathbf{1}-(\rho^{\alpha}/\rho^{\alpha}_{\mathrm{R}0})p^{\alpha}_{\mathrm{R}0}\mathbf{1}\\ &+\frac{\rho^{\alpha}}{\rho^{\alpha}_{\mathrm{R}0}}(1-\bar{D}^{\alpha})^{\bar{\vartheta}^{\alpha}}\mu^{\alpha}_{\mathrm{S}}[\tilde{\mathbf{B}}^{\alpha}-\tfrac{1}{3}(\mathrm{tr}\tilde{\mathbf{B}}^{\alpha})\mathbf{1}]\\ &+\frac{\rho^{\alpha}}{\rho^{\alpha}_{\mathrm{R}0}}\sum_{k}(1-D^{\alpha}_{k})^{\vartheta^{\alpha}_{k}}\mu^{\alpha}_{k}(I^{\alpha}_{k}-1)\\ &\qquad\times\exp[k^{\alpha}_{k}(I^{\alpha}_{k}-1)^2]\mathrm{H}(I^{\alpha}_{k}-1)\tilde{\mathbf{h}}^{\alpha}_{k}\\ &+\frac{\rho^{\alpha}}{\rho^{\alpha}_{\mathrm{R}0}}(1-\bar{D}^{\alpha})^{\bar{\vartheta}^{\alpha}}\sum_{l}\mathbf{F}^{\alpha}\mathbf{Q}^{\alpha}_{\mathrm{V}l}(\mathbf{F}^{\alpha})^{\mathsf{T}}\\ &+\frac{\rho^{\alpha}}{\rho^{\alpha}_{\mathrm{R}0}}(1-\bar{D}^{\alpha})^{\bar{\vartheta}^{\alpha}}\sum_{m}\mathbf{F}^{\alpha}\mathbf{Q}^{\alpha}_{\mathrm{S}m}(\mathbf{F}^{\alpha})^{\mathsf{T}}\\ &+\frac{\rho^{\alpha}}{\rho^{\alpha}_{\mathrm{R}0}}\sum_{k}[(1-D^{\alpha}_{k})^{\vartheta^{\alpha}_{k}}\sum_{n}\mathbf{F}^{\alpha}\mathbf{Q}^{\alpha}_{\Phi k,n}(\mathbf{F}^{\alpha})^{\mathsf{T}}]\\ &+\frac{\rho^{\alpha}}{\rho^{\alpha}_{\mathrm{R}0}}\sum_{k}\frac{1}{\lambda^{\alpha}_{k}}\frac{\partial\Lambda^{\alpha}_{k}}{\partial\lambda^{\alpha}_{k}}\tilde{\mathbf{h}}^{\alpha}_{k}.\end{aligned}\tag{174}$$

To preclude damage induced by normal muscle contraction, the final term in Eq. 174 is decoupled from $\{\mathbf{D}^{\alpha}\}$ consistently with Eqs. 128 and 129. If Eq. 139 is used instead of Eq. 133, then spherical terms on the right in Eq. 174 should appeal to Eq. 141 rather than Eq. 135.

Let $\Psi^{\alpha}_{\mathrm{D}}=U^{\alpha}_{\mathrm{D}}$ comprise cohesive and surface energies of fracture per unit referential volume scaled by contributions of dimensionless Finsler-type metric[94,97] $\hat{\mathbf{G}}^{\alpha}$ in Eq. 118, where $\hat{G}^{\alpha}=\hat{G}^{\alpha}(\{\boldsymbol{\xi}^{\alpha}\},\mathbf{X}^{\alpha},\mathbf{x})$ via Eq. 92. Extending usual single-parameter phase-field theories, quadratic forms for matrix $[\bar{(\cdot)}^{\alpha}]$ and fiber $[(\cdot)^{\alpha}_{k}]$ contributions are

$$\begin{aligned}\hat{\Psi}^{\alpha}_{\mathrm{D}}=\Psi^{\alpha}_{\mathrm{D}}/\sqrt{\hat{G}^{\alpha}}=&\bar{E}^{\alpha}_{\mathrm{C}}|\bar{D}^{\alpha}|^2+\bar{\Upsilon}^{\alpha}\bar{l}^{\alpha}_{\mathrm{R}}|\nabla^{\alpha}_{0}\bar{D}^{\alpha}|^2\\ &+\sum_{k}[E^{\alpha}_{\mathrm{C}k}|D^{\alpha}_{k}|^2+\Upsilon^{\alpha}_{k}l^{\alpha}_{\mathrm{R}k}|\nabla^{\alpha}_{0}D^{\alpha}_{k}|^2].\end{aligned}\tag{175}$$

In Eq. 175, cohesive energies per unit volume are $\bar{E}^{\alpha}_{\mathrm{C}}$ and $E^{\alpha}_{\mathrm{C}k}$, surface energies per

unit area are $\bar{\Upsilon}^\alpha$ and Υ^α_k, and gradient regularization lengths are

$$\bar{l}^\alpha_{\mathrm{R}} = \bar{\alpha}^\alpha \bar{l}^\alpha, \qquad l^\alpha_{\mathrm{R}k} = \alpha^\alpha_k l^\alpha_k, \tag{176}$$

all nonnegative constants. For solids, typically $\bar{E}^\alpha_{\mathrm{C}} = \bar{\Upsilon}^\alpha/\bar{l}^\alpha$ and $E^\alpha_{\mathrm{C}k} = \Upsilon^\alpha_k/l^\alpha_k$.

Dimensionless factors $\bar{\alpha}^\alpha \in [0,\infty)$ and $\alpha^\alpha_k \in [0,\infty)$ allow independent cohesive energies and gradient regularization lengths.[151] For cavitation of a fluid, gradient terms can be dropped[52] (i.e., $\bar{\alpha}^\alpha \to 0$); cohesion energy $\bar{E}^\alpha_{\mathrm{C}}$ will capture fracture of the fluid for tensile pressure. Isotropic surface energies are assumed for gradient terms of Eq. 175. These could be extended to anisotropic contributions[38,181] if data exist. However, $\{D^\alpha_k\}$ furnish stress-damage anisotropy regardless.

When $\hat{G}^\alpha \to 1$, corresponding to a classical Euclidean material metric, Eq. 175 is justified as a standard model of phase-field fracture mechanics.[50,51,151] In the classical case ($\bar{\alpha}^\alpha \to 1$), only two parameters are needed for matrix and each fiber family, with physical meaning (i.e., cohesive energy and surface energy). A novelty is scaling of energy by $|\hat{G}^\alpha|^{1/2}$. Physically, as justified by studies of hard[94,96] and soft[97] solids, this scaling, when greater than unity, accounts for increases in internal free surface area of the material with microstructure as cavities enlarge or cracks slide and open. This, in turn, increases the material's resistance to fracture since the total surface energy is proportional to the surface area. Given the metric tensors of Section 3.4, $\hat{G}^\alpha \geq 1$ for the physically rational case of positive remnant strain. The increase in toughness due to remnant strain or collagen fiber sliding and remodeling[18] is akin to toughening of an elastic–plastic solid from plasticity at a crack tip.

3.3 Generalized Finsler Metric Tensors

Coordinate forms of Eqs. 117 and 118 are, respectively,

$$\mathbf{g}(\mathbf{x},t) = \bar{g}_{ik}(\mathbf{x})\, \hat{g}^k_j(\{\boldsymbol{\xi}^\alpha(\mathbf{x},t)\})\mathbf{g}^i \otimes \mathbf{g}^j, \tag{177}$$

$$\mathbf{G}^\alpha(\mathbf{X}^\alpha,t) = (\bar{G}^\alpha)_{IK}(\mathbf{X}^\alpha)\,(\hat{G}^\alpha)^K_J(\{\boldsymbol{\Xi}^\alpha(\mathbf{X}^\alpha,t)\})\,(\mathbf{G}^\alpha)^I \otimes (\mathbf{G}^\alpha)^J. \tag{178}$$

Canonical transformations[94,96,97] between representations of state variables on $\mathfrak{m}$ and $\mathfrak{M}^\alpha$ are used for Eq. 92:

$$\{\boldsymbol{\Xi}^\alpha(\mathbf{X}^\alpha,t)\} = \{\boldsymbol{\xi}^\alpha(\mathbf{x},t)\} \circ \boldsymbol{\chi}^\alpha(\mathbf{X}^\alpha,t). \tag{179}$$

Though other relationships are admissible, the analogous transformation law[97] between components of $\hat{\mathbf{G}}^\alpha$ and $\hat{\mathbf{g}}$ is prescribed here, with δ^i_j Kronecker's delta symbols:

$$(\hat{G}^\alpha)^I_J(\mathbf{X}^\alpha, t) = \delta^I_i \delta^j_J \hat{g}^i_j(\boldsymbol{\chi}^\alpha(\mathbf{X}^\alpha, t), t), \tag{180}$$

Only $\{\boldsymbol{\xi}^\alpha\}$ and $\hat{g}^i_j(\{\boldsymbol{\xi}^\alpha\})$ need be defined constitutively, with Eq. 179 yielding $\{\boldsymbol{\Xi}^\alpha\}$ and Eq. 180 yielding $(\hat{G}^\alpha)^I_J(\{\boldsymbol{\Xi}^\alpha\})$, or vice-versa if referential (i.e., Lagrangian) versions of metric components are defined explicitly instead. Dependence of $\hat{\mathbf{g}}$ on $\{\boldsymbol{\xi}^\alpha\}$ is henceforth restricted to dependence on damage parameters $(\{\bar{D}^\alpha\}, \{D^\alpha_k\})$; Eq. 179 is $\bar{D}^\alpha(\mathbf{X}^\alpha, t) = \bar{D}^\alpha(\boldsymbol{\chi}^\alpha(\mathbf{X}^\alpha, t), t) \circ \boldsymbol{\chi}^\alpha_t$ and so on for $\{D^\alpha_k\}$.

If the geometric framework is extended to describe biologic growth[99,100] and remodeling,[105,136] then $\{\boldsymbol{\xi}^\alpha\}$ can be expanded with internal state variable(s) associated with such processes, for which kinetics of Eq. 97 are needed. For theories like those of Yavari[99] and Sadik et al.,[100] $\hat{\mathbf{G}}^\alpha$ should depend on some additional (e.g., growth) function(s), $\hat{g}^i_j \to \delta^i_j$, but Eq. 180 is not enforced, so $\mathfrak{m}$ is Euclidean but $\mathfrak{M}^\alpha$ need not be.[98,105,139]

In the current application, as tears and commensurate fiber rearrangements arise in constituents of the mixture, the body manifold can expand and shear.[97] For brevity and sufficiency in applications of Section 4, the specialization is there restricted to a mixture having a single solid constituent. Fluids are devoid of microstructure that would affect metric tensors; any effects of fluid cavitation, irrelevant in later calculations as shown in Section 4.2.2, are omitted. Metric forms can be expanded with additional products and sums to allow for contributions from more constituents, as shown in Eqs. 181–187 for $\alpha = 1, 2, \ldots, N$ with $N > 1$.

The mixed-variant tensor $\hat{\mathbf{g}}$ is a product of matrix and fiber terms:

$$\hat{g}^i_j(\{\bar{D}^\alpha\}, \{D^\alpha_k\}) = \bar{\gamma}^i_k(\{\bar{D}^\alpha\})\tilde{\gamma}^k_j(\{D^\alpha_k\}). \tag{181}$$

Contributions from isotropic matrix damage $\{\bar{D}^\alpha\}$ in $\bar{\gamma}^i_j$ are assumed spherical (e.g., Weyl-type scaling[95]), measured by determinants $\bar{\gamma}^\alpha = \bar{\gamma}^\alpha(\bar{D}^\alpha)$. Spherical contributions of phases $\alpha = 1, \ldots, N$ are merged multiplicatively in $\hat{\mathbf{g}}$ since their sequence

is irrelevant. Forms for each contribution are

$$\bar{\gamma}^i_j = \delta^i_j \prod_\alpha (\bar{\gamma}^\alpha)^{1/3}, \qquad \bar{\gamma}^\alpha = \exp\left[\frac{2n_0^\alpha \bar{\kappa}^\alpha}{\bar{r}^\alpha}(\bar{D}^\alpha)^{\bar{r}^\alpha}\right]. \tag{182}$$

Recall $n_0^\alpha(\mathbf{X}^\alpha) \in [0,1]$ is a reference volume fraction of phase α, and $\bar{r}^\alpha > 0$ and $\bar{\kappa}^\alpha$ are constants, the latter positive for dilatant damage. Remnant volumetric strain[97] at $\bar{D}^\alpha = 1$ is the ratio of constants

$$\bar{\epsilon}^\alpha = \frac{n_0^\alpha \bar{\kappa}^\alpha}{\bar{r}^\alpha}. \tag{183}$$

Fiber contributions from constituents α and fiber families k are merged additively into $\hat{\mathbf{g}}$ since these terms are generally anisotropic.[94,97] Defining $(H_k^\alpha)^i_j = \delta^i_I \delta^J_j (H_k^\alpha)^I_J$ with $(H_k^\alpha)^I_J = \kappa_k^\alpha \delta^I_J + (1 - 3\kappa_k^\alpha)(\iota_k^\alpha)^I(\iota_k^\alpha)_J$ from Eq. 147,

$$\tilde{\gamma}^i_j = \delta^i_j + \sum_\alpha \sum_k (H_k^\alpha)^i_j \{\exp\left[\frac{2n_0^\alpha \tilde{\kappa}_k^\alpha}{\tilde{r}_k^\alpha}(D_k^\alpha)^{\tilde{r}_k^\alpha}\right] - 1\}. \tag{184}$$

Constants $\tilde{r}_k^\alpha > 0$ and $\tilde{\kappa}_k^\alpha$ measure the logarithmic remnant strain contributions from fibers at $D_k^\alpha = 1$:

$$\tilde{\epsilon}_k^\alpha = \frac{n_0^\alpha \tilde{\kappa}_k^\alpha}{\tilde{r}_k^\alpha}. \tag{185}$$

Noting determinants of metrics $\hat{G}^\alpha = \det \hat{\mathbf{G}}^\alpha = \det \hat{\mathbf{g}} = \hat{g}$ are related through Eq. 180, derivatives in conjugate forces of Eqs. 198 and 203 are calculated from Eqs. 182 and 184 as follows:

$$\partial(\ln \sqrt{\hat{G}^\alpha})/\partial \bar{D}^\alpha = n_0^\alpha \bar{\kappa}^\alpha (\bar{D}^\alpha)^{\bar{r}^\alpha - 1}, \tag{186}$$

$$\frac{\partial(\ln \sqrt{\hat{G}^\alpha})}{\partial D_k^\alpha} = \exp\left[\frac{2n_0^\alpha \tilde{\kappa}_k^\alpha}{\tilde{r}_k^\alpha}(D_k^\alpha)^{\tilde{r}_k^\alpha}\right](\tilde{\gamma}^{-1})^i_j (H_k^\alpha)^j_i n_0^\alpha \tilde{\kappa}_k^\alpha (D_k^\alpha)^{\tilde{r}_k^\alpha - 1}. \tag{187}$$

Values $\bar{r}^\alpha \in (0,1)$ and $\tilde{r}_k^\alpha \in (0,1)$ produce nonsingular $\hat{\mathbf{g}}$ and admit solutions to some equilibrium problems.[97] However, these ranges can result in singularities at $\bar{D}^\alpha = 0$ and $D_k^\alpha = 0$ in respective Eqs. 186 and 187. Such singularities can be avoided by choosing $\bar{r}^\alpha \geq 1$ and $\tilde{r}_k^\alpha \geq 1$. Stronger conditions $\bar{r}^\alpha > 1$ and $\tilde{r}_k^\alpha > 1$ usefully ensure Eqs. 186 and 187 vanish at (e.g., initial) states having $\bar{D}^\alpha = 0$ and $D_k^\alpha = 0$.

Partitions in Eqs. 177 and 178 and exponential forms in Eqs. 182 and 184 are chosen based on successful use in prior work.[97,99,105] The latter are convenient for deriving analytical solutions to problems since Christoffel symbols (i.e., spatial derivatives of metric tensor components) are of relatively simple form. Only a few parameters are required to fit data,[97] physically related to measurable remnant strains in the case of degradation.

3.4 Kinetics for Soft-Tissue Biomechanics

3.4.1 Viscous Stress

Isotropic Newtonian behavior is usually adequate for each constituent α. Denote by $\hat{B}^\alpha(\theta^\alpha) \geq 0$ and $\hat{\mu}^\alpha(\theta^\alpha) \geq 0$ respective bulk and shear viscosities, possibly temperature dependent, of isolated constituents. Viscous stresses and dissipation are, respectively,

$$\hat{\boldsymbol{\sigma}}^\alpha = n_0^\alpha[\hat{B}^\alpha - \tfrac{2}{3}\hat{\mu}^\alpha]\mathrm{tr}(\mathbf{d}^\alpha)\mathbf{1} + 2n_0^\alpha\hat{\mu}^\alpha\mathbf{d}^\alpha, \tag{188}$$

$$\hat{\mathfrak{D}}^\alpha = \hat{\boldsymbol{\sigma}}^\alpha : \mathbf{d}^\alpha = n_0^\alpha\hat{B}^\alpha|\mathrm{tr}(\mathbf{d}^\alpha)|^2 + 2n_0^\alpha\hat{\mu}^\alpha|\mathbf{d}^\alpha - \tfrac{1}{3}\mathrm{tr}(\mathbf{d}^\alpha)\mathbf{1}|^2 \geq 0. \tag{189}$$

Viscous pressure and deviatoric stress contributions are $\hat{p}^\alpha = -n_0^\alpha\hat{B}^\alpha\nabla\cdot\boldsymbol{\upsilon}^\alpha$ and $\hat{\boldsymbol{\sigma}}^\alpha_{\mathrm{S}}$, whereby the total contribution to Cauchy stress is $\hat{\boldsymbol{\sigma}}^\alpha = -\hat{p}^\alpha\mathbf{1} + \hat{\boldsymbol{\sigma}}^\alpha_{\mathrm{S}}$. Equations 188 and 189 are standard, simple models for viscous fluids including air, water, and blood plasma,[3,72,182] needing only two measurable parameters. Any other viscosity model obeying Eq. 91 and $\hat{\mathfrak{D}}^\alpha \geq 0$ could be used (e.g., for whole blood) if justified by rheology.[3]

3.4.2 Viscoelasticity

Viscoelastic internal state variables are the subset of $\{\boldsymbol{\xi}^\alpha\}$ consisting of volumetric, deviatoric matrix, and fiber terms $\{\boldsymbol{\Gamma}^\alpha_{\mathrm{V}l}, \boldsymbol{\Gamma}^\alpha_{\mathrm{S}m}, \boldsymbol{\Gamma}^\alpha_{\Phi k,n}\}$. Conjugate forces entering Eq. 113 are a subset of $\{\boldsymbol{\pi}^\alpha\}$:

$$\begin{aligned} \boldsymbol{\pi}^\alpha_{\mathrm{V}l} &= -\varsigma^\alpha_{\mathrm{S}}\frac{\rho^\alpha}{\rho^\alpha_{\mathrm{R}0}}\mathbf{Q}^\alpha_{\mathrm{V}l}, \qquad \boldsymbol{\pi}^\alpha_{\mathrm{S}m} = -\varsigma^\alpha_{\mathrm{S}}\frac{\rho^\alpha}{\rho^\alpha_{\mathrm{R}0}}\mathbf{Q}^\alpha_{\mathrm{S}m}, \\ \boldsymbol{\pi}^\alpha_{\Phi k,n} &= -\varsigma^\alpha_{\mathrm{F}k}\frac{\rho^\alpha}{\rho^\alpha_{\mathrm{R}0}}\mathbf{Q}^\alpha_{\Phi k,n}. \end{aligned} \tag{190}$$

Kinetic laws for internal variables[36,164,165] are

$$\begin{aligned} D_t^\alpha \mathbf{\Gamma}_{\mathrm{V}l}^\alpha &= \frac{\mathbf{Q}_{\mathrm{V}l}^\alpha}{\beta_{\mathrm{V}l}^\alpha B_\theta^\alpha \tau_{\mathrm{V}l}^\alpha}, \qquad D_t^\alpha \mathbf{\Gamma}_{\mathrm{S}m}^\alpha = \frac{\mathbf{Q}_{\mathrm{S}m}^\alpha}{\beta_{\mathrm{S}m}^\alpha \mu_{\mathrm{S}}^\alpha \tau_{\mathrm{S}m}^\alpha}, \\ D_t^\alpha \mathbf{\Gamma}_{\Phi k,n}^\alpha &= \frac{\mathbf{Q}_{\Phi k,n}^\alpha}{\beta_{\Phi k,n}^\alpha \mu_k^\alpha \tau_{\Phi k,n}^\alpha}. \end{aligned} \tag{191}$$

Dissipation from viscoelasticity is unconditionally nonnegative in Eq. 113:

$$\begin{aligned} \mathfrak{D}_\Gamma^\alpha = \quad & \frac{\rho^\alpha}{\rho_{\mathrm{R}0}^\alpha} \sum_l \frac{\varsigma_{\mathrm{S}}^\alpha \mathbf{Q}_{\mathrm{V}l}^\alpha : \mathbf{Q}_{\mathrm{V}l}^\alpha}{\beta_{\mathrm{V}l}^\alpha B_\theta^\alpha \tau_{\mathrm{V}l}^\alpha} \\ & + \frac{\rho^\alpha}{\rho_{\mathrm{R}0}^\alpha} \sum_m \frac{\varsigma_{\mathrm{S}}^\alpha \mathbf{Q}_{\mathrm{S}m}^\alpha : \mathbf{Q}_{\mathrm{S}m}^\alpha}{\beta_{\mathrm{S}m}^\alpha \mu_{\mathrm{S}}^\alpha \tau_{\mathrm{S}m}^\alpha} \\ & + \frac{\rho^\alpha}{\rho_{\mathrm{R}0}^\alpha} \sum_k \sum_n \frac{\varsigma_{\mathrm{F}k}^\alpha \mathbf{Q}_{\Phi k,n}^\alpha : \mathbf{Q}_{\Phi k,n}^\alpha}{\beta_{\Phi k,n}^\alpha \mu_k^\alpha \tau_{\Phi k,n}^\alpha} \geq 0. \end{aligned} \tag{192}$$

The initial conditions for state variables are $\mathbf{\Gamma}_{\mathrm{V}l0}^\alpha = \mathbf{0}$, $\mathbf{\Gamma}_{\mathrm{S}m}^\alpha = \mathbf{0}$, and $\mathbf{\Gamma}_{\Phi k,n}^\alpha = \mathbf{0}$. For energies, $\Psi_{\mathrm{V}l}^\alpha(\mathbf{0}, \mathbf{C}^\alpha) = \hat{\Psi}_{\mathrm{V}l}^\alpha(\mathbf{C}^\alpha)$, $\Psi_{\mathrm{S}m}^\alpha(\mathbf{0}, \mathbf{C}^\alpha) = \hat{\Psi}_{\mathrm{S}m}^\alpha(\mathbf{C}^\alpha)$, and $\Psi_{\Phi k,n}^\alpha(\mathbf{0}, \mathbf{C}^\alpha) = \hat{\Psi}_{\Phi k,n}^\alpha(\mathbf{C}^\alpha)$. Configurational energies are integrated over time as

$$\begin{aligned} \Psi_\Gamma^\alpha = & \sum_l \left[\hat{\Psi}_{\mathrm{V}l}^\alpha - \int_0^t \mathbf{Q}_{\mathrm{V}l}^\alpha : D_s^\alpha \mathbf{\Gamma}_{\mathrm{V}l}^\alpha \, \mathrm{d}s \right] \\ & + \sum_m \left[\hat{\Psi}_{\mathrm{S}m}^\alpha - \int_0^t \mathbf{Q}_{\mathrm{S}m}^\alpha : D_s^\alpha \mathbf{\Gamma}_{\mathrm{S}m}^\alpha \, \mathrm{d}s \right], \end{aligned} \tag{193}$$

$$\Psi_\Phi^\alpha = \sum_k \sum_n \left[\hat{\Psi}_{\Phi k,n}^\alpha - \int_0^t \mathbf{Q}_{\Phi k,n}^\alpha : D_s^\alpha \mathbf{\Gamma}_{\Phi k,n}^\alpha \mathrm{d}s \right]. \tag{194}$$

Viscoelastic kinetics are consistent with Eqs. 151–169 and prior works.[36,164,165] This theory is further justified by its need for only two parameters for each mode $(\cdot)_{k,n}^\alpha$: glassy factor β and relaxation time τ. In Section 4.2, this framework depicts compression and tension data well on liver and muscle across a wide range of loading rates.

3.4.3 Active Tension

Internal state variables in $\{\boldsymbol{\xi}^\alpha\}$ are the scalar functions $\{\Delta_k^\alpha\}$ with k the fiber family number. Kinetic equations with initial conditions are imposed directly[31,178,179] rather

than by more sophisticated electrochemical physics[177] outside the present scope:

$$D_t^\alpha\{D_t^\alpha\Delta_k^\alpha\} = \{D_t^\alpha\Delta_k^\alpha\}(\mathbf{X}^\alpha, t), \qquad \{\Delta_k^\alpha\}(\mathbf{X}^\alpha, 0) = \{\Delta_{k0}^\alpha\}(\mathbf{X}^\alpha). \tag{195}$$

Evolution equations in Eq. 195 should implicitly be affected by local states; for example, the history of fiber damage $\{D_k^\alpha\}$, if severe, should limit maximum contractile stress. Conjugate forces in Eq. 113 are the following parts of $\{\boldsymbol{\pi}^\alpha\}$:

$$\{\pi_{\mathrm{A}k}^\alpha\}(\lambda_k^\alpha, \{\Delta_k^\alpha\}) = \varsigma_{\mathrm{F}k}^\alpha \frac{\rho^\alpha}{\rho_{\mathrm{R}0}^\alpha} \frac{\partial}{\partial\{\Delta_k^\alpha\}}[\Lambda_k^\alpha(\lambda_k^\alpha, \{\Delta_k^\alpha\}) + \chi_k^\alpha(\{\Delta_k^\alpha\})]. \tag{196}$$

Dissipation from activation or passivation should be nonnegative, to be ensured by storage-release functions χ_k^α:

$$\mathfrak{D}_{\mathrm{A}}^\alpha = -\sum_k \{\pi_{\mathrm{A}k}^\alpha\} \cdot \{D_t^\alpha\Delta_k^\alpha\} \geq 0. \tag{197}$$

The framework of Eqs. 195–197 is justified by compatibility with Eqs. 128, 170 and 171, and nonnegative dissipation. A specialization in Section 4.2.2 provides validation in the context of experimental data.[31,183]

3.4.4 Damage

From Eqs. 128 and 175, conjugate forces to damage measures for the matrix in $\{\boldsymbol{\pi}^\alpha\}$ and $\{\boldsymbol{\zeta}^\alpha\}$ are

$$\begin{aligned}
\bar{\pi}_{\mathrm{D}}^\alpha &= \rho^\alpha \frac{\partial\psi^\alpha}{\partial\bar{D}^\alpha} = \frac{\rho^\alpha}{\rho_{\mathrm{R}0}^\alpha} \frac{\partial}{\partial\bar{D}^\alpha}[\sqrt{\hat{G}^\alpha}\hat{\Psi}_{\mathrm{D}}^\alpha + \varsigma_{\mathrm{V}}^\alpha\Psi_{\mathrm{V}}^\alpha + \varsigma_{\mathrm{S}}^\alpha(\Psi_{\mathrm{S}}^\alpha + \Psi_\Gamma^\alpha)] \\
&= \frac{\rho^\alpha}{\rho_{\mathrm{R}0}^\alpha}[2\sqrt{\hat{G}^\alpha}\bar{E}_{\mathrm{C}}^\alpha\bar{D}^\alpha + \Psi_{\mathrm{D}}^\alpha \frac{\partial}{\partial\bar{D}^\alpha}\ln\sqrt{\hat{G}^\alpha}] \\
&\quad - \frac{\rho^\alpha}{\rho_{\mathrm{R}0}^\alpha}\bar{\vartheta}^\alpha[1 - \bar{D}^\alpha\mathrm{H}(\ln J^\alpha)]^{\bar{\vartheta}^\alpha - 1}\mathrm{H}(\ln J^\alpha)\Psi_{\mathrm{V}}^\alpha \\
&\quad - \frac{\rho^\alpha}{\rho_{\mathrm{R}0}^\alpha}\bar{\vartheta}^\alpha[1 - \bar{D}^\alpha]^{\bar{\vartheta}^\alpha - 1}(\Psi_{\mathrm{S}}^\alpha + \Psi_\Gamma^\alpha),
\end{aligned} \tag{198}$$

$$\begin{aligned}
\bar{\boldsymbol{\zeta}}_{\mathrm{D}}^\alpha &= \rho^\alpha\mathbf{F}^\alpha \frac{\partial\psi^\alpha}{\partial\nabla_0^\alpha\bar{D}^\alpha} = \frac{\rho^\alpha}{\rho_{\mathrm{R}0}^\alpha}\sqrt{\hat{G}^\alpha}\mathbf{F}^\alpha \frac{\partial\hat{\Psi}_{\mathrm{D}}^\alpha}{\partial\nabla_0\bar{D}^\alpha} \\
&= 2\frac{\rho^\alpha}{\rho_{\mathrm{R}0}^\alpha}\sqrt{\hat{G}^\alpha}\bar{\Upsilon}^\alpha\bar{l}_{\mathrm{R}}^\alpha\mathbf{F}^\alpha[(\nabla\bar{D}^\alpha)\mathbf{F}^\alpha].
\end{aligned} \tag{199}$$

Define the total conjugate force to damage in the matrix:

$$\bar{F}^{\alpha}_{\mathrm{D}} = -\bar{\pi}^{\alpha}_{\mathrm{D}} + \nabla \cdot \bar{\boldsymbol{\zeta}}^{\alpha}_{\mathrm{D}}. \tag{200}$$

Define the viscosity $\bar{\nu}^{\alpha}_{\mathrm{D}} \geq 0$. A Ginzburg–Landau kinetic law[114,148,151,180] and nonnegative dissipation for the matrix in Eq. 113 are, respectively,

$$n^{\alpha}_0 \bar{\nu}^{\alpha}_{\mathrm{D}} D^{\alpha}_t \bar{D}^{\alpha} = \bar{F}^{\alpha}_{\mathrm{D}}, \tag{201}$$

$$\bar{\mathfrak{D}}^{\alpha}_{\mathrm{D}} = \bar{F}^{\alpha}_{\mathrm{D}} D^{\alpha}_t \bar{D}^{\alpha} = n^{\alpha}_0 \bar{\nu}^{\alpha}_{\mathrm{D}} |D^{\alpha}_t \bar{D}^{\alpha}|^2 \geq 0. \tag{202}$$

To render the damage rate always nonnegative, Eq. 201 can be modified to the form $n^{\alpha}_0 \bar{\nu}^{\alpha}_{\mathrm{D}} D^{\alpha}_t \bar{D}^{\alpha} = \bar{F}^{\alpha}_{\mathrm{D}} \mathrm{H}(\bar{F}^{\alpha}_{\mathrm{D}})$. Damage kinetics are suppressed for $\bar{\nu}^{\alpha}_{\mathrm{D}} \to \infty$ and rate-independent for $\bar{\nu}^{\alpha}_{\mathrm{D}} \to 0$ with equilibrium condition $\bar{F}^{\alpha}_{\mathrm{D}} = 0$. For rate insensitivity, irreversibility is enforced by setting $\bar{D}^{\alpha}(t)$ to the maximum of the argument of $\bar{F}^{\alpha}_{\mathrm{D}}(\bar{D}^{\alpha}; \cdot)(t) = 0$ and $\bar{D}^{\alpha}(s) \, \forall \, s < t$, where the latter renders $D^{\alpha}_t \bar{D}^{\alpha}(t^-) \to 0$. Usual, but inessential, initial conditions are $\bar{D}^{\alpha}_0 = 0$.

When $\hat{G}^{\alpha} \to 1$, this theory reduces to Ginzburg–Landau or Allen–Cahn kinetics,[148] justified as standard for phase-field modeling of fracture.[51,151] The nondissipative simplification $\bar{\nu}^{\alpha}_{\mathrm{D}} \to 0$ is popular for quasi-statics.[38,50] The formulation has been used elsewhere for arterial rupture.[37,38] As remarked following Eq. 175, a novelty is the factor $\hat{G}^{\alpha} > 1$, which increases fracture resistance due to microstructure changes associated with remnant strain, for example nonaffine collagen fiber deformations and fibril-matrix sliding.[18] This feature was instrumental for modeling skin tearing.[97] Factors proportional to $\Psi^{\alpha}_{\mathrm{D}}$ in Eq. 198 and later Eq. 203 contribute to dissipation in a similar way as the spherical part of the Eshelby stress, proportional to Helmholtz free energy, in finite plasticity theory[184] and growth mechanics.[185]

Damage in fiber families k is treated analogously. Viscosities are $\nu^{\alpha}_{\mathrm{D}k} \geq 0$. Conjugate thermodynamic forces and dissipative Ginzburg–Landau kinetics are

$$\begin{aligned}
\pi^{\alpha}_{\mathrm{D}k} &= \rho^{\alpha} \frac{\partial \psi^{\alpha}}{\partial D^{\alpha}_k} = \frac{\rho^{\alpha}}{\rho^{\alpha}_{\mathrm{R}0}} \frac{\partial}{\partial D^{\alpha}_k} [\sqrt{\hat{G}^{\alpha}} \hat{\Psi}^{\alpha}_{\mathrm{D}} + \varsigma^{\alpha}_{\mathrm{F}k} (\Psi^{\alpha}_{\mathrm{F}k} + \Psi^{\alpha}_{\Phi k})] \\
&= \frac{\rho^{\alpha}}{\rho^{\alpha}_{\mathrm{R}0}} [2\sqrt{\hat{G}^{\alpha}} E^{\alpha}_{\mathrm{C}k} D^{\alpha}_k + \Psi^{\alpha}_{\mathrm{D}} \frac{\partial}{\partial D^{\alpha}_k} \ln \sqrt{\hat{G}^{\alpha}}] \\
&\qquad - \frac{\rho^{\alpha}}{\rho^{\alpha}_{\mathrm{R}0}} \vartheta^{\alpha}_k [1 - D^{\alpha}_k]^{\vartheta^{\alpha}_k - 1} (\Psi^{\alpha}_{\mathrm{F}k} + \Psi^{\alpha}_{\Phi k}),
\end{aligned} \tag{203}$$

$$\boldsymbol{\zeta}^{\alpha}_{\mathrm{D}k} = \rho^{\alpha}\mathbf{F}^{\alpha}\frac{\partial\psi^{\alpha}}{\partial\nabla^{\alpha}_{0}D^{\alpha}_{k}} = \frac{\rho^{\alpha}}{\rho^{\alpha}_{\mathrm{R}0}}\sqrt{\hat{G}^{\alpha}}\mathbf{F}^{\alpha}\frac{\partial\hat{\Psi}^{\alpha}_{\mathrm{D}}}{\partial\nabla_{0}D^{\alpha}_{k}} = 2\frac{\rho^{\alpha}}{\rho^{\alpha}_{\mathrm{R}0}}\sqrt{\hat{G}^{\alpha}}\Upsilon^{\alpha}_{k}l^{\alpha}_{\mathrm{R}k}\mathbf{F}^{\alpha}[(\nabla D^{\alpha}_{k})\mathbf{F}^{\alpha}], \tag{204}$$

$$\digamma^{\alpha}_{\mathrm{D}k} = -\pi^{\alpha}_{\mathrm{D}k} + \nabla\cdot\boldsymbol{\zeta}^{\alpha}_{\mathrm{D}k}, \tag{205}$$

$$n^{\alpha}_{0}\nu^{\alpha}_{\mathrm{D}k}D^{\alpha}_{t}D^{\alpha}_{k} = \digamma^{\alpha}_{\mathrm{D}k}, \tag{206}$$

$$\mathfrak{D}^{\alpha}_{\mathrm{DF}} = \sum_{k}\mathfrak{D}^{\alpha}_{\mathrm{D}k} = \sum_{k}\digamma^{\alpha}_{\mathrm{D}k}D^{\alpha}_{t}D^{\alpha}_{k} = n^{\alpha}_{0}\sum_{k}\nu^{\alpha}_{\mathrm{D}k}|D^{\alpha}_{t}D^{\alpha}_{k}|^{2} \geq 0. \tag{207}$$

To forbid healing, $n^{\alpha}_{0}\nu^{\alpha}_{\mathrm{D}k}D^{\alpha}_{t}D^{\alpha}_{k} = \digamma^{\alpha}_{\mathrm{D}k}\mathrm{H}(\digamma^{\alpha}_{\mathrm{D}k})$ in lieu of Eq. 206. For rate insensitivity, $\nu^{\alpha}_{\mathrm{D}k} \to 0 \Rightarrow \digamma^{\alpha}_{\mathrm{D}k} = 0$ with possible irreversibility constraints analogous to those for $\bar{D}^{\alpha}(t)$. Usual initial conditions are $D^{\alpha}_{k0} = 0$.

3.4.5 Heat Conduction

Fourier conduction is usually sufficient for each bulk constituent α, with isotropic conductivity $\kappa^{\alpha}_{\theta}(\theta, \{\boldsymbol{\xi}^{\alpha}\}) \geq 0$, often temperature and internal-state dependent. Conductivity could degrade with damage via, for example, $\kappa^{\alpha}_{\theta} \approx \varsigma^{\alpha}_{\mathrm{V}}\kappa^{\alpha}_{\theta 0}$. Heat flux and entropy production are

$$\mathbf{q}^{\alpha} = -n^{\alpha}_{0}\kappa^{\alpha}_{\theta}\nabla\theta^{\alpha}, \qquad \mathfrak{D}^{\alpha}_{\mathrm{q}} = \frac{-\mathbf{q}^{\alpha}\cdot\nabla\theta^{\alpha}}{\theta^{\alpha}} = \frac{n^{\alpha}_{0}\kappa^{\alpha}_{\theta}|\nabla\theta^{\alpha}|^{2}}{\theta^{\alpha}} \geq 0. \tag{208}$$

Such textbook isotropic Fourier conduction has been used elsewhere for soft tissue.[186] Realism may improve with anisotropic conductivity, if measured. Any other model obeying Eq. 93 and $\mathfrak{D}^{\alpha}_{\mathrm{q}} \geq 0$ could be substituted.

3.4.6 Momentum Transfer

Momentum exchange includes Darcy-like contributions[73,84,87] from velocity differences $\boldsymbol{v}^{\alpha} - \boldsymbol{v}^{\beta} = \boldsymbol{\mu}^{\alpha} - \boldsymbol{\mu}^{\beta}$ and mass exchange to satisfy Eq. 65:

$$\mathbf{h}^{\alpha} = -\sum_{\beta}[\lambda^{\alpha\beta}(\boldsymbol{\mu}^{\alpha} - \boldsymbol{\mu}^{\beta})] - \hat{c}^{\alpha}\boldsymbol{\mu}^{\alpha}. \tag{209}$$

The inverse hydraulic-type conductivity matrix is $\lambda^{\alpha\beta} = \lambda^{\beta\alpha}$. Summing Eq. 209 over α, total contributions to linear momentum from the first sum on the right of Eq. 209 vanish, producing Eq. 65, consistent with Bowen[67] and the mixture momentum balance in the second of Eq. 67. Forces $\mathbf{h}^{\alpha}$ do not necessarily sum to zero if mass supplies $\hat{c}^{\alpha}$ are nonzero. Entries $\lambda^{\alpha\beta} \geq 0$ can depend on temperature and volume of each phase (e.g., to account for changes in interphase viscosity with tem-

perature and in permeability with porosity[73]) and degrade with damage[75,76]:

$$\lambda^{\alpha\beta}(J^\alpha, J^\beta, \theta^\alpha, \theta^\beta, \bar{D}^\alpha, \bar{D}^\beta) = \bar{\lambda}^{\alpha\beta}(J^\alpha, J^\beta, \theta^\alpha, \theta^\beta)\sqrt{\varsigma_{\mathrm{V}}^\alpha \varsigma_{\mathrm{V}}^\beta}. \tag{210}$$

The form of Eq. 209 is justified as follows. As discussed by Bowen,[67,118] $\mathbf{h}^\alpha$ must be an odd function of phase velocity differences and conserve total momentum per Eq. 65. The first sum, linear in velocity differences, is a simple expression that fulfills the first requirement. The second sum in Eq. 209 is the simplest that can enforce the second requirement. Higher-order (e.g., cubic) terms could be added at the expense of more parameters. Only the linear terms affect weak-shock solutions derived in Section 4.3.3. In the absence of mass supplies, Eq. 209 is standard for poromechanics, including applications to biology.[72,74,87]

3.4.7 Energy Transfer

Energy exchange includes heat transfer from temperature differences $\theta^\alpha - \theta^\beta$ as well as momentum and mass exchange terms to satisfy Eq. 66:

$$\epsilon^\alpha = -\sum_\beta [\omega^{\alpha\beta}(\theta^\alpha - \theta^\beta)] - m^\alpha \sum_\beta \mathbf{h}^\beta \cdot \boldsymbol{\mu}^\beta - m^\alpha \sum_\beta \hat{c}^\beta (u^\beta + \tfrac{1}{2}|\boldsymbol{\mu}^\beta|^2), \tag{211}$$

recalling mass concentration $m^\alpha = \rho^\alpha/\rho$ from Eq. 87. The matrix of heat transfer coefficients $\omega^{\alpha\beta} = \omega^{\beta\alpha} \geq 0$ can depend on state variables and damage[76] like Eq. 210:

$$\omega^{\alpha\beta}(J^\alpha, J^\beta, \theta^\alpha, \theta^\beta, \bar{D}^\alpha, \bar{D}^\beta) = \bar{\omega}^{\alpha\beta}(J^\alpha, J^\beta, \theta^\alpha, \theta^\beta)\sqrt{\varsigma_{\mathrm{V}}^\alpha \varsigma_{\mathrm{V}}^\beta}. \tag{212}$$

In compression, contact among fully broken constituents permits momentum and heat transfer in respective Eqs. 210 and 212 even if $\bar{D}^\alpha \to 1$ or $\bar{D}^\beta \to 1$. Damage dependence differing from basic illustrations in Eqs. 210 and 212, for example as seen in other references merging poromechanics and phase-field mechanics,[75,76] can be substituted if found more appropriate. The form of Eq. 211 is motivated as follows. The linear term in temperature differences is standard for heat exchange in soft tissues.[186,187] The second and third sums are simple additions that can be used to satisfy mixture energy conservation in Eqs. 66 and 68. These are even functions of velocities per known thermodynamic restrictions.[67,118]

3.4.8 Mass Transfer

Terms $\hat{c}^\alpha$ sum to zero in Eq. 65; these account for mass transfer rates between constituents. In biology, such terms could originate from growth and remodeling, for example, exchange of nutrients dissolved in a fluid phase to support growth of new solid tissue. Detailed constitutive equations for $\hat{c}^\alpha$ are beyond the present scope. Thermodynamic constraints emerge from Eq. 106 with Eq. 209 and logical stipulation that the rightmost two sums in Eq. 106 should be nonnegative in concert:

$$\begin{aligned}\sum_\alpha \left[\frac{\epsilon^\alpha}{\theta^\alpha} + c^\alpha \eta^\alpha\right] = &\sum_\alpha \sum_\beta \frac{\omega^{\alpha\beta}(\theta^\alpha - \theta^\beta)^2}{2\theta^\alpha\theta^\beta} \\ &+ \sum_\alpha \frac{m^\alpha}{2\theta^\alpha} \sum_\beta \lambda^{\alpha\beta} |\boldsymbol{\mu}^\alpha - \boldsymbol{\mu}^\beta|^2 \\ &+ \sum_\alpha \frac{m^\alpha}{\theta^\alpha} \sum_\beta \hat{c}^\beta \left[\frac{|\boldsymbol{\mu}^\beta|^2}{2} - u^\beta\right] \\ &+ \sum_\alpha \hat{c}^\alpha \eta^\alpha + \rho\eta\, \partial_t \ln\sqrt{g} \geq 0. \end{aligned} \tag{213}$$

The first two double sums in Eq. 213 are always nonnegative. When all $\epsilon^\alpha = 0$ and $\hat{c}^\alpha = 0$ (i.e., no phase interactions), Eq. 213 becomes, with Eq. 117, $\eta\, \partial_t \hat{g} \geq 0$. Then when $\rho\eta = \sum_\alpha \rho^\alpha \eta^\alpha > 0$, the thermodynamic consequence implies that the generalized metric $\hat{\mathbf{g}}$ should only be dilating, not contracting, to ensure unconditionally nonnegative entropy production in this special scenario. This is consistent with nonnegative remnant strains from matrix and fiber degradation in Section 3.3.

Differentiating Eq. 87 in conjunction with use of Eqs. 16, 57, 58, and 65 relates rates of mass concentration m^α to $\hat{c}^\alpha$ as shown by Bowen[67]:

$$\hat{c}^\alpha = \rho \dot{m}^\alpha + \nabla \cdot (\rho^\alpha \boldsymbol{\mu}^\alpha), \qquad \sum_\alpha \dot{m}^\alpha = 0. \tag{214}$$

Kinetic equations for $\dot{m}^\alpha$ or $D_t^\alpha m^\alpha$ could be prescribed in lieu of $\hat{c}^\alpha$. Detailed constitutive equations for growth and remodeling are beyond the present scope. Examples for soft tissues respecting mass conservation and thermodynamics can be found in recent references.[146,188,189]

The Allen–Cahn equation has been used for kinetics of remodeling processes that do not affect mass density.[86] This equation, in bare form, is likely unsuitable for $\dot{m}^\alpha$ and $\hat{c}^\alpha$ since it need not respect Eqs. 65, 213, and 214. A variation on the

Cahn–Hilliard equation with source term $\hat{c}^\alpha$ might be admitted for $\dot{m}^\alpha$ by allowing energy density to depend on mass concentration and concentration gradients[190] and accounting for work of the latter in the energy balance.[148] The Cahn–Hilliard equation is classically used to simulate spinodal decomposition.[191] The current theory is unable to predict spinodal decomposition; aforementioned adaptations could permit this, but spontaneous agglomeration of phases might not be realistic for tissues, depending on their microstructures.

3.5 Summary

The total Cauchy stress tensor $\boldsymbol{\sigma}^\alpha$ for constituent α is the sum of Eqs. 174 and 188. The total stress tensor for the mixture $\boldsymbol{\sigma}$ is Eq. 60.

The total constituent dissipation $\mathfrak{D}^\alpha$ entering Eq. 113 is the sum of Eqs. 189, 192, 197, 202, 207, and 208, each individually nonnegative:

$$\mathfrak{D}^\alpha - (\mathbf{q}^\alpha \cdot \nabla\theta^\alpha)/\theta^\alpha = \hat{\mathfrak{D}}^\alpha + \mathfrak{D}^\alpha_\Gamma + \mathfrak{D}^\alpha_\mathrm{A} + \bar{\mathfrak{D}}^\alpha_\mathrm{D} + \mathfrak{D}^\alpha_\mathrm{DF} + \mathfrak{D}^\alpha_\mathrm{q} \geq 0. \tag{215}$$

The total dissipation inequality of Eq. 106 is then

$$\sum_\alpha \left[\frac{\mathfrak{D}^\alpha + \mathfrak{D}^\alpha_\mathrm{q}}{\theta^\alpha}\right] + \sum_\alpha \left[\frac{\epsilon^\alpha}{\theta^\alpha} + c^\alpha \eta^\alpha\right] \geq 0. \tag{216}$$

From Eq. 15, boundary conditions are required for each constituent $\alpha = 1, \ldots, N$. Mechanical conditions are prescribed histories of traction $\mathbf{t}^\alpha$ or velocity $\boldsymbol{v}^\alpha$ on $\partial\Omega$. Thermal conditions are histories of flux q^α_n or temperature θ^α on $\partial\Omega$. For internal variables $\{\boldsymbol{\xi}^\alpha\}$ with gradient energetic dependence (e.g., order parameters for damage), histories of fluxes $\{\mathbf{z}^\alpha\} = (\rho^\alpha \partial\psi^\alpha/\partial\{\nabla\boldsymbol{\xi}\}^\alpha) \cdot \mathbf{n}$ or conjugate rates $D^\alpha_t \boldsymbol{\xi}^\alpha$ are needed on $\partial\Omega$. Histories of body force $\mathbf{b}^\alpha$ and heat source r^α are prescribed over Ω.

The constitutive framework of Section 3 is now summarized. The mixture consists of one or more coexisting phases $\alpha = 1, \ldots, N$. The total free and internal energies of each constituent α are Eqs. 128 and 129. A single phase can include any or all of the following features: EOS (ideal gas or condensed matter), matrix elasticity, fiber elasticity, matrix viscoelasticity, fiber viscoelasticity, active fiber tension, damage (fluid cavitation, matrix and/or fiber fractures), non-Euclidean (e.g., Finsler or Riemannian) metric tensor contribution, Newtonian viscosity, and Fourier conduction. When $N > 1$, the material is further described by momentum, energy, and mass

exchanges among (all) phases.

Typically, as is in Section 4, a subset of features is sufficient to describe a real biologic material over a given loading regime. For example, an EOS is all that is needed for modeling the shock Hugoniot of isolated fluids. Active tension is intended for muscle contraction and is not relevant for passive constituents. In all applications of Section 4, $\hat{c}^\alpha = 0 \forall\, \alpha = 1, \ldots, N$ is imposed since growth and remodeling usually require much longer time scales than the prescribed loading durations.[166]

Governing equations of Section 2 and constitutive theory of Section 3 are used for all applications in Section 4. No new theories or models are introduced, only material parameters and specialized forms of some equations of Sections 2 and 3.

4. Soft Tissue Physics

4.1 Shock Hugoniot Response

4.1.1 Fluids

The theory is first exercised for three fluids that comprise the majority of soft tissues: water, extracellular fluid (ECF, representative of blood plasma[3] and interstitial fluid in skeletal muscle and skin), and whole blood, the latter with a realistic hematocrit of 0.4. Shock responses are modeled via theory of Section 2.3 with each fluid a single-phase material ($\alpha = N = 1$, superscript henceforth suppressed). Planar (1-D) impact is along the $x = x^1$ direction. Fluid is quiescent upstream, at density ρ_0, temperature θ_0, and ambient pressure $p_0 = p_{\mathrm{R}0} = 1$ atm.

Eulerian and Lagrangian shock speeds are identical, labeled $\mathcal{U}$. Particle velocity in Hugoniot states is $v^- = v$. In Hugoniot (i.e., downstream shocked) $(\cdot)^-$ states,

$$\rho = \rho_0/J, \qquad J = F^1_1 = F = \partial\chi/\partial X, \tag{217}$$

$$u = U/\rho_0, \qquad t_1 = \sigma^1_1 = -P = -p, \tag{218}$$

where U is energy per unit reference volume and P is longitudinal Cauchy stress, positive in compression. Since volume fraction $n^1_0 = n^1 = 1$, $\rho_{\mathrm{R}0} = \rho_0$, and $\rho_{\mathrm{R}} = \rho$.

To calculate the material response, J is decremented from unity. For each decrement, the constitutive model, here the condensed matter EOS for U_{V} and p_{V} in

Eqs. 139–141, is solved concurrently with the Hugoniot energy balance in Eq. 44 for P and η. With macroscopically adiabatic conditions assumed and $\{z\} = 0$, the latter reduces to

$$U = \tfrac{1}{2}(P + p_0)(1 - J), \tag{219}$$

since $U_0 = 0$ and $J = 1$ upstream. Then υ, $\mathcal{U}$, and θ are found from Eqs. 42 and 142. For single-phase materials, $\boldsymbol{\mu}^\alpha = \mathbf{0}$, $\mathbf{h}^\alpha = \mathbf{0}$, $\epsilon^\alpha = 0$, and here $\hat{c}^\alpha = 0$. For compression, fluid cavitation is omitted, so no damage is modeled. Hence, all metrics reduce to their trivial Euclidean (i.e., unit) values: $g = G = \hat{g} = \hat{G} = 1$.

Table 1 Physical properties or model parameters for water, ECF, human blood, and porcine skeletal muscle (cells and matrix, $\alpha = k = 1$, vol. fract. $n_0^1 = 0.9$)

Property (units)	Water	ECF	Human blood	Porcine muscle
$\rho_{\mathrm{R}0}^\alpha$ (g/cm^3)	1.00	1.03	1.06	1.10
B_η^α (GPa)	2.10	2.20	2.64	3.28
c_ϵ^α (J/g K)	4.15	3.96	3.58	3.25
γ_0^α (-)	0.120	0.132	0.160	0.313
$B_{\eta\mathrm{p}}^\alpha$ (-)	6.96	6.96	12.0	8.0
k_{V}^α (-)	7.0	7.0	0.0	6.0
$\hat{B}^\alpha$ (mPa s)	2.1	...	...	...
$\hat{\mu}^\alpha$ (mPa s)	0.8	1.2	5.0	...
μ_{S}^α (kPa)	...	...	...	1.0
μ_k^α (kPa)	...	...	...	1.0
k_k^α (-)	...	...	...	10.0
$\beta_{\mathrm{S}}^\alpha$ (-)	...	...	...	1.0×10^5
$\beta_{\Phi k}^\alpha$ (-)	...	...	...	1.0×10^5
J_{C} (kJ/m^2)	...	...	...	0.84
l^α (mm)	...	...	...	0.88
ϑ^α (-)	...	...	...	2.0
$\epsilon_{\mathrm{r}}^\alpha$ (-)	...	...	...	0.2
$\bar{r}^\alpha = \tilde{r}_k^\alpha$ (-)	...	...	...	2.0

Properties entering the EOS are listed in Table 1. All are obtained or estimated from experimental literature[3,182,192–195] with the exception of nonlinear bulk stiffening parameters $B_{\eta\mathrm{p}}$ and k_{V} that are fit to the experimental Hugoniot data. The ambient bulk modulus is related to the bulk sound velocity via

$$c_{\mathrm{B}} = \sqrt{(B_\eta + p_0)/\rho_0}. \tag{220}$$

For water, the usual relationship $B_{\eta\mathrm{p}} = 4S - 1$ is used, where S is the slope of

a linear fit to the $\mathcal{U}$-υ Hugoniot.[121] Since shock compression data are apparently unavailable for ECF, $B_{\eta\mathrm{p}}$ and k_{V} for water are assigned. Newtonian viscosities $\hat{B}, \hat{\mu}$ are listed for completeness,[3,182] where $\hat{\mu}$ for blood is that estimated for strain high rates[3] and bulk viscosity is supplied only for water.[182] These do not enter the present analysis: Newtonian viscosity in Eq. 188 and Fourier conduction in Eq. 208 are necessarily omitted as both are incompatible with treatment of shocks as singular surfaces.[196,197]

Compared in Fig. 1a are P-ρ Hugoniot predictions and experimental data on water[193] ($\theta_0 = 297$ K) and human blood[198] ($\theta_0 \approx 310$ K). Shock data on ECF do not seem to exist; predictions are for $\theta_0 = 310$ K. Compared in Fig. 1b are $\mathcal{U}$-υ data for water[193] and predictions for all three fluids. Shock velocity data were not reported for blood in Nagoya et al.[198] The c_{B} value for blood, $\mathcal{U} \to c_{\mathrm{B}}$ as $\upsilon \to 0$, is from Jones et al.[195]

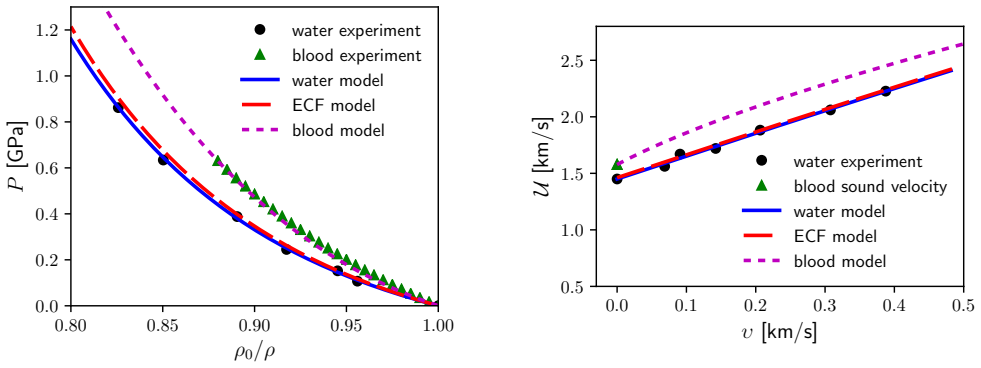

(a) shock pressure vs. density

(b) shock velocity vs. particle velocity

Fig. 1 Model results and shock data[193,198] for (a) Hugoniot stress vs. mass density and (b) shock velocity vs. particle velocity in water, ECF, and human blood.

Results in Fig. 1 confirm validity of the EOS for water and blood. The latter is stiffer than ECF, which is stiffer than water. Only two fitting parameters are needed. Neither vaporization nor solidification are addressed; the EOS would need substantial modification to account for latent heat and differing properties of phases. Temperature rise predicted at 20% compression is on the order of 20 K, by which water should remain in its liquid phase according to its P-θ phase diagram.[193] Solid-liquid-gas phase diagrams of ECF and blood appear to be unknown at high pressures, but neither experiments nor the EOS reported by Nagoya et al.[198] indicate any phase transition occurs.

4.1.2 Skeletal Muscle

The planar shock response of skeletal muscle is predicted next. Properties and loading conditions replicate impact experiments of Wilgeroth et al.[6,88] on porcine muscle tissue. The material is modeled as a mixture of two coexisting phases ($\alpha = 1, 2$): a "solid" tissue of initial volume fraction[199] $n_0^1 = 0.9$ and an interstitial fluid depicted by the ECF, comprising remaining fraction $n_0^2 = 0.1$. The first phase consists of the muscle cells (i.e., fibers), collagenous connective tissues, and ground substance between and encasing the cells (i.e., the extracellular matrix). Muscle cells contain significant internal fluid whose physical properties are included implicitly in the constitutive model for the first phase.

Experiments[88] show a single-wave structure with steep shock front (rise time on the order of μs or smaller) rather than multiple wave forms that would be expected if shock and particle velocities among the phases differed significantly.[87,118] This suggests inverse hydraulic conductivity is very large (e.g., $\lambda^{\alpha\beta} \tilde{\to} \infty$) at these high-pressure dynamic conditions, and diffusion velocities $\boldsymbol{\mu}^\alpha$ are negligible. It is thus assumed that particle velocity histories match in each phase: $v^\alpha(x,t) = v^1(x,t) = v^2(x,t) = v(x,t)$. Therefore, $J(x,t) = F(x,t) = \partial\chi/\partial X$ is identical in each constituent. Microsecond scales are too brief for biologic mass exchange: $\hat{c}^\alpha = 0$. Shock compression is adiabatic: $q^\alpha \to 0$. Heat transfer in ϵ^α of Eq. 211 is likewise assumed null in Hugoniot states: $\theta^\alpha = \theta^1 = \theta^2 = \theta$. Coincident velocities and temperatures have been used elsewhere in constrained mixture theories.[145,146,188,189]

The solution procedure is similar to that for single fluids, but the constitutive model is now much more complex. The shock response is that of the mixture, where governing and jump equations are in Eqs. 72–80. Both phases are quiescent and at reference $\theta_0 = 310$ K and $p_{\mathrm{R}0} = 1$ atm upstream; θ_0 was unreported in Wilgeroth et al.,[88] but model results are insensitive to θ_0.

From Eqs. 60 and 61 with $\boldsymbol{\mu}^\alpha = \mathbf{0}$, mixture stress and internal energy are

$$\boldsymbol{\sigma} = \sum_\alpha \boldsymbol{\sigma}^\alpha, \qquad U = \sum_\alpha n_0^\alpha \rho_{\mathrm{R}0}^\alpha u^\alpha = \sum_\alpha n_0^\alpha U^\alpha. \tag{221}$$

Because all phases deform equally without mass exchange, mixture density is $\rho = \rho_0/J$. As explained later in the context of Eq. 226, $\{\mathbf{z}^\alpha\} \to \{z^\alpha\} = 0$. The analog of Eq. 44 for the mixture reduces to Eq. 219 with $U_0 = 0$ and $p_0 = \sum_\alpha n_0^\alpha p_{\mathrm{R}0}^\alpha$.

In calculations, J is reduced incrementally from unity. In each decrement, energy equation Eq. 219 and constitutive equations for each phase are solved simultaneously and summed, if appropriate, to give mixture values P, U, and θ. Given θ and J, entropy η^α of each phase is found by inversion of Eq. 142. Particle and shock velocities are found from mixture analogs of Eq. 42. The response of the fluid phase (ECF, $\alpha = 2$) is calculated as before; its energy and pressure contributions are given fully by $U^\alpha_{\rm V}$ and $p^\alpha_{\rm V}$.

The tissue phase (including intracellular fluids), $\alpha = 1$, has a total internal energy per unit reference volume U^α:

$$U^1 = U^1_{\rm V} + \varsigma^1_{\rm S} \cdot (U^1_{\rm S} + U^1_\Gamma) + \varsigma^1_{\rm F} \circ (U^1_{\rm F} + U^1_\Phi) + U^1_{\rm D}. \tag{222}$$

The first term on the right is the EOS (noting $\varsigma_{\rm V} = 1$ for compression), the second and third are deviatoric matrix elasticity and viscoelasticity, the third and fourth are deviatoric fiber elasticity and viscoelasticity, and the last is surface energy of soft-tissue degradation (i.e., damage). Only passive states are modeled: $U^1_{\rm A} = 0$. Thermal variables θ^1 and η^1 only enter $U^1_{\rm V}$, which fully specifies the partial pressure $p^\alpha \to p^1$. Notation U and Ψ is interchangeable for remaining terms that only affect deviatoric response.

Matrix viscoelasticity is limited to the shear response, following typical assumptions for nearly incompressible soft materials.[27,164,165] For very rapid loading modeled here, viscous relaxation for all (m) configurational variables $\mathbf{\Gamma}^1_{{\rm S}m}$ is assumed negligible with $t/\tau^1_{{\rm S}m} \to 0$, so

$$U^1_{\rm S} + U^1_\Gamma \to U^1_{\rm S} + \sum_m \hat\Psi^1_{{\rm S}m} = U^1_{\rm S}(1 + \sum_m \beta^1_{{\rm S}m}). \tag{223}$$

Thus, $\breve\mu^1_{\rm S} = \mu^1_{\rm S}(1 + \sum_m \beta^1_{{\rm S}m})$ is the glassy shear modulus of the matrix, with static energy and modulus in Eq. 145.

Muscle fibers comprise one family, $k = 1$, of direction $\boldsymbol{\iota}^\alpha_k = \boldsymbol{\iota}$ with $\kappa^1_1 = 0$ in Eq. 147. Viscous relaxation for all (n) configurational variables $\mathbf{\Gamma}^1_{\Phi k,n}$ is assumed negligible:

$$U^1_{\rm F} + U^1_\Phi \to U^1_{\rm F} + \sum_n \hat\Psi^1_{\Phi 1,n} = U^1_{\rm F}(1 + \sum_n \beta^1_{\Phi 1,n}). \tag{224}$$

Static strain energy of fibers $U^1_{\rm F}$ is Eq. 149 with $\mu^\alpha_k = \mu^1_1$ and $\mathrm{H}(\cdot)$ omitted. The latter allows fibers to support compressive stress, considered a physically realistic assumption given the confinement of uniaxial strain. A dynamic fiber modulus is

$$\check{\mu}^1_1 = \mu^1_1(1 + \sum_n \beta^1_{\Phi 1,n}). \tag{225}$$

Fiber directions relative to $x = x^1$ are ambiguous in Wilgeroth et al.[88] Calculations apply loading parallel or transverse to $\boldsymbol{\iota}$, both pure mode directions. In the former, the longitudinal sound speed $\mathcal{C}$ obeys $\rho_0\mathcal{C}^2 = B_\eta + p_0 + \frac{4}{3}n^1_0(\check{\mu}^1_{\rm S} + \frac{2}{3}\check{\mu}^1_1)$. In the latter, $\rho_0\mathcal{C}^2 = B_\eta + p_0 + \frac{4}{3}n^1_0(\check{\mu}^1_{\rm S} - \frac{1}{3}\check{\mu}^1_1)$.

Damage order parameters for the matrix, $\bar{D}^\alpha = \bar{D}^1 = \bar{D} \in [0,1]$, and fibers, $D^\alpha_k = D^1_1 = D_1 \in [0,1]$, degrade respective deviatoric stress contributions from matrix and fibers in Eq. 174. They also supply surface energy $U^1_{\rm D} = \Psi^1_{\rm D}$ in Eq. 175.

Jumps in $\bar{D}$ and D_k are allowed across the shock front. This necessitates $\bar{\alpha}^\alpha = \alpha^\alpha_k = 0 \Rightarrow \bar{l}^\alpha_{\rm R} = l^\alpha_{{\rm R}k} = 0$ in Eq. 175 to avoid infinite energy in the front. Gradient energies and conjugate forces $\bar{\boldsymbol{\zeta}}^\alpha_{\rm D}$ and $\boldsymbol{\zeta}^\alpha_{{\rm D}k}$ vanish identically, as do $\{\mathbf{z}^\alpha\}$. Treatment of shocks as singular surfaces mandates viscosities $\bar{\nu}^\alpha_{\rm D} = \nu^\alpha_{{\rm D}k} = 0$ for fracture to avoid infinite dissipation in the shock front if $\bar{D}$ and D_k are discontinuous across the front.

Kinetic laws for fractures of the matrix in Eq. 201 and of the fibers in Eq. 206 therefore reduce as follows, with $\bar{\pi}^\alpha_{\rm D}$ and $\pi^\alpha_{{\rm D}k}$ defined in Eqs. 198 and 203:

$$\bar{\pi}^1_{\rm D} = 0, \qquad \pi^1_{\rm D1} = 0. \tag{226}$$

For each decrement of J, Eq. 226 is solved simultaneously for $\bar{D}$ and D_1, affecting P and U in the Hugoniot energy balance of Eq. 219.

Because damage can be nonzero, the generalized Finsler metrics of Section 3.3 are nontrivial. Here, $\bar{g}_{ij} = \delta_{ij}, \bar{G}^\alpha_{IJ} = \delta_{IJ}$, with $\hat{g}^i_j$ and $(\hat{G}^\alpha)^I_J$ in Eqs. 180–184. Isotropic matrix damage furnishes Eq. 182, and anisotropic fiber damage supplies Eq. 184. Determinants of metric tensors and their derivatives, Eqs. 186 and 187, enter Eqs. 175 and 226. For the present loading and material symmetries, with Eq. 180, $\hat{g}^i_j$ and $(\hat{G}^\alpha)^I_J$ do not affect J or $\mathrm{tr}\,\tilde{\mathbf{C}}$. Finsler or osculating Riemannian metrics enter the analysis only through Eqs. 175 and 226.

Properties for the ECF and tissue phase used in calculations are in Table 1. Experimental data on hydrated muscle (e.g., Wilgeroth et al.[88]) furnish properties of the mixture as a whole, but not the isolated $\alpha = 1$ phase. Given Eq. 221, the mixture density, isentropic bulk modulus, bulk sound speed, volumetric thermal expansion coefficient, specific heat, and Grüneisen parameter are, respectively,

$$\rho_0 = \sum_\alpha n_0^\alpha \rho_{\mathrm{R}0}^\alpha, \qquad B_\eta = \sum_\alpha n_0^\alpha B_\eta^\alpha, \tag{227}$$

$$c_{\mathrm{B}} = \sqrt{(B_\eta + p_0)/\rho_0}, \qquad A = \sum_\alpha n_0^\alpha A^\alpha, \tag{228}$$

$$\rho_0 c_{\mathrm{p}} = \sum_\alpha n_0^\alpha \rho_{\mathrm{R}0}^\alpha c_{\mathrm{p}}^\alpha = \rho_0 c_\epsilon (1 + A\gamma_0\theta_0), \tag{229}$$

$$\gamma_0 = AB_\eta/(\rho_0 c_{\mathrm{p}}) = AB_\theta/(\rho_0 c_\epsilon), \tag{230}$$

where c_{p}^α is specific heat at constant pressure of phase α. Given properties of the mixture[88,195] and ECF ($\alpha = 2$), Eqs. 227–230 are inverted and solved for thermoelastic properties of the tissue phase ($\alpha = 1$). Ultimately, experimental values[88] of ρ_0 and c_{B} yield tissue density and bulk modulus. Nonlinear bulk stiffening parameters $B_{\eta\mathrm{p}}^1$ and k_{V}^1 are fit to the shock Hugoniot data.[88]

Not all static and dynamic shear properties can be fully established from Wilgeroth et al.,[88] so order-of-magnitude estimates are used based on literature values for skeletal, and in some cases cardiac, muscle.[16,27,31,178,200,201] A standard scalar measure[121] of shear stress τ of the mixture for uniaxial shock compression is the first of

$$\tau = \tfrac{3}{4}(P - p); \qquad \tau = -\tfrac{3}{4}\sum_\alpha [(\sigma^\alpha)_1^1 + p^\alpha]. \tag{231}$$

If a material is isotropic, then τ is half the von Mises stress under uniaxial strain.[202] The second expression in Eq. 231 specializes the first. Both phases $\alpha = 1, 2$ contribute to p via each EOS; only the tissue phase contributes to τ via deviatoric matrix and fiber, elastic and viscoelastic, stresses. Low-rate data[16,27,31,178,200,201] suggest that μ_{S}^1 and μ_1^1 should be in the kPa range, with fiber exponential stiffening k_1^1 approximated on the order of 10.

Define the following sums of glassy viscoelastic stiffening factors:

$$\beta_{\mathrm{S}}^{1} = \sum_{m} \beta_{\mathrm{S}m}^{1}, \qquad \beta_{\Phi 1}^{1} = \sum_{n} \beta_{\Phi 1,n}^{1}. \tag{232}$$

Low- to moderate-rate data on cardiac tissue[27] suggest values of these factors near 10^3. Dynamic compression data on porcine muscle[200] show von Mises stresses in the MPa range at strain rates on the order of 10^3/s. Extrapolating, τ is anticipated up to the order of 10 MPa for *strong* shock loading, where strain rates are on the order of 10^5/s given rise times[88] under 1 μs. Accordingly, β_{S}^{1} and $\beta_{\Phi 1}^{1}$ are both estimated here for strong shock compression to be 10^5, probing very high-frequency modes.

For fracture cohesive energy in Eq. 175, the usual phase-field description is invoked for matrix and fibers:

$$\bar{E}_{\mathrm{C}}^{1} = \bar{\Upsilon}^{1}/\bar{l}^{1} = \bar{\mathsf{J}}_{\mathrm{C}}^{1}/(2\bar{l}^{1}), \qquad E_{\mathrm{C}1}^{1} = \Upsilon_{1}^{1}/l_{1} = \mathsf{J}_{\mathrm{C}1}^{1}/(2l_{1}^{1}). \tag{233}$$

Toughness J_{C} of muscle is known only for the whole tissue,[203] so here the simplest physical choice is used:

$$n_{0}^{1}\bar{\mathsf{J}}_{\mathrm{C}}^{1} = n_{0}^{1}\mathsf{J}_{\mathrm{C}1}^{1} = \frac{1}{2}\mathsf{J}_{\mathrm{C}}. \tag{234}$$

Similarly, length constants for each mechanism are both set equal to a value calibrated later for modeling tensile damage: $\bar{l}^{1} = l_{1}^{1} = l^{1}$, on the order of 10-15 single-fiber diameters.[88] Values are about $20\times$ those used elsewhere for modeling skin.[97] Standard[38,97] phase-field choices $\bar{\vartheta}^{1} = \vartheta_{1}^{1} = \vartheta^{1} = 2$ are used for degradation functions of Eqs. 172 and 173.

Regarding generalized Finsler metrics, $\bar{r}^{1} = \tilde{r}_{1}^{1} = 2$ is adopted from prior work on skin,[97] and remanent microstructure strain factors are set equal: $\bar{\epsilon}^{1} = n_{0}^{1}\bar{\kappa}^{1}/\bar{r}^{1} = \tilde{\epsilon}_{1}^{1} = n_{0}^{1}\tilde{\kappa}_{1}^{1}/\tilde{r}_{1}^{1} = \epsilon_{\mathrm{r}}^{1}$. Experimental data on vascular tissue[204] furnish $\epsilon_{\mathrm{r}}^{1} = 0.2$, set positive (dilative) here, as in other soft tissues.[25,97] Under uniaxial-stress compression,[204] axial shortening is overcompensated by radial and circumferential expansion: the arterial wall tissue is residually stretched. Arterial data[204] suggest $\epsilon_{\mathrm{r}}^{1}$ is higher (lower) for tissues with more collagen (less elastin), but experimental data on skeletal muscle components do not exist to substantiate different choices of $\epsilon_{\mathrm{r}}^{1}$ for matrix and fibers.

Figures 2 and 3 report model predictions for the Hugoniot response of porcine skeletal muscle. Shown in Fig. 2a for skeletal muscle is mixture Hugoniot stress P versus mixture density ratio ρ/ρ_0. Experimental data on muscle,[88] blood,[198] and water[193] are shown for comparison, along with model predictions for the ECF in isolation. The mixture theory captures most of the shock data well, exceptions being several anomalous points in the domain $\rho_0/\rho \in [0.82, 0.87]$. Similar statements apply for mixture $\mathcal{U}$ versus v data[88] and model results in Fig. 2b. Muscle is stiffer than blood, ECF, and water. Hugoniot θ predictions in Fig. 2c show a substantial temperature rise, with higher temperatures in muscle than ECF in isolation. This could cause burn damage or other structural changes, not modeled here. Crystal structure and properties of collagen immersed in water exhibit changes[205] at temperatures above 335 K, far exceeded in predictions of Fig. 2c for muscle.

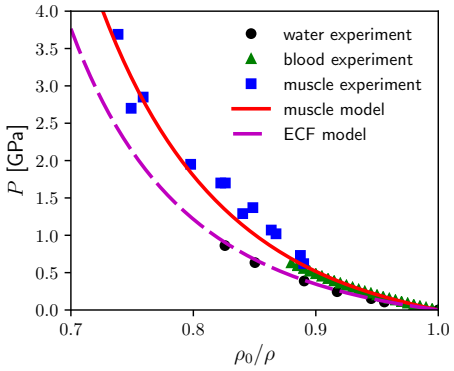

(a) shock pressure vs. density

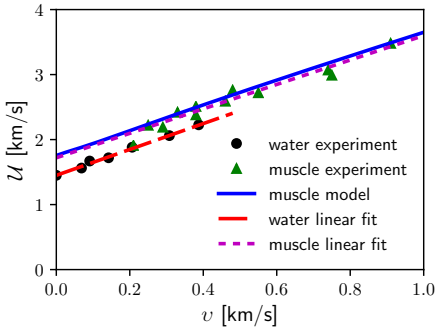

(b) shock velocity vs. particle velocity

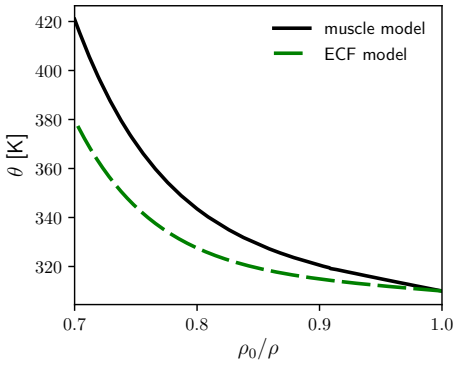

(c) temperature vs. density

Fig. 2 Model results and/or shock compression data for (a) Hugoniot stress vs. mass density, (b) shock velocity vs. particle velocity, and (c) temperature vs. mass density. Data in (a,b) are for water,[193] human blood,[198] and porcine skeletal muscle.[88]

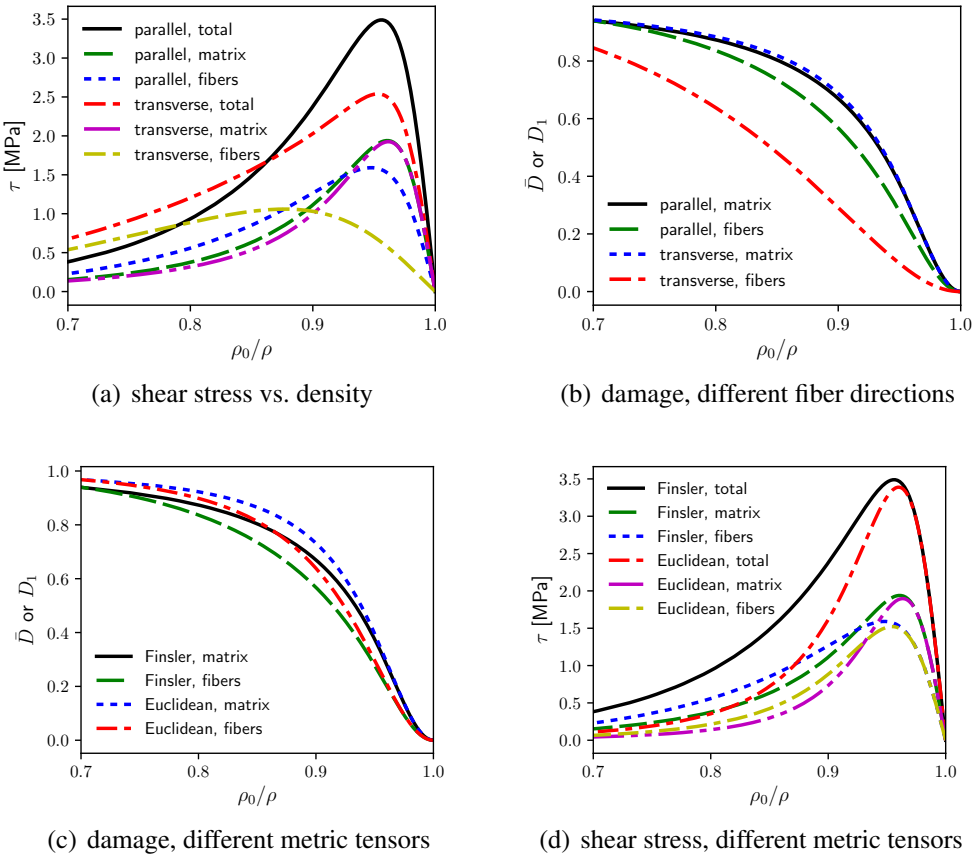

(a) shear stress vs. density

(b) damage, different fiber directions

(c) damage, different metric tensors

(d) shear stress, different metric tensors

Fig. 3 Theoretical predictions for parallel and transverse fiber orientations and Finsler metrics: (a) shear stress vs. mass density and (b) damage. Model results for Finsler and Euclidean metrics and parallel orientation: (c) damage and (d) shear stress.

Results in Fig. 2 are for shock compression parallel to the fiber direction $\boldsymbol{\iota}$. Shear stress of the mixture (supplied only by the tissue phase) τ is predicted in Fig. 3a for tissue shocked parallel and transverse to the fiber direction. Contributions of matrix and fiber deviatoric stresses are delineated; these simply sum to give τ.

For parallel compression, matrix and fibers contribute similarly in magnitude. For transverse compression, fibers support less load, and τ is lower. In both arrangements, τ is at most on the order of $10^{-2}P$, so orientation does not discernibly influence the Hugoniot stress that is dominated by $p = P - \frac{4}{3}\tau$. For $\rho_0/\rho \lesssim 0.95$, damage in matrix and fibers causes a reduction in strength, leading to reduced total shear stress τ at high compressions.

Order parameters $\bar{D}$ (matrix) and D_1 (muscle fibers) at Hugoniot states are shown in

Fig. 3b. For parallel loading, degradation occurs similarly for matrix and fibers. For transverse loading, less degradation occurs in the fibers; their strain energy is lower in this arrangement, giving smaller elastic driving force in $\pi^1_{\mathrm{D}1}$. Shock-recovered samples[6] show microstructure changes indicative of damage in fibers (myofibrils) and slippage at cellular interfaces, implying matrix damage. Other experiments, including microscopy and histology after static crushing of muscle, show shear-induced damage in fibers, interfaces, and extracellular matrix.[206,207] The current model can reflect these trends. Other phase-field approaches that do not delineate between fiber and matrix fractures[37,38] would be unable to give such insight into microstructure.

Model results for muscle in Figs. 2 and 3a,b use the generalized Finsler metric with remnant strain $\epsilon^1_{\mathrm{r}} = 0.2$ (Table 1). Predictions in Fig. 3c,d compare aforementioned results for damage and τ with those obtained when $\epsilon^1_{\mathrm{r}} = 0$, producing Euclidean metrics. Recall $\epsilon^1_{\mathrm{r}} > 0$ depicts dilatation of the material manifold $\mathfrak{M}^\alpha = \mathfrak{M}^1$ as tearing commences and internal surfaces enlarge.

Under shock compression, shear-induced dilatation can occur in solid phases as fracture surfaces slide and open.[121] As a result, area of free surfaces increases, leading to an increase in total fracture surface energy in the model at fixed damage order parameters. As corroborated by Fig. 3c, damage is suppressed (i.e., more diffuse tearing and rupture) at large deformation when a Finsler metric is used relative to a Euclidean metric. Higher energetic cost of fracture in Eq. 175 for the former ($\hat{G}^\alpha > 1$) explains this. Conversely, with higher values of $\bar{D}$ and D_1, τ decays more rapidly with increasing compression in Fig. 3d when a Euclidean metric ($\hat{G}^\alpha = 1$) is used.

More experimental information (e.g., lateral stress readings[121] of τ) is needed to better validate the choice of metric. Past modeling and experiments on skin tissue[18,97] suggest results from a Finsler metric may generally be more realistic: nonaffine fiber rearrangements and fiber-matrix sliding embodied by $\hat{G}^\alpha > 1$ lead to diffusion of damage, crack blunting, and gradual softening.

For compressive shock stability,[117] along the Hugoniot,

$$P > 0, \qquad \mathrm{d}P/\mathrm{d}J < 0, \qquad \mathrm{d}^2P/\mathrm{d}J^2 > 0. \tag{235}$$

These conditions, and complementary conditions along isentropes in conjunction with $\partial P/\partial \eta > 0$,[116] were verified for $J \in [0.7, 1]$ for all cases in Fig. 3. Damage reduces the tangent shear modulus, but this is more than offset by increasing tangent elastic parts of bulk and shear moduli under compression (e.g., exponential stiffening).

4.2 Static and Dynamic Uniaxial Stress Response

4.2.1 Liver

The theory is implemented to model uniaxial-stress compression of bovine liver across a wide range of strain rates as studied experimentally,[208] demonstrating efficacy of the model's viscoelastic and damage kinetics. Liver parenchyma is comprised of cells (hepatocytes), blood vessels (sinusoids), lymphatic vessels, bile ducts, and fibrous extracellular matrix (ECM). The organ is encased in a membrane (peritoneum) and connective tissue (Glisson's capsule). In vivo, the liver is internally pressurized, expanded, and perfused with blood, with a fluid volume fraction[14] on the order of 0.5. Most experimental characterizations, including those modeled here,[208] consider excised samples of the parenchyma, initially at ambient pressure (i.e., not perfused), excluding the peritoneum, Glisson's capsule, and major vessels and ligaments. In these cases, initial blood volume fraction is substantially lower than 50%, and the response is usually isotropic.

The material is depicted as a mixture of two phases ($N = 2$): a solid tissue phase ($\alpha = 1$) and a fluid phase ($\alpha = 2$) consisting of blood. The EOS used in Section 4.1 is reinvoked, with properties in Table 1, any differences between bovine and human blood ignored. In the nonperfused state,[209] the initial fluid fraction is $n_0^2 = 0.12$, the solid fraction $n_0^1 = 0.88$. Effects of intracellular and extracellular fluids other than blood are encompassed by the EOS of the first phase, with the free energy of Eqs. 133 and 134.

In addition, the free energy of the solid phase ($\alpha = 1$) consists of matrix deviatoric elastic (Ψ_{S}^1) and viscoelastic (Ψ_{Γ}^1) terms, fiber elastic (Ψ_{F1}^1) and viscoelastic ($\Psi_{\Phi 1}^1$) terms, and damage to matrix and fibers (Ψ_{D}^1). A single fiber family is sufficient ($k = 1$), fully dispersed with $\kappa_k^\alpha \to \kappa_1^1 = \frac{1}{3}$ in Eq. 147 for isotropy. Damage order parameters for matrix and fibers, $\bar{D}^\alpha \to \bar{D}^1 = \bar{D}$ and $D_k^\alpha \to D_1^1 = D_1$, reduce the tissue deviatoric stress in Eq. 174 and furnish the fracture surface energy in Eq. 175. For loading rates up to the order of 10^3/s and viscosities $\hat{B}^\alpha$ and $\hat{\mu}^\alpha$ in Table 1,

viscous stress from blood should not exceed tens of Pa. This is negligible relative to total stresses in the kPa to MPa range,[208] and thus ignored. For compression, cavitation damage in the fluid is irrelevant.

The sample is a cylindrical annulus,[208] deformed uniformly in the longitudinal (i.e., axial) direction to a stretch of $F_1^1(t) = \lambda(t) = 1 - \dot{\epsilon}t \leq 1$ at constant "engineering strain" rate of $\dot{\epsilon}$. A Cartesian coordinate frame defines the axial 1-direction and orthogonal (radial) 2- and 3-directions. Longitudinal velocity history $(\upsilon^\alpha)^1(t)$ and axial deformation gradient $(F^\alpha)_1^1(t)$ are identical in each phase. In the initial state, partial pressure in each phase is equilibrated to reference ambient pressure: $p_0^\alpha = n_0^\alpha p_{\mathrm{R}0}^\alpha$ with $p_{\mathrm{R}0}^\alpha = 1$ atm. At low rates ($\dot{\epsilon} \lesssim 10^2$/s), isothermal conditions apply: $\theta^\alpha = \theta_0 = 310$ K. For high rates ($\dot{\epsilon} \gtrsim 10^2$/s), macroscopically adiabatic conditions apply: $\mathbf{q}^\alpha = \mathbf{0}$. Interphase mass transfer is excluded: $\hat{c}^\alpha = 0$.

Two different boundary conditions are considered for transverse (i.e., radial) stress and deformation. First is a "drained" condition, whereby each phase expands or contracts independently to maintain equilibrium with external atmosphere: $(\sigma^\alpha)_2^2 = (\sigma^\alpha)_3^3 = p_0^\alpha$. Transverse velocities $(\upsilon^1)^2 = (\upsilon^1)^3$ and $(\upsilon^2)^2 = (\upsilon^2)^3$ are not necessarily equal in each phase, so transverse diffusion velocities $(\mu^\alpha)^2, (\mu^\alpha)^3$ need not vanish. Hydraulic conductivity is assumed infinite as a limiting case, so $\lambda^{\alpha\beta} \to 0$ and $\mathbf{h}^\alpha \to \mathbf{0}$ in Eq. 209. For the drained case, each α likewise maintains its own temperature $\theta^\alpha(t)$, with $\omega^{\alpha\beta} \to 0$ in Eq. 211 as a similarly limiting case, so $\epsilon^\alpha \to 0$. Temperatures are updated by solving Eq. 116 separately for $\alpha = 1, 2$.

Second is an "undrained" or "tied" condition, whereby each phase expands or contracts radially with the same transverse velocity history. All diffusion velocities vanish: $\boldsymbol{\mu}^\alpha = \mathbf{0}$. Transverse deformation is obtained by equilibrating the total transverse stress of Eq. 60 to atmospheric pressure: $\sigma_2^2 = \sum_{\alpha=1,2}(\sigma^\alpha)_2^2 = p_{\mathrm{R}0}^\alpha = 1$ atm. Consistently, for high-rate loading, each phase has the same temperature: $\theta^1(t) = \theta^2(t) = \theta(t)$, updated by integrating the sum of Eq. 116 over $\alpha = 1, 2$. Undrained conditions are consistent with limiting very high, yet still finite, $\lambda^{\alpha\beta} \tilde{\to} \infty$ and $\omega^{\alpha\beta} \tilde{\to} \infty$, so $\mathbf{h}^\alpha \to \mathbf{0}$ and $\epsilon^\alpha \to 0$. The tied condition is used elsewhere for biologic solids in "constrained reactive mixture theory."[145,146,188,189]

Axial deformation $\lambda(t)$ is imposed over small time steps Δt. Thermomechanical responses of each phase and the mixture as a whole are obtained by solution and integration of the constitutive (i.e., stress-deformation-temperature) equations, Eq. 116

if high-rate loading, and kinetic laws for viscoelasticity and damage. For viscoelasticity, two relaxation modes are sufficient for the deviatoric matrix ($m = 1, 2$ in Eq. 151) and one for fiber ($n = 1$ in Eq. 162) contributions to stress, with volumetric (pressure) contributions omitted for reasons explained in Section 4.1.2. The algorithm of several related references[27,165] is used to solve the differential equations in Eqs. 154 and 164 over the time history of loading.

Damage is absent in the fluid and spatially homogeneous in the solid: $\nabla \bar{D} = \nabla D_1 = \mathbf{0}$, ensuring stress fields are homogeneous within each phase, consistent with momentum conservation in the absence of acceleration waves. Gradient energies in Eq. 175 and conjugate forces $\bar{\boldsymbol{\zeta}}^{\alpha}_{\mathrm{D}}$ and $\boldsymbol{\zeta}^{\alpha}_{\mathrm{D}k}$ in Eqs. 199 and 204 vanish. Order parameters and dissipated energies are obtained by integrating kinetic laws of Eqs. 201, 202, 206, and 207 over the load history with nonzero fracture viscosities $\bar{\nu}^1_{\mathrm{D}}$ and $\nu^1_{\mathrm{D}1}$.

Properties for the isolated solid tissue phase ($\alpha = 1$) of bovine liver are given in Table 2. EOS properties, namely $\rho^{\alpha}_{\mathrm{R}0}$, B^{α}_{η}, γ^{α}_{0}, and c^{α}_{ϵ}, are calculated from mixture rules in Eqs. 227–230 using known values for the fluid ($\alpha = 2$) phase (i.e., blood in Table 1), initial volume fraction[209] $n^1_0 = 0.88$, and available properties for the liver as a whole (solid + fluid).[195,210,211] Bulk nonlinear stiffening coefficients k^{α}_{V} and $B^{\alpha}_{\eta\mathrm{p}} = B^{\alpha}_{\theta\mathrm{p}}$ are assumed identical to those of skeletal muscle in Table 1 since high-pressure data are not available for their determination. Values are inconsequential for pressures obtained here under uniaxial-stress compression, wherein $|J^{\alpha} - 1| < 10^{-4}$.

Table 2 Physical properties or model parameters ($\alpha = k = 1$) for bovine liver ($n_0^1 = 0.88$) and rabbit muscle ($n_0^1 = 0.9$)

Property (units)	Bovine liver	Rabbit muscle
$\rho^\alpha_{\mathrm{R}0}$ (g/cm^3)	1.06	1.10
B^α_η (GPa)	2.67	3.28
c^α_ϵ (J/g K)	3.51	3.25
γ^α_0 (-)	0.114	0.313
$B^\alpha_{\eta\mathrm{p}}$ (-)	8.0	8.0
k^α_{V} (-)	6.0	6.0
μ^α_{S} (kPa)	1.0	1.0
μ^α_k (kPa)	100	600
k^α_k (-)	1.0×10^{-6}	2.1
$\beta^\alpha_{\mathrm{S}1}$ (-)	20	900
$\beta^\alpha_{\mathrm{S}2}$ (-)	150	...
$\beta^\alpha_{\Phi k,1}$ (-)	1.0	0.1
$\tau^\alpha_{\mathrm{S}1}$ (s)	0.05	0.05
$\tau^\alpha_{\mathrm{S}2}$ (s)	1.0×10^{-3}	...
$\tau^\alpha_{\Phi k,1}$ (s)	1.0×10^{-3}	0.05
$\hat{\nu}^\alpha_{\mathrm{D}}$ (s)	0.05	0
J_{C} (kJ/m^2)	0.08	0.84
l^α (mm)	1.00	0.88
ϑ^α (-)	2.0	2.0
$\epsilon^\alpha_{\mathrm{r}}$ (-)	0.2	0.2
$\bar{r}^\alpha = \tilde{r}^\alpha_k$ (-)	2.0	2.0

Shear moduli μ^α_{S} and μ^α_k, stiffening k^α_k, viscoelastic strength factors $\beta^\alpha_{\mathrm{S}m}$ and $\beta^\alpha_{\Phi k,n}$, and relaxation times $\tau^\alpha_{\mathrm{S}m}$ and $\tau^\alpha_{\Phi k,n}$ for $\alpha = k = 1$, $m = 1, 2$ and $n = 1$ are fit to data[208] in Fig. 4a,b at rates $\dot\epsilon = 0.01$/s, $\dot\epsilon = 10$/s, and $\dot\epsilon = 2000$/s. The total first Piola–Kirchhoff or "engineering" stress magnitude for this purpose, noting $J^1 \approx 1$ and $(\sigma^\alpha)^1_1 \leq -n^\alpha_0 p^\alpha_{\mathrm{R}0}$, is measured relative to ambient pressure $p^\alpha_{\mathrm{R}0}$:

$$P = \frac{J^1|(\sigma^1_1 + p^1_{\mathrm{R}0})|}{(F^1)^1_1} = \frac{J^1}{\lambda}\Big|\sum_\alpha [(\sigma^\alpha)^1_1 + n^\alpha_0 p^\alpha_{\mathrm{R}0}]\Big|. \tag{236}$$

The fracture toughness of the mixture, J_{C}, is obtained from Azar and Hayward,[212] presumed similar for porcine and bovine liver. Procedures of Section 4.1.2 give $n^1_0 \bar{\mathsf{J}}^1_{\mathrm{C}} = n^1_0 \mathsf{J}^1_{\mathrm{C}1} = \frac{1}{2}\mathsf{J}_{\mathrm{C}}$. Length constants for matrix and fibers are set equal to the value in Table 2 to best represent data in Figs. 4a and 4b: $\bar{l}^1 = l^1_1 = l^1 = 1$ mm. Recalling $\bar{E}^1_{\mathrm{C}} = \bar{\Upsilon}^1/\bar{l}^1 = \bar{\mathsf{J}}^1_{\mathrm{C}}/(2\bar{l}^1)$ and $E^1_{\mathrm{C}1} = \Upsilon^1_1/l_1 = \mathsf{J}^1_{\mathrm{C}1}/(2l^1_1)$, for homogeneous damage, Eq. 175 and evolution of order parameters depend only on

the ratio of toughness to length (i.e., cohesive energies $\bar{E}^1_{\mathrm{C}}$, E^1_{C1}) and not toughness and length independently. If gradient regularization lengths $\bar{l}^1_{\mathrm{R}}, l^1_{\mathrm{R1}}$ must be chosen in Eq. 175 based on mesh size constraints rather than physical observations, for example the smaller value of 0.1 mm used for arterial rupture by Gultekin et al.,[38] then $\bar{\alpha}^1 = \bar{l}^1_{\mathrm{R}}/\bar{l}^1$ and $\alpha^1_1 = l^1_{\mathrm{R1}}/l^1_1$ can be invoked independently without affecting the cohesive energy.

Standard[38,97] values of $\bar{\vartheta}^1 = \vartheta^1_1 = \vartheta^1 = 2$ enter Eqs. 172 and 173. The same rate dependence of damage, $\hat{\nu}^\alpha_{\mathrm{D}}$, normalized by cohesive energy $E^\alpha_{\mathrm{C}} = \bar{E}^\alpha_{\mathrm{C}} = E^\alpha_{\mathrm{C}k}$ and with units of time, is used for matrix and fibers ($\alpha = k = 1$): $n^\alpha_0 \bar{\nu}^\alpha_{\mathrm{D}} = n^\alpha_0 \nu^\alpha_{\mathrm{D}k} = E^\alpha_{\mathrm{C}} \hat{\nu}^\alpha_{\mathrm{D}}$. The value in Table 2 produces credible results in the context of Fig. 4c. The same parameters for generalized Finsler metrics $\mathbf{G}^\alpha$ are used for liver and muscle, justified by explanation in Section 4.1.2.

The high-rate response of compressed liver is shown in Fig. 4a. Model results assume adiabatic conditions, but predicted temperature change is negligible. Damage order parameters attain small maxima at high rates (i.e., $\bar{D} \lesssim 0.03$ and $D_1 \lesssim 0.003$ in Fig. 4c) due to the viscosity $\hat{\nu}^\alpha_{\mathrm{D}}$ preventing notable degradation over the brief time period of deformation. This is consistent with data[208] that show continuously increasing stiffness at this loading rate, with no evidence of material failure. Differences between drained and undrained conditions are indiscernible because the solid tissue is nearly incompressible.

Low and moderate-rate stress histories are shown in Fig. 4b. These model predictions are isothermal and for drained conditions only; results for undrained, not shown, are nearly identical. This theory captures the mechanical response of liver spanning five decades in strain rate. Previous viscoelastic modeling has been limited to much lower rates.[213,214] Model fits to data are deemed reasonable, but they are not as close to experimental data as those for high-rate loading in Fig. 4a.

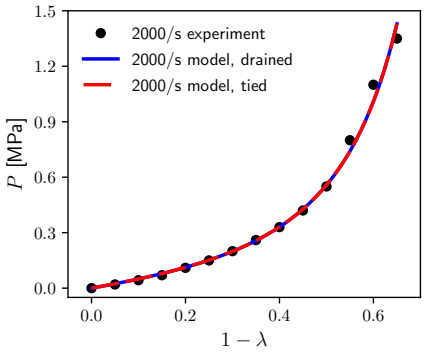

(a) axial stress vs. strain, high strain rate

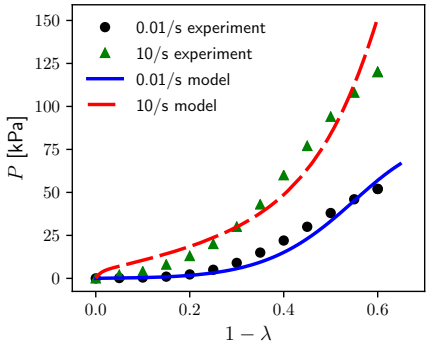

(b) axial stress, low and moderate rates

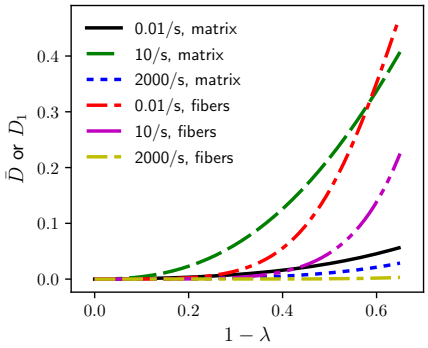

(c) damage vs. strain, all three rates

Fig. 4 Model results and experimental data[208] for bovine liver compressed to stretch λ: (a) axial stress P at strain rate $\dot{\epsilon} = 2000$/s, (b) P at $\dot{\epsilon} = 0.01$/s and $\dot{\epsilon} = 10$/s, and (c) predicted matrix and fiber damage $\bar{D}$ and D_1 at all three rates

At low strain rates, the data show reduction in the degree of stiffening at large compression, indicative of strength degradation.[3,18,107] This phenomenon is captured by damage kinetics, Fig. 4c. Damage increases monotonically with compressive strain $1 - \lambda$. At moderate to high rates, damage is more severe in matrix than fibers.

Histological analysis after dynamic blunt impact[215] shows that fractures in the liver parenchyma tend to avoid fibers and interlobular septa and more often propagate along interfaces, consistent with higher levels of "matrix" damage $\bar{D}$ relative to fiber damage D_1 in Fig. 4c. Conversely, at the lowest strain rate (0.01/s), fiber damage overtakes matrix damage at large compression ($\lambda \lesssim 0.77$) and is more pronounced due to longer load times for relaxation to ensue.

The present theory uniquely addresses tissue damage, resolving that in cellular matrix and collagen fiber network seen experimentally.[215] Models for liver damage

at high strain rates appear to be scarce in the literature. One other study applies a cohesive zone model for relatively slow extension and tearing.[216]

4.2.2 Skeletal Muscle

The theory is now implemented to study uniaxial-stress tensile behavior of rabbit skeletal muscle at low and moderate strain rates, with and without activation from electrical stimulation. Model results seek to depict experiments reported by Taniguchi et al.[183] and Ito et al.[31]

Calculations proceed in the same manner as just described for modeling liver, with a few exceptions. First, tension is modeled rather than compression, with stretch ratio $F_1^1(t) = \lambda(t) = 1 + \dot{\epsilon}t \geq 1$ at two rates[183]: $\dot{\epsilon} = 0.17$/s and $\dot{\epsilon} = 15$/s. Engineering tensile stress is P of Eq. 236, where now $(\sigma^\alpha)_1^1 \geq -n_0^\alpha p_{\mathrm{R}0}^\alpha$. Both drained and undrained conditions are considered, all isothermal.

Second, the data do not indicate any consistent rate sensitivity of damage or failure stretch,[31] so equilibrium equations derived in Eq. 226 and used in Section 4.1.2 for porcine muscle still apply. These correspond to Eqs. 201 and 206 with null viscosities $\bar{\nu}_{\mathrm{D}}^\alpha = \nu_{\mathrm{D}k}^\alpha \to 0$, giving zero dissipation in Eqs. 202 and 207. Lastly, active tension, irrelevant for liver, is relevant and implemented for skeletal muscle.

Regarding muscle activation, the form of free energy Ψ_{A}^α in Eq. 170 and the resultant Cauchy stress term $\boldsymbol{\sigma}_{\mathrm{A}}^\alpha$ in Eq. 171 are adapted directly from Ito et al.[31] since they reproduce the over-stress from activation recorded in isometric experiments[183]:

$$\Psi_{\mathrm{A}}^1 = \tfrac{2}{3}\Delta_{\mathrm{A}}\mu_{\mathrm{A}}(\lambda_{\mathrm{A}1} - \lambda_{\mathrm{A}0})[\bar{\Lambda}^{p_{\mathrm{A}}}/p_{\mathrm{A}} - \bar{\Lambda}^{r_{\mathrm{A}}}/r_{\mathrm{A}}], \tag{237}$$

$$\boldsymbol{\sigma}_{\mathrm{A}}^1 = \tfrac{2}{3}\frac{\rho^\alpha}{\rho_{\mathrm{R}0}^\alpha}\frac{\Delta_{\mathrm{A}}\mu_{\mathrm{A}}}{\lambda_1^1}\bar{\Lambda}^{p_{\mathrm{A}}-1}[1 - \bar{\Lambda}^{q_{\mathrm{A}}-1}]\tilde{\mathbf{h}}_1^1, \tag{238}$$

$$\bar{\Lambda} = \begin{cases} \frac{\lambda_1^1 - \lambda_{\mathrm{A}0}}{\lambda_{\mathrm{A}1} - \lambda_{\mathrm{A}0}} & \forall\, \lambda_1^1 \in (\lambda_{\mathrm{A}0}, \lambda_{\mathrm{A}1}), \\ 0 & (\text{otherwise}). \end{cases} \tag{239}$$

Active tension vanishes for $\bar{\Lambda}$ outside domain $[0, 1]$. Recall that the fiber elastic stretch obeys $(\lambda_k^\alpha)^2 = I_k^\alpha = \tilde{\mathbf{C}}^\alpha : \mathbf{H}_k^\alpha$ with $\alpha = k = 1$. Parameters are μ_{A} (stress units) and the dimensionless set $(\lambda_{\mathrm{A}0}, \lambda_{\mathrm{A}1}, p_{\mathrm{A}}, q_{\mathrm{A}})$, with $r_{\mathrm{A}} = p_{\mathrm{A}} + q_{\mathrm{A}} - 1$. A dimensionless internal variable for activation is $\{\Delta_k^\alpha(t)\} \to \Delta_1^1(t) = \Delta_{\mathrm{A}}$. Only discrete states are considered: $\Delta_{\mathrm{A}} = 1$ in the fully active state and $\Delta_{\mathrm{A}} = 0$ in the fully passive state. Transient switching between states and partial activation are not

addressed here or in the experiments.[31,183] Neither the energy χ_k^α contributing to the sum in Eq. 170 nor the kinetic law in Eq. 195 be prescribed; no contribution to dissipation arises since $D_t^1 \Delta_\mathrm{A} = 0$ in Eq. 197. The factor of $\frac{2}{3}$ in Eq. 237 is missing in the article by Ito et al.[31] wherein compressibility is ignored.

As invoked in Section 4.1.2 for porcine muscle, here rabbit muscle consists of solid tissue $\alpha = 1$ and ECF ($\alpha = 2$), where parameters for ECF are in Table 1. The initial solid volume fraction remains $n_0^1 = 0.9$. Parameters for rabbit skeletal muscle are compiled in Table 2. Thermophysical properties entering the EOS are identical to those for porcine tissue in Table 1. Shear properties μ_S^α, μ_k^α, and k_k^α are calibrated to the experimental data,[31,183] with $k = 1$ sufficient. Fibers are fully aligned, $\kappa_k^\alpha \to \kappa_1^1 = 0$ in Eq. 147, giving anisotropic response.

The glassy viscoelastic assumption used for modeling shocks in Section 4.1.2 is inappropriate for low and moderate strain rates. Instead, viscoelastic strength factors $\beta_{\mathrm{S}m}^\alpha$ and $\beta_{\Phi k,n}^\alpha$ and relaxation times $\tau_{\mathrm{S}m}^\alpha$ and $\tau_{\Phi k,n}^\alpha$ are fit to experimental data; here, a single mode suffices: $m = n = 1$. The activation parameters in Eq. 237 are verbatim from Ito et al.[31]: $\mu_\mathrm{A} = 962$ kPa, $\lambda_{\mathrm{A}0} = 0.9$, $\lambda_{\mathrm{A}1} = 1.32$, $p_\mathrm{A} = 1.65$, and $q_\mathrm{A} = 2.0$. Assumptions for properties modulating matrix and fiber damage are the same as those explained for porcine tissue in Section 4.1.2, with matching toughness J_C.[203] Length $l^1 = \bar{l}^1 = l_1^1$ provides cohesive energies $E_\mathrm{C} = \bar{E}_\mathrm{C} = E_{\mathrm{C}1}$ in Eqs. 175 and 233. The value in Table 2 best fits softening and failure in test data[31,183] at the lowest loading rate. Finsler metric parameters in Table 2 match those of porcine muscle in Table 1; none are adjusted when fitting the data.

For tensile loading, cavitation of the fluid ($\alpha = 2$) is not impossible. Calibration of the model for water under isentropic expansion to its 8.7 MPa cavitation stress[91] gives $\bar{E}_\mathrm{C}^\alpha = 0.1818$ MPa. Use of the same cohesive energy for ECF gives a cavitation stress of 8.9 MPa, and $J^\alpha \gtrsim 1.001$ ($\alpha = 2$) is needed to initiate detectable damage $\bar{D}^\alpha$. Such fluid expansion is never achieved in the present modeling of muscle response. The conclusion is that cavitation "damage" to the ECF is negligible for the current application.

Model outcomes and experimental stress-stretch data are compared in Fig. 5a for active states and Fig. 5b for passive states, at engineering strain rates of $\dot{\epsilon} = 0.17$/s and $\dot{\epsilon} = 15$/s. The fiber direction $\boldsymbol{\iota} = \boldsymbol{\iota}_1^1$ is aligned with the direction of elongation.

Model results in Fig. 5 are for drained lateral boundaries; predictions for undrained conditions are nearly indiscernible from drained and thus not shown. For active and passive states, the material is stiffer at the higher rate, with larger peak (failure) stress. Predicted failure stretch is similar at both strain rates. The material supports larger P in the active state over domain $1 \leq \lambda \lesssim 1.32$, including an initial stress of $P = 0.192$ MPa at $\lambda(t = 0) = 1$ that matches experiments.

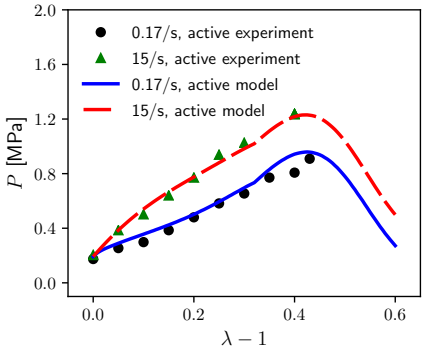

(a) axial stress vs. strain, active state

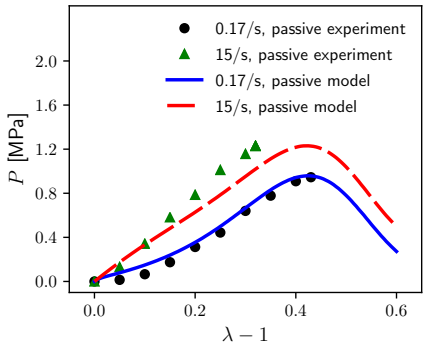

(b) axial stress vs. strain, passive state

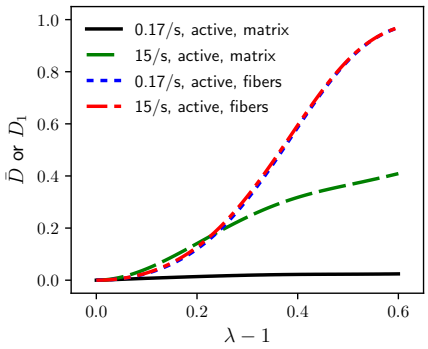

(c) damage vs. strain, active state

Fig. 5 Model results and experimental data[31,183] for rabbit skeletal muscle to tensile stretch λ at rates of $\dot{\epsilon} = 0.17$/s and $\dot{\epsilon} = 15$/s: (a) axial stress P in active state ($\Delta_{\rm A} = 1$), (b) P in passive state ($\Delta_{\rm A} = 0$), and (c) predicted matrix and fiber damage $\bar{D}$ and D_1, active state (passive nearly identical)

The model closely depicts the majority of data points,[31,183] an exception under-prediction of large P versus λ data at $\dot{\epsilon} = 15$/s for the passive state in Fig. 5b. An over-prediction of peak stress for active loading at the higher rate was obtained from a phenomenological model.[31] That model, however, contained five adjustable parameters, whereas only the length parameter l^1 was adjusted for damage modeling in application of the present theory. More elaborate coupling among viscoelastic

and damage kinetics, with more parameters, could improve agreement, but such an exercise is unjustified for closer fitting of relatively few data points.

Unlike results for uniaxial-strain compression in Section 4.1.2 where the matrix and fibers supported similar stress, here, under tensile loading, the fibers bear the majority of the load P, with the ratio of fiber to matrix stress increasing as stretch increases and strain rate decreases. The correspondingly larger strain energy in the fibers provides a larger driving force for fiber damage D_1 than matrix damage $\bar{D}$, the latter which is nearly negligible at $\dot{\epsilon} = 0.17$/s, as shown in Fig. 5c. The model of Ito et al.,[31] which contains more calibrated parameters, does not specifically delineate between matrix and fiber fractures, though it does feature a transversely isotropic representation for fiber failure versus fiber detachment.

As discussed by Lamsfuss and Bargmann,[217] under tensile loading at low rates, damage to muscle fibers is prominently observed over delamination and damage to the endomysium (i.e., the matrix including connective tissue in which fibers are embedded). The current predictions concur with these observations. At the higher rate of $\dot{\epsilon} = 15$/s, viscoelastic energy of the matrix is sufficient to induce matrix damage, though it remains less severe than fiber damage for $\lambda \gtrsim 1.23$, which is nearly the same at both rates. The damage model is decoupled from Ψ_{A}, so order parameters $\bar{D}$ and D_1 have indistinguishable histories for active versus passive states.

4.3 Shock Evolution

4.3.1 General Analytical Solution

Growth and decay of planar shock waves are studied, with shock fronts treated as singular surfaces per theory of Section 2.3. An analytical solution is derived for solid-fluid mixtures with viscoelastic and damage mechanisms, extending work of the author[87] that considered nonlinear elastic solid-fluid mixtures without internal variables and work of Chen and Gurtin[117] that considered fluids with internal state variables.

To streamline notation, let internal variables $\{\boldsymbol{\xi}^\alpha\} \rightarrow (\mathbf{a}^\alpha, \mathbf{b}^\alpha)$. Generic internal variable class $\mathbf{a}^\alpha$ obeys kinetic laws of the form in Eq. 97 specialized to

$$D_t^\alpha \mathbf{a}^\alpha = D_t^\alpha \mathbf{a}^\alpha(\mathbf{F}^\alpha, \eta^\alpha(\mathbf{F}^\alpha, \theta^\alpha, \mathbf{a}^\alpha, \mathbf{b}^\alpha), \mathbf{a}^\alpha, \mathbf{b}^\alpha). \tag{240}$$

Generic class $\mathbf{b}^\alpha$ obeys equilibrium conditions of form

$$\boldsymbol{\pi}_{\mathsf{b}}^\alpha = \rho^\alpha \partial u^\alpha / \partial \mathbf{b}^\alpha = \mathbf{0}. \tag{241}$$

Type $\mathbf{a}^\alpha$ include dissipative variables for viscoelasticity and order parameters for rate-dependent fracture; type $\mathbf{b}^\alpha$ include rate-insensitive order parameter(s). Now excluding gradient regularization and explicit $\mathbf{X}^\alpha$-dependence,

$$u^\alpha = u^\alpha(\mathbf{F}^\alpha, \eta^\alpha, \mathbf{a}^\alpha, \mathbf{b}^\alpha), \qquad \theta^\alpha = \theta^\alpha(\mathbf{F}^\alpha, \eta^\alpha, \mathbf{a}^\alpha, \mathbf{b}^\alpha) \tag{242}$$

are internal energy and temperature of Eqs. 107 and 108.

Unless $[\![\boldsymbol{\xi}^\alpha]\!] = \mathbf{0}$, gradient regularization yields infinite energy density in the shock front as its width approaches zero. It also introduces complexity in the Rankine–Hugoniot equations via $\boldsymbol{\zeta}^\alpha$, precluding analytical solutions without undue assumptions on shock structure[111] not used here.

From Eq. 180, $\hat{g} = \hat{G}^\alpha \Rightarrow g/G^\alpha = 1$. Then 1-D kinematics, continuum balance laws, and entropy production are, with $\hat{c}^\alpha = 0$, $\mathbf{q}^\alpha = \mathbf{0}$, $r^\alpha = 0$, $h^\alpha = \mathbf{h}^\alpha \cdot \mathbf{n}$, and $P^\alpha = -t^\alpha$,

$$F^\alpha = \partial \chi^\alpha / \partial X^\alpha = J^\alpha, \qquad D_t^\alpha J^\alpha = \partial v^\alpha / \partial X^\alpha, \tag{243}$$

$$\rho_0^\alpha = J^\alpha \rho^\alpha, \qquad \rho_0^\alpha D_t^\alpha v^\alpha = -(\partial P^\alpha / \partial X^\alpha) + J^\alpha h^\alpha, \tag{244}$$

$$\rho_0^\alpha D_t^\alpha u^\alpha = -P^\alpha (\partial v^\alpha / \partial X^\alpha) + J^\alpha \epsilon^\alpha, \tag{245}$$

$$\rho_0^\alpha \theta^\alpha D_t^\alpha \eta^\alpha = J^\alpha (\epsilon^\alpha - \boldsymbol{\pi}_{\mathsf{a}}^\alpha \cdot D_t^\alpha \mathbf{a}^\alpha), \tag{246}$$

$$\sum_\alpha (J^\alpha / \theta^\alpha)(\epsilon^\alpha - \boldsymbol{\pi}_{\mathsf{a}}^\alpha \cdot D_t^\alpha \mathbf{a}^\alpha + c^\alpha \theta^\alpha \eta^\alpha) \geq 0. \tag{247}$$

A single shock propagates in the (x, X^α)-direction at Lagrangian speed $\mathcal{U}^\alpha$. Ahead of the shock front Σ^α, each phase α obeys equilibrium and uniformity conditions:

$$\begin{aligned} &J^{\alpha+} = 1, \qquad v^{\alpha+} = 0, \qquad \theta^{\alpha+} = \theta_0, \qquad \eta^{\alpha+} = \text{constant} \\ &\quad \Rightarrow \quad \rho^{\alpha+} = \rho_0^\alpha, \qquad h^{\alpha+} = 0, \qquad \epsilon^{\alpha+} = 0, \qquad \mathcal{U}^\alpha = \mathcal{U}; \end{aligned} \tag{248}$$

$$\mathbf{a}^{\alpha+} = \mathbf{a}_0^\alpha = \text{constant}, \qquad \mathbf{b}^{\alpha+} = \mathbf{b}_0^\alpha = \text{constant}. \tag{249}$$

Rankine–Hugoniot equations ($P^\alpha > 0 \Leftrightarrow \text{compression}$) are

$$[\![v^\alpha]\!] = -\mathcal{U}[\![J^\alpha]\!], \qquad [\![P^\alpha]\!] = -\rho_0^\alpha \mathcal{U}^2 [\![J^\alpha]\!], \tag{250}$$

$$\rho_0^\alpha [\![u^\alpha]\!] = -\langle P^\alpha \rangle [\![J]\!], \qquad \sum_\alpha \rho_0^\alpha [\![\eta^\alpha]\!] \geq 0. \tag{251}$$

To avoid infinite dissipation in the shock front,[117,196,197]

$$[\![\mathbf{a}^\alpha]\!] = \mathbf{0} \;\Rightarrow\; \mathbf{a}^{\alpha-} = \mathbf{a}_0^\alpha. \tag{252}$$

Jumps $[\![\mathbf{b}^\alpha]\!]$ in nondissipative variables can be nonzero across Σ^α so long as Eq. 241 holds. However, it is assumed that Eq. 241 can be solved, at least implicitly, at any (X^α, t) with the first of each of Eqs. 242 and 244, and then via Eq. 252,

$$\mathbf{b}^\alpha = \bar{\mathbf{b}}^\alpha(J^\alpha, \eta^\alpha, \mathbf{a}^\alpha), \qquad \mathbf{b}^{\alpha-} = \bar{\mathbf{b}}^{\alpha-}(J^{\alpha-}, \eta^{\alpha-}, \mathbf{a}_0^\alpha). \tag{253}$$

Now with Eqs. 252 and 253 at a given $(\cdot)^+$ state, the first of Eq. 251 can be written $H(J^{\alpha-}, \eta^{\alpha-}, \bar{\mathbf{b}}^{\alpha-}(J^{\alpha-}, \eta^{\alpha-})) = 0$. Again, at least implicitly, this can be solved for entropy along the Hugoniot and then the other state variables:

$$[\![\eta^\alpha]\!] = \eta_{\mathrm{H}}^\alpha([\![J^\alpha]\!]), \qquad [\![\mathbf{b}^\alpha]\!] = \mathbf{b}_{\mathrm{H}}^\alpha([\![J^\alpha]\!]), \tag{254}$$

$$[\![P^\alpha]\!] = P_{\mathrm{H}}^\alpha([\![J^\alpha]\!]), \qquad [\![u^\alpha]\!] = u_{\mathrm{H}}^\alpha([\![J^\alpha]\!]). \tag{255}$$

Hugoniot states do not depend explicitly on $h^{\alpha-}$ or $\epsilon^{\alpha-}$. From Eq. 109 with $\mathbf{F}^\alpha = \mathrm{diag}(J^\alpha, 1, 1)$, calculate or define the following quantities:

$$P^\alpha = -\rho_0^\alpha \partial u^\alpha / \partial J^\alpha, \qquad \theta^\alpha = \partial u^\alpha / \partial \eta^\alpha; \tag{256}$$

$$\mathsf{C}^\alpha = -\partial P^\alpha / \partial J^\alpha = \rho_0^\alpha \partial^2 u^\alpha / \partial (J^\alpha)^2, \tag{257}$$

$$\mathsf{G}^\alpha = -\partial P^\alpha / \partial \eta^\alpha = -\rho_0^\alpha J^\alpha \theta^\alpha (\gamma^\alpha)_1^1, \tag{258}$$

$$\mathbf{A}^\alpha = -\partial P^\alpha / \partial \mathbf{a}^\alpha, \qquad \mathbf{B}^\alpha = -\partial P^\alpha / \partial \mathbf{b}^\alpha, \tag{259}$$

$$\mathbf{b}'^\alpha = \partial \bar{\mathbf{b}}^\alpha / \partial J^\alpha, \qquad \mathbf{b}''^\alpha = \partial^2 \bar{\mathbf{b}}^\alpha / (\partial J^\alpha)^2, \tag{260}$$

$$\hat{\mathsf{C}}^\alpha = \mathsf{C}^\alpha + \mathbf{B}^\alpha \cdot \mathbf{b}'^\alpha, \qquad \mathbf{B}'^\alpha = \partial \mathbf{B}^\alpha / \partial J^\alpha, \tag{261}$$

$$\mathsf{C}'^\alpha = \partial \mathsf{C}^\alpha / \partial J^\alpha = \rho_0^\alpha \partial^3 u^\alpha / \partial (J^\alpha)^3, \tag{262}$$

$$\hat{\mathsf{C}}'^\alpha = \mathsf{C}'^\alpha + \mathbf{B}'^\alpha \cdot \mathbf{b}'^\alpha + \mathbf{B}^\alpha \cdot \mathbf{b}''^\alpha, \tag{263}$$

$$\hat{\mathsf{G}}^\alpha = \mathsf{G}^\alpha + \mathbf{B}^\alpha \cdot \mathbf{b}_\eta^\alpha. \tag{264}$$

Weak shocks are analyzed later, in the limit $[\![J^\alpha]\!] \to 0$. Applying theorems[116] relating isentropic and tangent moduli, Eqs. 254 and 255 are expanded from a $(\cdot)^+$ state, as is Hugoniot temperature $\theta^\alpha_{\rm H}([\![J^\alpha]\!])$:

$$[\![P^\alpha]\!] = -\hat{\mathsf{C}}^{\alpha+}[\![J^\alpha]\!] - \tfrac{1}{2}\hat{\mathsf{C}}'^{\alpha+}[\![J^\alpha]\!]^2 + O([\![J^\alpha]\!]^3), \tag{265}$$

$$[\![\rho_0^\alpha u^\alpha]\!] = -P^{\alpha+}[\![J^\alpha]\!] + \tfrac{1}{2}\hat{\mathsf{C}}^{\alpha+}[\![J^\alpha]\!]^2 + O([\![J^\alpha]\!]^3), \tag{266}$$

$$[\![\rho_0^\alpha \theta^\alpha]\!] = \hat{\mathsf{G}}^{\alpha+}[\![J^\alpha]\!] + \tfrac{1}{2}(\tfrac{\partial \hat{\mathsf{G}}}{\partial J})^{\alpha+}[\![J^\alpha]\!]^2 + O([\![J^\alpha]\!]^3), \tag{267}$$

$$[\![\mathbf{b}^\alpha]\!] = \mathbf{b}'^{\alpha+}[\![J^\alpha]\!] + \tfrac{1}{2}\mathbf{b}''^{\alpha+}[\![J^\alpha]\!]^2 + O([\![J^\alpha]\!]^3), \tag{268}$$

$$[\![\eta^\alpha]\!] = \tfrac{1}{12}\{\hat{\mathsf{C}}'^{\alpha+}/(\rho_0^\alpha\theta_0)\}[\![J^\alpha]\!]^3 + O([\![J^\alpha]\!]^4). \tag{269}$$

From Eq. 269, $[\![\eta^\alpha]\!]$ is of order three in $[\![J^\alpha]\!]$, and $[\![J^\alpha]\!] \leq 0$ when $\hat{\mathsf{C}}'^{\alpha+} < 0$ to satisfy the second of Eq. 251 for a single constituent α.

Interactions $\mathbf{h}^\alpha$ and ϵ^α are respectively odd and even functions[87,118] of v^β, so from Eqs. 248, 250, and 267,

$$h^{\alpha-} = -\mathcal{U}\sum_\beta (\partial h^\alpha/\partial v^\beta)^+[\![J^\beta]\!] + O([\![J^\beta]\!]^2), \tag{270}$$

$$\epsilon^{\alpha-} = \sum_\beta (\partial \epsilon^\alpha/\partial\theta^\beta)^+(\hat{\mathsf{G}}^\beta/\rho_0^\beta)^+[\![J^\beta]\!] + O([\![J^\beta]\!]^2). \tag{271}$$

From Eqs. 251 and 265, $\mathcal{U}^\beta$ the weak-shock propagation velocity approaches the sound speed:

$$\begin{aligned}(\mathcal{U}^\beta)^2 &= (\mathcal{C}^\beta)^2 + \tfrac{1}{2}(\hat{\mathsf{C}}'^\beta/\rho_0^\beta)^+[\![J^\beta]\!] + O([\![J^\beta]\!]^2),\\ \mathcal{C}^\beta &= \sqrt{\hat{\mathsf{C}}^{\beta+}/\rho_0^\beta}.\end{aligned} \tag{272}$$

Considering $\alpha \neq \beta$ and $\mathcal{C}^\alpha \neq \mathcal{C}^\beta$, Eq. 272 implies[87,118]

$$\begin{aligned}&\{(\mathcal{C}^\alpha)^2 - (\mathcal{C}^\beta)^2\}[\![J^\beta]\!] + O([\![J^\alpha]\!][\![J^\beta]\!]) + O([\![J^\beta]\!]^2) = 0\\ &\Rightarrow \mathcal{U}^2 = (\mathcal{C}^\alpha)^2 + O([\![J^\alpha]\!]) \qquad (\text{for one } [\![J^\alpha]\!] \neq 0),\\ &\quad [\![J^\beta]\!] = 0 \qquad (\forall\, \beta = 1, 2, \ldots, \alpha-1, \alpha+1, \ldots, N).\end{aligned} \tag{273}$$

Each distinct wave speed $\mathcal{C}^\alpha$ corresponds to an isolated jump $[\![J^\alpha]\!]$. From Eqs. 265–269, a weak shock in phase α does not induce jumps $[\![P^\beta]\!]$, $[\![u^\beta]\!]$, $[\![\theta^\beta]\!]$, etc. in other

phases β. Since $[\![J^\beta]\!] = 0$ for $\beta \neq \alpha$, Eqs. 270 and 271 become

$$h^{\alpha-} = -\mathcal{C}^\alpha (\partial h^\alpha / \partial \upsilon^\alpha)^+ [\![J^\alpha]\!] + O([\![J^\alpha]\!]^2), \tag{274}$$

$$\epsilon^{\alpha-} = (\partial \epsilon^\alpha / \partial \theta^\alpha)^+ (\hat{\mathsf{G}}^\alpha / \rho_0^\alpha)^+ [\![J^\alpha]\!] + O([\![J^\alpha]\!]^2). \tag{275}$$

The same expressions in Eqs. 274 and 275 also apply[118] for $h^{\beta-}, \epsilon^{\beta-}$, and $\beta \neq \alpha$ with $(\partial h^\alpha / \partial \upsilon^\alpha)^+ \to (\partial h^\beta / \partial \upsilon^\alpha)^+$ and $(\partial \epsilon^\alpha / \partial \theta^\alpha)^+ \to (\partial \epsilon^\beta / \partial \theta^\alpha)^+$.

Resuming analysis of the nonlinear (i.e., strong-shock) regime, denote by f^α any of (J^α, P^α, η^α, θ^α, ρ^α, υ^α, u^α, $\mathbf{b}^\alpha$). Recall that across surface Σ^α, any or all of f^α, $D_t^\alpha f^\alpha$, and $\nabla_0^\alpha f^\alpha = \partial f^\alpha / \partial X^\alpha$ can be discontinuous. From Eq. 252, $\mathbf{a}^\alpha$ is continuous; however, $D_t^\alpha \mathbf{a}^\alpha$ and $\nabla_0^\alpha \mathbf{a}^\alpha$ need not be so. Applying Eq. 45 with the last of Eq. 248 gives[117]

$$\delta_t [\![f^\alpha]\!] = [\![D_t^\alpha f^\alpha]\!] + \mathcal{U} [\![\nabla_0^\alpha f^\alpha]\!], \tag{276}$$

$$[\![D_t^\alpha \mathbf{a}^\alpha]\!] = -\mathcal{U} [\![\nabla_0^\alpha \mathbf{a}^\alpha]\!]. \tag{277}$$

Recall Eq. 9 in 1-D is $D_t^\alpha J^\alpha = \nabla_0^\alpha \upsilon^\alpha$ via Eq. 243. Using Eq. 276 on $[\![J^\alpha]\!]$ and using $[\![\upsilon^\alpha]\!]$ and Eq. 45 on $\mathcal{U}$ in the first of Eq. 250 gives

$$2\mathcal{U} \delta_t [\![J^\alpha]\!] + [\![J^\alpha]\!] \delta_t \mathcal{U} = \mathcal{U}^2 [\![\nabla_0^\alpha J^\alpha]\!] - [\![D_t^\alpha \upsilon^\alpha]\!]. \tag{278}$$

From Eqs. 244, 246, 248, 250, and 256–259,

$$\begin{aligned} \rho_0^\alpha [\![D_t^\alpha \upsilon^\alpha]\!] = {} & \mathsf{C}^{\alpha-} [\![\nabla_0^\alpha J^\alpha]\!] + \mathsf{G}^{\alpha-} [\![\nabla_0^\alpha \eta^\alpha]\!] + J^{\alpha-} [\![h^\alpha]\!] \\ & + \mathbf{A}^{\alpha-} \cdot [\![\nabla_0^\alpha \mathbf{a}^\alpha]\!] + \mathbf{B}^{\alpha-} \cdot [\![\nabla_0^\alpha \mathbf{b}^\alpha]\!], \end{aligned} \tag{279}$$

$$\rho_0^\alpha \theta^{\alpha-} [\![D_t^\alpha \eta^\alpha]\!] = J^{\alpha-} ([\![\epsilon^\alpha]\!] - \boldsymbol{\pi}_{\mathsf{a}}^{\alpha-} \cdot [\![D_t^\alpha \mathbf{a}^\alpha]\!]), \tag{280}$$

where $\boldsymbol{\pi}_{\mathsf{a}}^\alpha = \rho^\alpha \partial u^\alpha / \partial \mathbf{a}^\alpha$. With $f^\alpha \to \eta^\alpha$, putting Eq. 280 into Eq. 276 gives $[\![\nabla_0^\alpha \eta^\alpha]\!]$ in terms of $\delta_t [\![\eta^\alpha]\!]$ and jumps on the right side of Eq. 280. This result for $[\![\nabla_0^\alpha \eta^\alpha]\!]$ is substituted for the second term on the right in Eq. 279.

The fourth term on the right of Eq. 279 is $-\frac{1}{\mathcal{U}} \mathbf{A}^{\alpha-} \cdot [\![D_t^\alpha \mathbf{a}^\alpha]\!]$ via Eq. 277. Using this

result and Eqs. 260 and 280, the fifth term includes

$$\begin{aligned}\llbracket \nabla_0^\alpha \mathbf{b}^\alpha \rrbracket &= \mathbf{b}'^{\alpha-} \llbracket \nabla_0^\alpha J^\alpha \rrbracket - (1/\mathcal{U})\, \mathbf{b}_{\mathsf{a}}^{\alpha-} \cdot \llbracket D_t^\alpha \mathbf{a}^\alpha \rrbracket \\ &\quad + \frac{\mathbf{b}_\eta^{\alpha-}}{\mathcal{U}} \left\{ \delta_t \llbracket \eta^\alpha \rrbracket - \frac{J^{\alpha-}(\llbracket \epsilon^\alpha \rrbracket - \boldsymbol{\pi}_{\mathsf{a}}^{\alpha-} \cdot \llbracket D_t^\alpha \mathbf{a}^\alpha \rrbracket)}{\rho_0^\alpha \theta^{\alpha-}} \right\}, \qquad (281) \\ \mathbf{b}_{\mathsf{a}}^\alpha &= \partial \bar{\mathbf{b}}^\alpha / \partial \mathbf{a}^\alpha, \qquad \mathbf{b}_\eta^\alpha = \partial \bar{\mathbf{b}}^\alpha / \partial \eta^\alpha. \qquad (282)\end{aligned}$$

Putting Eq. 281 into Eq. 279, the latter is inserted into Eq. 278:

$$\begin{aligned}\delta_t \llbracket J^\alpha \rrbracket = \frac{1}{2\mathcal{U}} \Bigg\{ &\left(\mathcal{U}^2 - \frac{\hat{\mathsf{C}}^{\alpha-}}{\rho_0^\alpha} \right) \llbracket \nabla_0^\alpha J^\alpha \rrbracket - \frac{\hat{\mathsf{G}}^{\alpha-}}{\rho_0^\alpha \mathcal{U}} \delta_t \llbracket \eta^\alpha \rrbracket \\ &- \delta_t \mathcal{U} \llbracket J^\alpha \rrbracket - \frac{J^{\alpha-}}{\rho_0^\alpha} \llbracket h^\alpha \rrbracket + \frac{J^{\alpha-} \hat{\mathsf{G}}^{\alpha-}}{(\rho_0^\alpha)^2 \mathcal{U} \theta^{\alpha-}} \llbracket \epsilon^\alpha \rrbracket \\ &+ \mathbf{L}^{\alpha-} \cdot \llbracket D_t^\alpha \mathbf{a}^\alpha \rrbracket \Bigg\}, \qquad (283) \\ \mathbf{L}^\alpha = \frac{1}{\rho_0^\alpha \mathcal{U}} &\left\{ \mathbf{A}^\alpha + \mathbf{B}^\alpha \cdot \mathbf{b}_{\mathsf{a}}^\alpha - \frac{J^\alpha \hat{\mathsf{G}}^\alpha}{\rho_0^\alpha \theta^\alpha} \boldsymbol{\pi}_{\mathsf{a}}^\alpha \right\}. \qquad (284)\end{aligned}$$

From Eqs. 241, 250, 251, 256, 261, 277, and 264,

$$\begin{aligned}\rho_0^\alpha \delta_t \llbracket u^\alpha \rrbracket &= -(P^{\alpha-} + \rho_0^\alpha \mathcal{U}^2 \llbracket J^\alpha \rrbracket) \delta_t \llbracket J^\alpha \rrbracket \\ &\quad - \llbracket J^\alpha \rrbracket \delta_t P^{\alpha-} - \rho_0^\alpha \mathcal{U} \llbracket J^\alpha \rrbracket^2 \delta_t \mathcal{U}, \qquad (285) \\ \rho_0^\alpha \delta_t \llbracket u^\alpha \rrbracket &= -P^{\alpha-} \delta_t \llbracket J^\alpha \rrbracket + \rho_0^\alpha \theta^{\alpha-} \delta_t \llbracket \eta^\alpha \rrbracket, \qquad (286) \\ \delta_t P^{\alpha-} &= \delta_t \llbracket P^\alpha \rrbracket = -\hat{C}^{\alpha-} \delta_t \llbracket J^\alpha \rrbracket - \hat{G}^{\alpha-} \delta_t \llbracket \eta^\alpha \rrbracket. \qquad (287)\end{aligned}$$

Using Eqs. 285–287 to eliminate $\delta_t \llbracket u^\alpha \rrbracket$ and $\delta_t P^{\alpha-}$, then differentiating Eq. 250 produces the following, where $\hat{\xi}^\alpha$ and $\hat{\zeta}^\alpha$ are definitions:

$$\begin{aligned}&\rho_0^\alpha \llbracket J^\alpha \rrbracket^2 \mathcal{U} \delta_t \mathcal{U} = \mathsf{G}^{\alpha-} \llbracket J^\alpha \rrbracket (1 - 1/\hat{\zeta}^\alpha) \delta_t \llbracket \eta^\alpha \rrbracket + \hat{\mathsf{C}}^{\alpha-} (1 - \hat{\xi}^\alpha) \llbracket J^\alpha \rrbracket, \qquad (288) \\ &\hat{\xi}^\alpha = \rho_0^\alpha \mathcal{U}^2 / \hat{\mathsf{C}}^{\alpha-}, \qquad \hat{\zeta}^\alpha = \hat{\mathsf{G}}^{\alpha-} \llbracket J^\alpha \rrbracket / (\rho_0^\alpha \theta^{\alpha-}); \qquad (289) \\ &2\rho_0^\alpha \llbracket J^\alpha \rrbracket \mathcal{U} \delta_t \mathcal{U} = \hat{\mathsf{C}}^{\alpha-} (1 - \hat{\xi}^\alpha) \delta_t \llbracket J^\alpha \rrbracket + \hat{G}^{\alpha-} \delta_t \llbracket \eta^\alpha \rrbracket. \qquad (290)\end{aligned}$$

4.3.2 Nonlinear Solution for Strong Shocks

Solving Eqs. 288 and 290 simultaneously for $\delta_t \mathcal{U}$ and $\delta_t \llbracket \eta^\alpha \rrbracket$, then insertion into Eq. 283 with Eqs. 248 and 287 yields the fully nonlinear shock evolution equations

for $\delta_t[\![J^\alpha]\!]$ and $\delta_t[\![P^\alpha]\!]$:

$$\delta_t\mathcal{U} = \mathcal{U}\frac{(1-\hat{\xi}^\alpha)}{(2-\hat{\zeta}^\alpha)\hat{\xi}^\alpha[\![J^\alpha]\!]}\delta_t[\![J^\alpha]\!], \tag{291}$$

$$\delta_t[\![\eta^\alpha]\!] = \frac{\hat{\mathsf{C}}^{\alpha-}}{\hat{\mathsf{G}}^{\alpha-}}\frac{\hat{\zeta}^\alpha(1-\hat{\xi}^\alpha)}{(2-\hat{\zeta}^\alpha)}\delta_t[\![J^\alpha]\!], \tag{292}$$

$$\delta_t[\![J^\alpha]\!] = \mathcal{U}\frac{(1-\hat{\xi}^\alpha)(2-\hat{\zeta}^\alpha)\{\Lambda^\alpha - (\nabla_0^\alpha J^\alpha)^-\}}{(3\hat{\xi}^\alpha+1)-\hat{\zeta}^\alpha(3\hat{\xi}^\alpha-1)}, \tag{293}$$

$$\delta_t[\![P^\alpha]\!] = -\hat{\mathsf{C}}^{\alpha-}\mathcal{U}\frac{\{3-\hat{\xi}^\alpha(1+\hat{\zeta}^\alpha)\}\{\Lambda^\alpha - (\nabla_0^\alpha J^\alpha)^-\}}{(3\hat{\xi}^\alpha+1)-\hat{\zeta}^\alpha(3\hat{\xi}^\alpha-1)}, \tag{294}$$

$$\Lambda^\alpha = \frac{1+[\![J^\alpha]\!]}{(1-\hat{\xi}^\alpha)\hat{\mathsf{C}}^{\alpha-}}\Big\{\frac{\rho_0^\alpha}{J^{\alpha-}}[\mathbf{L}^{\alpha-}\cdot(D_t^\alpha\mathbf{a}^\alpha)^-] - h^{\alpha-} + [\hat{\mathsf{G}}^{\alpha-}/(\rho_0^\alpha\mathcal{U}\theta^{\alpha-})]\epsilon^{\alpha-}\Big\}. \tag{295}$$

When $(\nabla_0^\alpha J^\alpha)^-$ equals a critical strain gradient Λ^α, the latter a function of the $(\cdot)^-$ conditions immediately behind the wave front, the time derivatives witnessed by an observer moving with the wave front in Eqs. 291–294 all vanish identically. In that ideal case, the shock is steady.

The preceding derivations apply for shocked phase α. Now let $\mathcal{U}$ for phase α be imposed simultaneously on another constituent $\beta \neq \alpha$. The trivial solution to Eq. 250 is $[\![J^\beta]\!] = 0$. However, since Eqs. 290 and 292 still apply with $\alpha \to \beta$, substitution of Eq. 291 into the former gives a different, nontrivial solution (i.e., a nonlinear shock interaction law) for the strain jump in a different phase β when that phase inherits the shock velocity $\mathcal{U}$ assigned first to phase α as a loading condition[87,118]:

$$\delta_t[\![J^\beta]\!] = \frac{(2-\hat{\zeta}^\beta)\hat{\xi}^\beta(1-\hat{\xi}^\alpha)}{(2-\hat{\zeta}^\alpha)\hat{\xi}^\alpha(1-\hat{\xi}^\beta)}\frac{[\![J^\beta]\!]}{[\![J^\alpha]\!]}\delta_t[\![J^\alpha]\!]. \tag{296}$$

4.3.3 Linearized Solution for Weak Shocks

In the weak limit, $\mathcal{U} = \mathcal{U}^\alpha \to \mathcal{C}^\alpha = \text{constant}$ and shock evolution depends only on $(\cdot)^+$ states. As $[\![J^\alpha]\!] \to 0$, from Eqs. 250, 251, 265, 267, 270, 271, 293, and 295,

$$\hat{\xi}^\alpha = 1 - \tfrac{1}{2}(\hat{\mathsf{C}}'^{\alpha+}/\hat{\mathsf{C}}^{\alpha+})[\![J^\alpha]\!] + O([\![J^\alpha]\!]^2), \tag{297}$$

$$\hat{\zeta}^\alpha = \{\hat{\mathsf{G}}^{\alpha+}/(\rho_0^\alpha\theta_0)\}[\![J^\alpha]\!] + O([\![J^\alpha]\!]^2), \tag{298}$$

$$\Lambda^\alpha = -4\,\mathcal{C}^\alpha\rho_0^\alpha\omega^\alpha/\hat{\mathsf{C}}'^{\alpha+} + O([\![J^\alpha]\!]), \tag{299}$$

$$\omega^\alpha = -\frac{1}{2\rho_0^\alpha}\Bigg\{\frac{1}{(\mathcal{C}^\alpha)^2}\left[\mathbf{A}^{\alpha+} + \mathbf{B}^{\alpha+}\cdot\mathbf{b}_{\mathsf{a}}^{\alpha+} - \frac{\hat{\mathsf{G}}^{\alpha+}}{\rho_0^\alpha\theta_0}\boldsymbol{\pi}_{\mathsf{a}}^{\alpha+}\right]$$
$$\cdot\left[\left(\frac{\partial(D_t^\alpha\mathbf{a}^\alpha)}{\partial J^\alpha}\right)^+ + \left(\frac{\partial(D_t^\alpha\mathbf{a}^\alpha)}{\partial\mathbf{b}^\alpha}\cdot\mathbf{b}'^\alpha\right)^+\right]$$
$$+\left(\frac{\partial h^\alpha}{\partial\upsilon^\alpha}\right)^+ + \frac{1}{\theta_0}\left(\frac{\hat{\mathsf{G}}^{\alpha+}}{\rho_0^\alpha\mathcal{C}^\alpha}\right)^2\left(\frac{\partial\epsilon^\alpha}{\partial\theta^\alpha}\right)^+\Bigg\}, \tag{300}$$

$$\delta_t[\![J^\alpha]\!] = -\omega^\alpha[\![J^\alpha]\!] + O([\![J^\alpha]\!][\![\nabla_0^\alpha J^\alpha]\!]; [\![J^\alpha]\!]^2). \tag{301}$$

Omitting all higher-order products[87,118] on the right of Eq. 301, the closed-form analytical solution to this ordinary differential equation predicts exponential decay for $\omega^\alpha > 0$, the physically relevant and thermodynamically expected case:

$$[\![J^\alpha]\!](t) = \Delta J_0^\alpha \exp(-\omega^\alpha t), \qquad \Delta J_0^\alpha = [\![J^\alpha]\!](t=0). \tag{302}$$

For small $[\![J^\alpha]\!]$, if $\nabla_0^\alpha J^\alpha$ remains negligible behind the wave front Σ^α, then the shock amplitude evolves at a rate determined by $\omega^\alpha = \text{constant}$. Jumps $[\![P^\alpha]\!]$, $[\![u^\alpha]\!]$, $[\![\theta^\alpha]\!]$, and $[\![\mathbf{b}^\alpha]\!]$ evolve proportionally via Eqs. 265–268. For weak shocks, $[\![\eta^\alpha]\!] \to 0$ by Eq. 269.

4.3.4 Homogenized Mixture Response

Preceding derivations and solutions of Sections 4.3.1–4.3.3 apply trivially for a single-phase material: $\alpha = N = 1$, $h^\alpha \to 0$, $\epsilon^\alpha \to 0$. They can also describe a shock moving with velocity $\mathcal{U}$ through the mixture as a whole per Section 2.4.2. Assuming $\upsilon^\alpha = \upsilon$ and $\theta^\alpha = \theta$ for all constituents, then $J^\alpha = J$, diffusion velocities $\boldsymbol{\mu}^\alpha = \mathbf{0}$, and thus $h^\alpha = 0$ and $\epsilon^\alpha = 0$. Then from Section 2.4, mixture quantities include Helmholtz free energy density $\psi = u - \theta\eta$ and

$$P = \sum_\alpha P^\alpha, \quad \rho_0 = \sum_\alpha n_0^\alpha\rho_{\mathrm{R}0}^\alpha, \qquad \rho_0 u = \sum_\alpha \rho_0^\alpha u^\alpha,$$
$$\hat{\mathsf{C}} = \sum_\alpha \hat{\mathsf{C}}^\alpha, \qquad \hat{\mathsf{G}} = \sum_\alpha \frac{\partial P^\alpha}{\partial\eta}, \qquad \eta = -\frac{\partial\psi}{\partial\theta}. \tag{303}$$

Since u^α is independent of $(\mathbf{a}^\beta, \mathbf{b}^\beta)\,\forall\,\beta \neq \alpha$ per Eq. 242 and here $\boldsymbol{\mu}^\alpha = \mathbf{0}$, it follows from Eq. 58 that

$$\mathbf{L}\cdot[\![\dot{\mathbf{a}}]\!] = \sum_\alpha \mathbf{L}^\alpha\cdot[\![D_t^\alpha\mathbf{a}^\alpha]\!]. \tag{304}$$

4.3.5 Weak Shocks in Soft Biologic Tissues

Quantities entering Λ^α of Eq. 299 and ω^α of Eq. 300 are evaluated for constitutive frameworks of Section 3. First, consider an ideal gas. Variables $(\mathbf{a}^\alpha, \mathbf{b}^\alpha)$ are irrelevant, $\rho_0^\alpha = n_0^\alpha \rho_{\mathrm{R}0}^\alpha$, and Eq. 130 for the ideal gas partial pressure and Eq. 132 for the ideal gas internal energy give

$$P^{\alpha+} = n_0^\alpha p_{\mathrm{R}0}^\alpha, \qquad \hat{\mathsf{C}}^{\alpha+} = n_0^\alpha p_{\mathrm{R}0}^\alpha (1+\gamma_0^\alpha), \tag{305}$$

$$\hat{\mathsf{C}}'^{\alpha+} = -n_0^\alpha p_{\mathrm{R}0}^\alpha (1+\gamma_0^\alpha)(2+\gamma_0^\alpha), \tag{306}$$

$$\hat{\mathsf{G}}^{\alpha+} = -\rho_0^\alpha \theta_0 \gamma_0^\alpha, \qquad \mathcal{C}^\alpha = [n_0^\alpha p_{\mathrm{R}0}^\alpha (1+\gamma_0^\alpha)/\rho_0^\alpha]^{1/2}, \tag{307}$$

$$(\partial \hat{\mathsf{G}}^\alpha / \partial J^\alpha)^+ = -\hat{\mathsf{G}}^{\alpha+}(1+\gamma_0^\alpha). \tag{308}$$

Next, consider a compressible fluid obeying the condensed matter EOS expressed in terms of internal energy density in Eqs. 139–142. With null cavitation for compression, internal variables ($\mathbf{a}^\alpha$, $\mathbf{b}^\alpha$) are again irrelevant, $\rho_0^\alpha = n_0^\alpha \rho_{\mathrm{R}0}^\alpha$, Eq. 308 holds, and

$$P^{\alpha+} = n_0^\alpha p_{\mathrm{R}0}^\alpha, \qquad \hat{\mathsf{C}}^{\alpha+} = n_0^\alpha (p_{\mathrm{R}0}^\alpha + B_\eta^\alpha), \tag{309}$$

$$\hat{\mathsf{C}}'^{\alpha+} = -n_0^\alpha \{2p_{\mathrm{R}0}^\alpha + B_\eta^\alpha (1 + B_{\eta\mathrm{p}}^\alpha)\}, \tag{310}$$

$$\hat{\mathsf{G}}^{\alpha+} = -\rho_0^\alpha \theta_0 \gamma_0^\alpha, \qquad \mathcal{C}^\alpha = [n_0^\alpha (p_{\mathrm{R}0}^\alpha + B_\eta^\alpha)/\rho_0^\alpha]^{1/2}. \tag{311}$$

Last, a solid tissue with the condensed matter EOS given by Eqs. 139–142, viscoelastic matrix, viscoelastic fibers, matrix- and fiber-damage is addressed. Bulk and shear viscoelasticity and fiber family $k = 1$ furnish internal variables $\mathbf{a}^\alpha \rightarrow \{\mathbf{\Gamma}_{\mathrm{V}l}^\alpha, \mathbf{\Gamma}_{\mathrm{S}m}^\alpha, \mathbf{\Gamma}_{\Phi k,n}^\alpha\}$ with initial conditions $\{\mathbf{\Gamma}_{\mathrm{V}l}^{\alpha+} = \mathbf{\Gamma}_{\mathrm{S}m}^{\alpha+} = \mathbf{\Gamma}_{\Phi k,n}^{\alpha+} = \mathbf{0}\}$. Rate-insensitive damage supplies order parameters $\mathbf{b}^\alpha \rightarrow \{\bar{D}^\alpha, D_k^\alpha\}$ with initial conditions $\{\bar{D}^{\alpha+} = D_k^{\alpha+} = 0\}$.

Fibers are either aligned, $\kappa_k^\alpha = 0$ parallel to (x, X^α), or isotropic, $\kappa_k^\alpha = \frac{1}{3}$. Constant active tension is permitted, affecting energy, stress $(\sigma_{\mathrm{A}})_1^1$, and stiffness via the energy density in Eq. 170 and the partial Cauchy stress in Eq. 171. Since $\Delta_k^\alpha = \mathrm{constant}$, active tension does not affect dissipation nor need enter $\mathbf{a}^\alpha$.

As usual, $\rho_0^\alpha = n_0^\alpha \rho_{\rm R0}^\alpha$ and $(\mathcal{C}^\alpha)^2 = \hat{\mathsf{C}}^{\alpha+}/\rho_0^\alpha$. Lengthy, yet routine, derivations yield

$$P^{\alpha+} = n_0^\alpha\{p_{\rm R0}^\alpha - (\sigma_{\rm A}^\alpha)_1^{1+}\}, \qquad \mathsf{G}^{\alpha+} = -\rho_0^\alpha\theta_0\gamma_0^\alpha; \tag{312}$$

$$(\partial\hat{\mathsf{G}}^\alpha/\partial J^\alpha)^+ = -\hat{\mathsf{G}}^{\alpha+}(1+\gamma_0^\alpha), \tag{313}$$

$$\hat{\mathsf{C}}^{\alpha+} = \mathsf{C}^{\alpha+}, \qquad \hat{\mathsf{C}}'^{\alpha+} = \mathsf{C}'^{\alpha+}, \qquad \hat{\mathsf{G}}^{\alpha+} = \mathsf{G}^{\alpha+}, \tag{314}$$

$$\mathsf{C}^{\alpha+} = \mathsf{C}_{\rm V}^{\alpha+} + \mathsf{C}_{\rm S}^{\alpha+} + \mathsf{C}_\Gamma^{\alpha+} + \mathsf{C}_{\rm A}^{\alpha+} + \mathsf{C}_{\rm F}^{\alpha+} + \mathsf{C}_\Phi^{\alpha+}, \tag{315}$$

$$\mathsf{C}'^{\alpha+} = \mathsf{C}_{\rm V}'^{\alpha+} + \mathsf{C}_{\rm S}'^{\alpha+} + \mathsf{C}_\Gamma'^{\alpha+} + \mathsf{C}_{\rm A}'^{\alpha+} + \mathsf{C}_{\rm F}'^{\alpha+} + \mathsf{C}_\Phi'^{\alpha+}; \tag{316}$$

$$\mathsf{C}_{\rm V}^{\alpha+} = n_0^\alpha(p_{\rm R0}^\alpha + B_\eta^\alpha), \qquad \mathsf{C}_{\rm S}^{\alpha+} = \tfrac{4}{3}n_0^\alpha\mu_{\rm S}^\alpha, \tag{317}$$

$$\mathsf{C}_\Gamma^{\alpha+} = n_0^\alpha\big(B_\theta^\alpha\sum_l \beta_{{\rm V}l}^\alpha + \tfrac{4}{3}\mu_{\rm S}^\alpha\sum_m \beta_{{\rm S}m}^\alpha\big), \tag{318}$$

$$\mathsf{C}_{\rm A}^{\alpha+} = n_0^\alpha(\partial^2\Psi_{{\rm A}k}^\alpha/\partial(J^\alpha)^2)^+ \qquad (k=1), \tag{319}$$

$$\mathsf{C}_{\rm F}^{\alpha+} = \begin{cases} \frac{8}{9}n_0^\alpha\mu_k^\alpha & (\kappa_k^\alpha = 0), \\ 0 & (\kappa_k^\alpha = \frac{1}{3}), \end{cases} \tag{320}$$

$$\mathsf{C}_\Phi^{\alpha+} = \begin{cases} \frac{8}{9}n_0^\alpha\mu_k^\alpha\sum_n \beta_{\Phi k,n}^\alpha & (\kappa_k^\alpha = 0), \\ 0 & (\kappa_k^\alpha = \frac{1}{3}); \end{cases} \tag{321}$$

$$\mathsf{C}_{\rm V}'^{\alpha+} = -n_0^\alpha\{2p_{\rm R0}^\alpha + B_\eta^\alpha(1+B_{\eta{\rm p}}^\alpha)\}, \tag{322}$$

$$\mathsf{C}_{\rm S}'^{\alpha+} = -\tfrac{28}{9}n_0^\alpha\mu_{\rm S}^\alpha, \tag{323}$$

$$\mathsf{C}_\Gamma'^{\alpha+} = -3n_0^\alpha\big(B_\theta^\alpha\sum_l \beta_{{\rm V}l}^\alpha + \tfrac{28}{27}\mu_{\rm S}^\alpha\sum_m \beta_{{\rm S}m}^\alpha\big), \tag{324}$$

$$\mathsf{C}_{\rm A}'^{\alpha+} = n_0^\alpha(\partial^3\Psi_{{\rm A}k}^\alpha/\partial(J^\alpha)^3)^+ \qquad (k=1), \tag{325}$$

$$\mathsf{C}_{\rm F}'^{\alpha+} = \begin{cases} \frac{24}{27}n_0^\alpha\mu_k^\alpha & (\kappa_k^\alpha = 0), \\ 0 & (\kappa_k^\alpha = \frac{1}{3}), \end{cases} \tag{326}$$

$$\mathsf{C}_\Phi'^{\alpha+} = \begin{cases} \frac{24}{27}n_0^\alpha\mu_k^\alpha\sum_n \beta_{\Phi k,n}^\alpha & (\kappa_k^\alpha = 0), \\ 0 & (\kappa_k^\alpha = \frac{1}{3}); \end{cases} \tag{327}$$

$$\mathbf{B}^{\alpha+} \to \mathbf{0}, \qquad \mathbf{b}_{\mathsf{a}}^{\alpha+} \to \mathbf{0}, \qquad \mathbf{b}'^{\alpha+} \to \mathbf{0}, \qquad \mathbf{b}_\eta^{\alpha+} \to \mathbf{0}, \tag{328}$$

$$\mathbf{A}^{\alpha+} \to -n_0^\alpha\left\{\frac{\partial\mathbf{Q}_{{\rm V}l}^\alpha}{\partial J^\alpha}, \frac{\partial\mathbf{Q}_{{\rm S}m}^\alpha}{\partial J^\alpha}, \frac{\partial\mathbf{Q}_{\Phi k,n}^\alpha}{\partial J^\alpha}\right\}^+, \tag{329}$$

$$\left(\frac{\partial(D_t^\alpha \mathbf{a}^\alpha)}{\partial J^\alpha}\right)^+ \to \left\{\frac{\partial \mathbf{Q}_{\mathrm{V}l}^\alpha/\partial J^\alpha}{\beta_{\mathrm{V}l}^\alpha B_\theta^\alpha \tau_{\mathrm{V}l}^\alpha}, \frac{\partial \mathbf{Q}_{\mathrm{S}m}^\alpha/\partial J^\alpha}{\beta_{\mathrm{S}m}^\alpha \mu_{\mathrm{S}}^\alpha \tau_{\mathrm{S}m}^\alpha}, \frac{\partial \mathbf{Q}_{\Phi k,n}^\alpha/\partial J^\alpha}{\beta_{\Phi k,n}^\alpha \mu_k^\alpha \tau_{\Phi k,n}^\alpha}\right\}^+,$$

$$\boldsymbol{\pi}_{\mathsf{a}}^{\alpha+} \to \mathbf{0}, \tag{330}$$

$$\mathbf{A}^{\alpha+} \cdot \left(\partial(D_t^\alpha \mathbf{a}^\alpha)/\partial J^\alpha\right)^+ \to \mathcal{A}_{\Gamma\mathrm{V}}^\alpha + \mathcal{A}_{\Gamma\mathrm{S}}^\alpha + \mathcal{A}_\Phi^\alpha, \tag{331}$$

$$\mathcal{A}_{\Gamma\mathrm{V}}^\alpha = -3n_0^\alpha B_\theta^\alpha \sum_l \frac{\beta_{\mathrm{V}l}^\alpha}{\tau_{\mathrm{V}l}^\alpha}, \qquad \mathcal{A}_{\Gamma\mathrm{S}}^\alpha = -\tfrac{8}{3} n_0^\alpha \mu_{\mathrm{S}}^\alpha \sum_m \frac{\beta_{\mathrm{S}m}^\alpha}{\tau_{\mathrm{S}m}^\alpha},$$

$$\mathcal{A}_\Phi^\alpha = \begin{cases} -\frac{32}{27} n_0^\alpha \mu_k^\alpha \sum_n \beta_{\Phi k,n}^\alpha / \tau_{\Phi k,n}^\alpha & (\kappa_k^\alpha = 0), \\ 0 & (\kappa_k^\alpha = \frac{1}{3}). \end{cases} \tag{332}$$

For rate-insensitive damage, from $\bar{\pi}_{\mathrm{D}}^\alpha = 0$ and $\pi_{\mathrm{D}k}^\alpha = 0$ via Eq. 241, and using Eqs. 268 and 328 with $\bar{\vartheta}^\alpha = \vartheta_k^\alpha = 2$, a quadratic approximation for matrix and fiber damages incurred across the shock front is derived:

$$\bar{D}^{\alpha-} = \frac{1}{n_0^\alpha \bar{E}_{\mathrm{C}}^\alpha} (\mathsf{C}_{\mathrm{S}}^{\alpha+} + \mathsf{C}_\Gamma^{\alpha+}) [\![J^\alpha]\!]^2 + O([\![J^\alpha]\!]^3), \tag{333}$$

$$D_k^{\alpha-} = \frac{1}{n_0^\alpha E_{\mathrm{C}k}^\alpha} (\mathsf{C}_{\mathrm{F}}^{\alpha+} + \mathsf{C}_\Phi^{\alpha+}) [\![J^\alpha]\!]^2 + O([\![J^\alpha]\!]^3). \tag{334}$$

Notice $D_k^{\alpha-} \to 0$ in Eq. 334 if $\kappa_k^\alpha = \frac{1}{3}$. To at least $O([\![J^\alpha]\!]^2)$, matrix fracture in Eq. 333 and fiber fracture Eq. 334 are unaffected by Finsler versus Euclidean metrics $(\mathbf{g}, \mathbf{G}^\alpha)$ for current prescriptions $\bar{r}^\alpha \geq 2$ and $\tilde{r}_k^\alpha \geq 2$. From $\mathbf{b}^{\alpha+} \to \mathbf{0}$ and Eq. 328, rate-insensitive fractures do not affect weak-shock evolution in Eqs. 299–302 to second order in $[\![J^\alpha]\!]$.

If fractures are instead rate dependent (i.e., dissipative), then $\mathbf{b}^\alpha \to \mathbf{0}$ and $\mathbf{a}^\alpha \to \{\boldsymbol{\Gamma}_{\mathrm{V}l}^\alpha, \boldsymbol{\Gamma}_{\mathrm{S}m}^\alpha, \boldsymbol{\Gamma}_{\Phi k,n}^\alpha, \bar{D}^\alpha, D_k^\alpha\}$. Then Eq. 252 yields $\bar{D}^{\alpha-} = 0$ and $D_k^{\alpha-} = 0$ in lieu of Eqs. 333 and 334. From Eq. 201 for matrix rupture and Eq. 206 for fiber fracture, damage kinetics do not contribute to $\mathbf{A}^{\alpha+}$ or $\boldsymbol{\pi}_{\mathsf{a}}^{\alpha+}$. Nor do such kinetics affect Λ^α of Eq. 299 or ω^α of Eq. 300. Equations 329–331 are unchanged.

Thus, an important conclusion is that *weak* shock decay distances, in the setting of the present linear approximation and phase-field type energy functions with equilibrium conditions (i.e., rate independence) or Ginzburg–Landau type kinetics (i.e., rate dependence), are not affected by either rate-independent or rate-dependent damage to first order in $[\![J^\alpha]\!]$. Importantly, damage, regardless of any rate dependence, can still affect *strong* shock evolution in Eqs. 291–295.

Phase interactions, in contrast, strongly affect Λ^α and ω^α. From Eqs. 209–212,

$$\left(\frac{\partial h^\alpha}{\partial \upsilon^\alpha}\right)^+ = -\sum_{\beta\neq\alpha} \bar{\lambda}^{\alpha\beta+}, \qquad \left(\frac{\partial \epsilon^\alpha}{\partial \theta^\alpha}\right)^+ = -\sum_{\beta\neq\alpha} \bar{\omega}^{\alpha\beta+}. \tag{335}$$

Consider now a two-phase mixture of solid ($\alpha = 1 \to \mathrm{s}$) and fluid ($\alpha = 2 \to \mathrm{f}$). Adopting physics of Regueiro et al.[72] and Suh and Sun,[76]

$$\bar{\lambda}^{12+} = (n_0^{\mathrm{f}})^2 \hat{\mu}^{\mathrm{f}}/\Xi, \qquad \bar{\omega}^{12+} = \alpha_{\mathrm{v}} \kappa^{\mathrm{fs}}, \tag{336}$$

with fluid viscosity $\hat{\mu}^{\mathrm{f}}$, system permeability Ξ, interfacial area per unit volume α_{v}, and heat transfer coefficient κ^{fs}. Although macroscopic Newtonian viscosity and Fourier conduction are excluded for singular shocks,[196,197] microscopic h^α and ϵ^α include viscosity and heat transfer. As noted in Section 1, the effect of fluid viscosity $\hat{\mu}^{\mathrm{f}}$ manifests through a finite permeability Ξ. In the limit that $\Xi \to \infty$ or $\hat{\mu}^{\mathrm{f}} \to 0$, effects of viscous drag are negligible.

Recall from Eq. 273 that the weak-shock solution in Eq. 302 for a multi-phase material corresponds to strain jump ΔJ_0^α and resulting discontinuities in P^α and θ^α applied as a loading condition for one phase α, with all other phase $\beta = 1, 2, \ldots \alpha - 1, \alpha + 1, \ldots, N$ witnessing no discontinuities in J^β, P^β, or θ^β. This shock moves through all phases at speed $\mathcal{C}^\alpha$; phase interactions h^α and ϵ^α induce decay in amplitude $[\![J^\alpha]\!](t)$ so long as $\bar{\lambda}^{\alpha\beta} > 0$ and $\bar{\omega}^{\alpha\beta} > 0$. Velocities υ^β and temperatures θ^β ($\beta \neq \alpha$) can evolve continuously in space–time behind the wave front from such interactions, their values indeterminate from the outcome of the linear analysis.

In contrast, if the mixture is idealized as homogeneous with matching υ^α and θ^α, then h^α and ϵ^α do not explicitly affect shock evolution. In this "tied" case, ΔJ_0^α is applied simultaneously at $t = 0$ to all phases $\alpha = 1, \ldots, N$ as a loading condition. Speed $\mathcal{C} = (\hat{\mathsf{C}}/\rho_0)^{1/2}$ results from stiffness and density of the whole mixture in Eq. 303, and

$$\hat{\mathsf{C}}'^{+} = \sum_\alpha \hat{\mathsf{C}}'^{\alpha+}, \qquad \hat{\mathsf{G}}^+ = -\rho_0 \theta_0 \frac{\sum_\alpha \gamma_0^\alpha \rho_0^\alpha c_\epsilon^\alpha}{\sum_\alpha \rho_0^\alpha c_\epsilon^\alpha}. \tag{337}$$

4.4 Properties and Predictions

4.4.1 Skeletal Muscle, Liver, and Lung

The analytical solution for weak shock evolution, Eqs. 299–302, is applied in Section 4.4.1 to three biologic systems at $\theta_0 = 310\,\mathrm{K}$, each comprised of one solid tissue phase and one fluid: skeletal muscle with interstitial fluid, liver with blood, and lung with air. Physical properties or parameters, ω^α, and Λ^α are given in Table 3 for each component, and for the homogeneous idealization of Eqs. 303, 304, and 337 labeled "Mixture." Shock loading of skin tissue is modeled in Section 4.4.2.

Constitutive and metric-tensor parameters are those for rabbit skeletal muscle and bovine lung of Section 4.2, Table 1 (ECF, blood) and Table 2 (solid phases). For muscle, active tension from Eq. 238 affects initial stress but does not appreciably change tabulated results (not shown).

Air is modeled as an ideal gas[87] with $\mathfrak{R}^\alpha = 287\,\mathrm{J/kg\,K}$ and $\gamma_0^\alpha = 0.4$. Viscosity for air[72] in Eq. 336 is $\hat{\mu}^\mathrm{f} = 18.3\,\mu\mathrm{Pa\,s}$. Solid properties are for canine lung[8,36,87] with bulk and shear viscoelasticity ($l = m = 1$), isotropic fibers ($\kappa_k^\alpha = \frac{1}{3}$), solid fraction $n_0^1 = 0.336$, $B_\eta^\alpha = 164\,\mathrm{kPa}$, $\mu_\mathrm{S}^\alpha = 2.98\,\mathrm{kPa}$, $\beta_{\mathrm{V}l}^\alpha = 0.009$, $\beta_{\mathrm{S}m}^\alpha = 1.5$, and $\tau_{\mathrm{V}l}^\alpha = \tau_{\mathrm{S}m}^\alpha = 0.5\,\mathrm{s}$. Values $\gamma_0^\alpha = 0.114$ and $\bar{E}_\mathrm{C}^\alpha = 22.7\,\mathrm{kPa}$, unmeasured for lung parenchyma, are borrowed from liver parenchyma. This value of γ_0^α for lung is approximately twice that of Clayton,[87] with the latter estimate $10^3\times$ that of classical thermodynamics[103] using the low B_θ^α of the highly porous structure.

In Eq. 336, $\Xi = 6.7 \times 10^{-18}\mathrm{m}^2$ for muscle,[218] $\Xi = 1.5 \times 10^{-14}\mathrm{m}^2$ for liver,[15] and $\Xi = 1.83 \times 10^{-10}\mathrm{m}^2$ for lung.[72] Regarding heat transfer, $\kappa^\mathrm{fs} = 6\,\mathrm{W/m^2\,K}$ for muscle and liver,[187] and $\kappa^\mathrm{fs} = 41.2\,\mathrm{W/m^2\,K}$ for lung.[219] From idealized microstructure geometries,[2,209,218] a contact area estimate for muscle is $\alpha_\mathrm{v} = \pi/R_0$ with $R_0 = 30\,\mu\mathrm{m}$ the fiber radius,[88] for liver $\alpha_\mathrm{v} = 2n_0^\mathrm{f}/R_0$ with $R_0 = 4\,\mu\mathrm{m}$ the capillary radius,[187] and for lung $\alpha_\mathrm{v} = \pi/(2R_0)$ with $R_0 = 30\,\mu\mathrm{m}$ the alveolar radius.[36]

Table 3 Shock evolution parameters for rabbit muscle comprising ECF and solid ($n_0^1 = 0.9$), bovine liver (blood and solid, $n_0^1 = 0.88$), and canine lung (air and solid, $n_0^1 = 0.336$). "Mixture" invokes same shock simultaneously to each phase. $(\Delta P)_0^\alpha$, $(\Delta\theta)_0^\alpha$, $(\Delta\bar{D})_0^\alpha$, and $(\Delta D_1)_0^\alpha$ are initial stress, temperature, and matrix and fiber damage jumps, respectively, for initial strain change $\Delta J_0^\alpha = [\![J^\alpha]\!](t=0) = -0.1$.

Property or		**Muscle**			**Liver**			**Lung**	
prediction (units)	**ECF**	**Solid**	**Mixture**	**Blood**	**Solid**	**Mixture**	**Air**	**Solid**	**Mixture**
ρ_0^α (g/cm^3)	0.103	0.990	1.093	0.127	0.933	1.060	7.56×10^{-4}	0.337	0.338
$\hat{\mathsf{C}}^{\alpha+}$ (GPa)	0.220	2.954	3.174	0.317	2.350	2.667	9.42×10^{-5}	9.26×10^{-5}	1.87×10^{-4}
$\hat{\mathsf{C}}'^{\alpha+}$ (GPa)	-1.751	-26.57	-28.32	-4.118	-21.15	-25.27	-2.26×10^{-4}	-2.42×10^{-4}	-4.68×10^{-4}
$\mathcal{C}^\alpha$ (km/s)	1.462	1.727	1.704	1.578	1.587	1.586	0.353	1.66×10^{-2}	2.35×10^{-2}
$\hat{\mathsf{G}}^{\alpha+}$ (g K/cm^3)	-4.215	-96.06	-99.15	-6.309	-32.97	-39.31	-9.38×10^{-2}	-11.91	-11.95
ω^α (1/s)	8.69×10^{9}	9.05×10^{8}	7.01×10^{-3}	1.89×10^{7}	2.57×10^{6}	6.62×10^{-2}	2.97×10^{4}	1.13×10^{2}	2.95×10^{-2}
Λ^α (1/m)	2.99×10^{6}	2.33×10^{5}	1.84×10^{-6}	3.68×10^{3}	7.21×10^{2}	1.76×10^{-5}	1.40×10^{2}	1.04×10^{1}	2.01×10^{-3}
$(\Delta P)_0^\alpha$ (MPa)	30.8	428	459	52.3	341	393	1.06×10^{-2}	1.05×10^{-2}	2.10×10^{-2}
$(\Delta\theta)_0^\alpha$ (K)	4.32	10.3	9.66	5.25	3.73	3.92	13.3	3.73	3.74
$(\Delta\bar{D})_0^\alpha$ (-) matrix	...	0.045	0.045	...	0.100	0.100	...	5.03×10^{-3}	5.03×10^{-3}
$(\Delta D_1)_0^\alpha$ (-) fibers	...	0.022	0.022	...	0	0	...	0	0

The lower four rows of Table 3 contain initial jumps in stress of Eq. 265, temperature of Eq. 267, matrix damage of Eq. 333, and fiber fracture of Eq. 334, each to $O([\![J^\alpha]\!]^2)$ for initial strain jump $\Delta J_0^\alpha = -0.1$. If damage is modeled as rate dependent, its jumps must vanish instead in the infinitesimal-width shock approximation of Eq. 252 to avoid infinite dissipation in the shock front. Normalized exponential decay of $[\![P^\alpha]\!]$ and $[\![\theta^\alpha]\!]$ arising from Eq. 302 is shown for each component of each two-phase system in Fig. 6. When mixtures are shocked uniformly, decay from viscoelastic dissipation alone manifests over much larger distances (not shown).

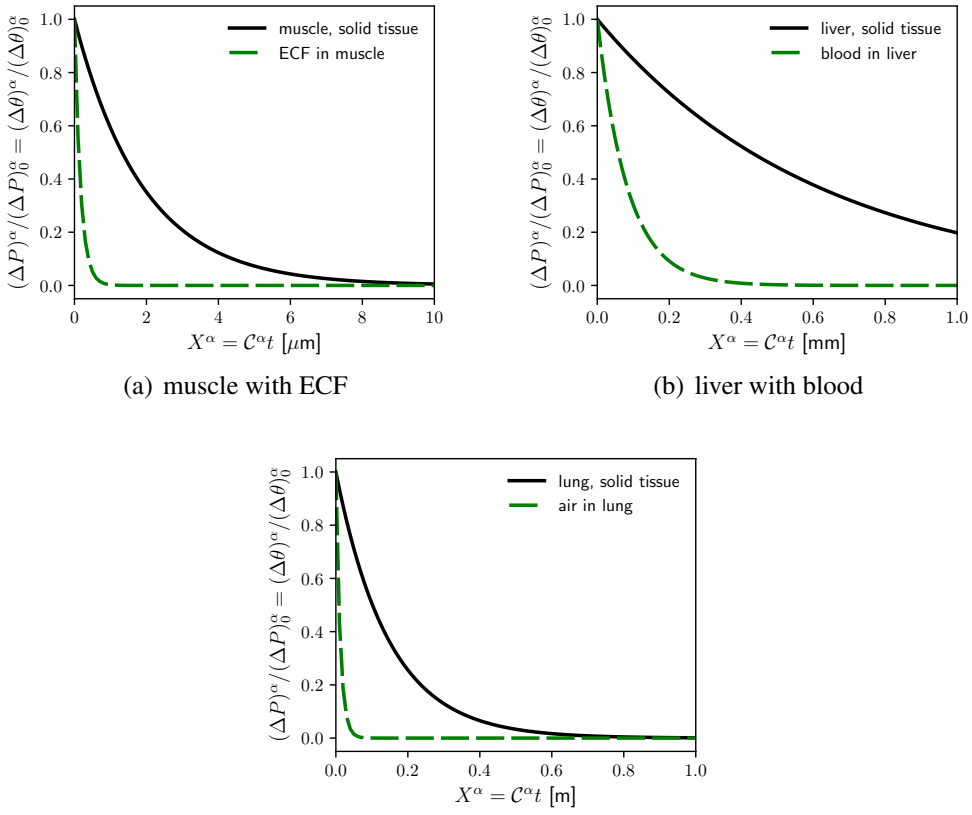

(a) muscle with ECF

(b) liver with blood

(c) lung with air

Fig. 6 Predicted ratio of jump in shock stress $(\Delta P)^\alpha$ or temperature $(\Delta\theta)^\alpha$ normalized by initial magnitude $(\Delta P)_0^\alpha$ or $(\Delta\theta)_0^\alpha$, for shock amplitude ΔJ_0^α applied individually to phase α, vs. propagation distance X^α in the weak shock limit: (a) rabbit muscle, (b) bovine liver, and (c) canine lung. Wave speed is $\mathcal{C}^\alpha$; different scales (i.e., μm, mm, or m) used for X^α.

From Table 3 and Fig. 6, when ΔJ_0^α is applied to one constituent alone, then $|\Lambda^\alpha|$ and $|\omega^\alpha|$ are relatively large, with $\omega^\alpha > 0$ for transient decay. For $\mathrm{d}P_{\mathrm{H}}^\alpha/\mathrm{d}[\![J^\alpha]\!] \approx -\hat{\mathsf{C}}^{\alpha-} < 0$ and since $\Lambda^\alpha > 0$, a negative stress gradient $\nabla_0 P^{\alpha-}$ is needed for a steady shock. In a steady shock, P^α should decrease steeply as Σ^α is approached from the $(\cdot)^-$ side.

For muscle and liver, $(\partial h^\alpha/\partial \upsilon^\alpha)^+$ is the dominant contribution to ω^α due to relatively large $1/\Xi$ and $\hat{\mu}^{\mathrm{f}}$ in Eq. 336. For lung, both $(\partial h^\alpha/\partial \upsilon^\alpha)^+$ and $(\partial \epsilon^\alpha/\partial \theta^\alpha)^+$ have significant influence on shock decay, the latter due to a comparatively low $\mathcal{C}^\alpha$. Viscoelastic dissipation embodied in $\mathcal{A}_{\Gamma\mathrm{V}}$, $\mathcal{A}_{\Gamma\mathrm{S}}$, and $\mathcal{A}_\Phi$ has relatively small effects, negligible compared to interphase drag and heat exchange. The nearly incompressible viscoelastic response of these soft biologic tissues, also typical of soft polymers at high rates,[220] leads to small glassy shear moduli relative to bulk moduli, the latter (bulk moduli) modeled here as having little or no viscoelastic relaxation.

From Fig. 6, decay distance is shortest in muscle and longest in lung. In each system, a shock applied to the fluid decays over a much shorter distance than one applied to the solid. From Table 3, stress rises $(\Delta P)_0^\alpha$ are highest in solid phases of muscle and liver having largest tangent moduli. Temperature $(\Delta\theta)_0^\alpha$ is greatest in air in the lung.

Damage is greatest in liver and smallest in lung. Fiber damage is absent in both of these organs (i.e., liver and lung) in the weak-shock limit because their fiber distributions are idealized as isotropic. In anisotropic muscle, fiber damage $(\Delta D_k)_0^\alpha$ is $\approx \frac{1}{2}\times$ matrix damage $(\Delta \bar{D})_0^\alpha$, in contrast to (strong-shock) Hugoniot solutions of Figs. 3b and 3c whereby these damage mechanisms evolve more similarly.

When ΔJ_0^α is applied to both phases at once and the homogeneous idealization is invoked, $|\Lambda^\alpha|$ and $|\omega^\alpha|$ are deemed small, with contributions only from viscoelasticity. As noted in Section 4.3.5, damage does not affect $|\Lambda^\alpha|$ or $|\omega^\alpha|$ in the linear weak-shock limit. Furthermore, dissipative transfers of momentum and energy cannot contribute to decay of a shock applied uniformly to all constituents in the "Mixture" idealization because velocity and temperature differences among constituents are not resolved. For these homogenized conditions, weak shocks should be steady with near-uniform stress–strain states trailing their wave fronts. Weak-shock experiments are needed to confirm this prediction; known data[88] are for strong shocks.

4.4.2 Skin

Skin exhibits a complex layered microstructure. The middle and outer layers of skin are the dermis and epidermis, with elastin and collagen fibers embedded in a ground matrix. Underlying hypodermis (i.e., adipose) can be labeled an inner layer of the skin. The collagenous microstructure dictates finite-strain nonlinear, anisotropic, viscoelastic, and tearing behaviors. Orthotropy of skin arises from preferred arrangements of the collagen fibers, leading to greater stiffness in directions along which proportionally more fibers are aligned. In the plane of the dermis, fibers tend to be dispersed about a primary axis along which stiffness is greatest. In vivo, resting skin tension is greatest along this axis, parallel to Langer's lines.[221] In typical uniaxial and biaxial tests,[3,18,128,222] extracted skin is unstretched initially, but the greater stiffness along the primary direction parallel to Langer's lines persists. Differences in elastic stiffness also emerge between orthogonal in-plane and out-of-plane directions.[221,222]

Damage processes in skin tissue are also anisotropic due to fiber degradation that differs with respect to direction of loading relative to the microstructure.[18,97,223] Rupture stress tends to be larger, and failure elongation lower, for stretching in the stiffer direction.[18,221,224] The Finsler-geometric model of Clayton[97] predicts that skin is more brittle in directions parallel to Langer's lines than perpendicular to Langer's lines, in concurrence with experiment.[18,224] Collagen fibers are less coiled initially in directions parallel to Langer's lines,[221] giving the skin lower compliance and less potential strain accommodation at rupture in those directions.

Skin, like most biological tissue, is simultaneously nonlinear anisotropic elastic, viscoelastic, and poroelastic.[3,225] Poromechanical effects are not explicitly resolved in most continuum mechanical treatments[18,25,97,221,224,226] that focus on skin's nonlinear elastic, and possibly viscoelastic, response. Nonetheless, a few models for skin tissue mechanics resolving the solid and fluid phases and their interactions exist. A continuum mixture theory similar to that of Bowen[67] was applied to the skin in the mid-1980s.[227–229] More recent works account for layered and fibrous microstructures in the context of a nonlinear poroelastic theory.[17,230] The total liquid content of the dermis is around 70% by weight,[17,230–232] whereas the epidermis contains around 15% water weight. However, not all fluid is mobile: some is entrapped in cells or otherwise locally bound to the microstructure. Samant and Prausnitz[232] report that the *mobile* interstitial fluid makes up 24% by weight of hydrated pig

skin, corresponding to a mobile interstitial fluid volume fraction of approximately 27%.

In the present subsection of this report, the 3-D theory and constitutive framework of Sections 2 and 3 are applied to the skin, treated as a two-phase mixture of *mobile* interstitial fluid represented as ECF and a solid-tissue phase comprised of matrix (including cells, blood vessels, ground substance, and trapped fluids) and collagen fibers. Bound fluid distinct from the mobile ECF contributes to compressibility and viscoelastic properties of the solid-tissue phase. The resulting model and properties are then used to study shock decay in the skin according to the analysis and solutions derived in Section 4.3, in a manner fully analogous to that invoked for muscle, liver, and lung in Section 4.4.1.

Many aspects and properties are adapted from a previous 2-D differential-geometric model[97] of orthotropic skin that addressed nonlinear elastic and tearing behaviors in rabbit skin but did not consider temperature changes, viscoelasticity, or poromechanics explicitly. As noted in Section 1, processes of fiber uncoiling and reorientation[18] are not modeled explicitly, but their effects are embedded implicitly in constitutive functions and parameters for nonlinear elasticity, viscoelasticity, and damage. Time durations for shock wave loading may be too brief to allow for transient (but not a priori) remodeling, regardless of its likely observation at low tensile strain rates near crack tips.[18] Initial fiber or matrix tensions are likewise omitted in the analysis.

Let superscript index $\alpha = 1$ for the solid, with $\alpha = 2$ for the fluid. The initial, respective solid and mobile fluid volume fractions[232] are $n_0^1 = 0.73$ and $n_0^2 = 0.27$. The interstitial fluid phase is modeled identically to the ECF used for skeletal muscle in Sections 4.1.2 and 4.4.1, with properties listed in Table 1. The solid tissue is modeled with two families of dispersed fibers, having subscript $k = 1$ or $k = 2$, within the plane of the dermis.[128] Physical properties and model parameters for each family are identical, and the smaller of the two angles between the fiber directions $(\boldsymbol{\iota}_1, \boldsymbol{\iota}_2)$ is of magnitude $2\varphi = \cos^{-1}(\boldsymbol{\iota}_1 \cdot \boldsymbol{\iota}_2)$. See Fig. 7 that shows the fiber geometry relative to the primary direction of Langer's lines. Taking data from Annaidh et al.[128] on human torso skin as representative, $\varphi = 41^\circ$ and the fiber dispersion factor in Eq. 147 is $\kappa_k^\alpha = \kappa_1^1 = \kappa_2^1 = 0.15$.

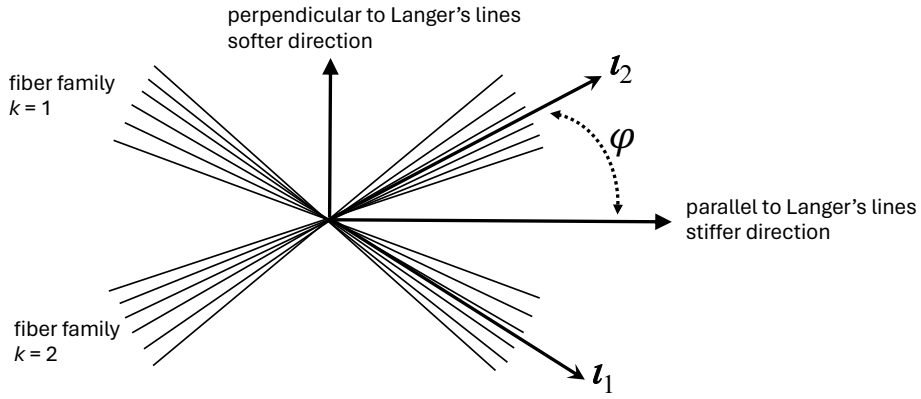

Fig. 7 Geometry of dispersed skin fibers. Two fiber families $k = 1, 2$ with identical physical properties and dispersion factors $\kappa_k^\alpha = \kappa_1^1 = \kappa_2^1$ have referential director vectors $\boldsymbol{\iota}_1$ and $\boldsymbol{\iota}_2$ and are subtended by an angle of magnitude 2φ. Shock loading is applied independently in directions parallel or perpendicular to Langer's lines in the plane of the skin, or is applied normal to the plane of the skin.

The theory of Sections 2 and 3 applies verbatim, as do the treatment of shock evolution and general analytical solutions in Sections 4.3.1–4.3.4. Several additions are needed for the current application to fibrous biologic tissues in Section 4.3.5. The treatment in Section 4.3.5 considered only one family of fibers ($k = 1$) either fully dispersed ($\kappa_k^\alpha = \frac{1}{3}$) or fully aligned ($\kappa_k^\alpha = 0$), with the shock wave moving parallel to the fiber direction in the latter case. Here, two equivalent families of fibers can be partially dispersed (i.e., $0 < \kappa_k^\alpha < \frac{1}{3}$) and three possible directions are considered for shock-wave loading. Referring to Fig. 7, the first is parallel to Langer's lines, the second perpendicular to Langer's lines, and the third direction is normal to both of the former two, corresponding to impact through the thickness of the skin.

Specifically, Eqs. 320 and 321 for fiber contributions to longitudinal elastic and viscoelastic stiffness, their volume derivatives in Eqs. 326 and 327, and the contribution of viscous dissipation to shock decay in Eq. 332 all require extension for two families of partially dispersed fibers. For the first case (i.e., shock loading parallel to Langer's line direction), differentiation of the elastic and viscoelastic energy densities produces, for the total contributions from both fiber families having identical

properties besides orientation,

$$\mathsf{C}_{\mathrm{F}}^{\alpha+} = \tfrac{16}{9} n_0^\alpha \mu_k^\alpha (1 - 3\kappa_k^\alpha)^2 (\cos^2\varphi - \tfrac{1}{2}\sin^2\varphi), \tag{338}$$

$$\mathsf{C}_{\Phi}^{\alpha+} = \tfrac{16}{9} n_0^\alpha \mu_k^\alpha (1 - 3\kappa_k^\alpha)^2 (\cos^2\varphi - \tfrac{1}{2}\sin^2\varphi) \{\sum_n \beta_{\Phi k,n}^\alpha\}; \tag{339}$$

$$\begin{aligned}\mathsf{C}_{\mathrm{F}}'^{\alpha+} = {} & \tfrac{8}{9} n_0^\alpha \mu_k^\alpha (1 - 3\kappa_k^\alpha) \{\tfrac{2}{3} + 2\kappa_k^\alpha + (1 - 3\kappa_k^\alpha)\sin^2\varphi \\ & + 4(\cos^2\varphi - \tfrac{1}{2}\sin^2\varphi)[2\kappa_k^\alpha + \tfrac{1}{3}(1 - 3\kappa_k^\alpha)(\cos^2\varphi - 5\sin^2\varphi)]\},\end{aligned} \tag{340}$$

$$\begin{aligned}\mathsf{C}_{\Phi}'^{\alpha+} = {} & \tfrac{8}{9} n_0^\alpha \mu_k^\alpha (1 - 3\kappa_k^\alpha) \{\tfrac{2}{3} + 2\kappa_k^\alpha + (1 - 3\kappa_k^\alpha)\sin^2\varphi + 4(\cos^2\varphi - \tfrac{1}{2}\sin^2\varphi) \\ & \times [2\kappa_k^\alpha + \tfrac{1}{3}(1 - 3\kappa_k^\alpha)(\cos^2\varphi - 5\sin^2\varphi)]\} \{\sum_n \beta_{\Phi k,n}^\alpha\};\end{aligned} \tag{341}$$

$$\mathcal{A}_{\Phi}^{\alpha} = -\tfrac{32}{81} n_0^\alpha \mu_k^\alpha [5 + 9(\sin^2\varphi - \tfrac{1}{3})^2 + 18\sin^2\varphi\cos^2\varphi] \{\sum_n \beta_{\Phi k,n}^\alpha / \tau_{\Phi k,n}^\alpha\}. \tag{342}$$

For case 2, namely shock compression along the direction perpendicular to Langer's lines, Eqs. 338–342 apply after making the transformation $\varphi \to 90^\circ - \varphi$. For case 3, meaning compression normal to the plane of the skin tissue, Eqs. 338–342 apply upon setting $\varphi = 90^\circ$.

Parameters, excluding those for phase interactions, are listed in Table 4. Values of the ECF are repeated for reference, and properties of the mixture as a whole are shown for completeness. For the solid tissue phase, properties entering the EOS, specifically $\rho_{\mathrm{R}0}^\alpha$, B_η^α, γ_0^α, and c_ϵ^α, are found via use of the mixture rules in Eqs. 227–230 in conjunction with known values for the fluid ($\alpha = 2$) phase (i.e., ECF), initial volume fraction $n_0^1 = 0.73$, and properties for the skin as a whole (solid + fluid). The latter include the bulk sound speed,[233] pressure derivative of the bulk modulus,[234] mass density and specific heat,[235,236] and thermal expansion coefficient[186] used to calculate the Grüneisen parameter. Nonlinear stiffening coefficient k_{V}^α is assumed to match that of muscle and liver in the absence of sufficient data for its precise calibration. Shear moduli μ_{S}^α and μ_k^α and the fiber stiffening factor $k_k^\alpha = k_1^1 = k_2^1$ are obtained from several prior works on nonlinear elasticity of rabbit and human skin.[97,128]

Viscoelastic stiffening at strain rates ranging from approximately 0.01/s to 3000/s is of similar strength in porcine skin,[237] liver,[208] and skeletal muscle.[200] Therefore, order-of-magnitude estimates for $\beta_{\mathrm{S}m}^\alpha$ and $\beta_{\Phi k,n}^\alpha$ and relaxation times $\tau_{\mathrm{S}m}^\alpha$ and $\tau_{\Phi k,n}^\alpha$ are based on high-rate data for skin[237] and comparable values for liver and muscle (Table 2). For the present shock evolution analysis, the viscoelastic response is

dominated by the relaxation mode of matrix or fibers with the largest stiffening factor $\beta^\alpha_{\mathrm{S}m}$ or $\beta^\alpha_{\Phi k,n}$ and shortest relaxation time $\tau^\alpha_{\mathrm{S}m}$ or $\tau^\alpha_{\Phi k,n}$. Therefore, one primary mode labeled by $m = n = 1$ is sufficient, with $\alpha = 1$ and $k = 1, 2$.

Table 4 Physical properties or model parameters for rabbit skin: interstitial fluid phase (ECF, $\alpha = 2$), solid tissue phase ($\alpha = 1$), and homogenized mixture ($n^1_0 = 0.73$)

Property (units)	ECF (fluid phase)	Rabbit skin (solid)	Mixture
$\rho^\alpha_{\mathrm{R}0}$ (g/cm^3)	1.03	1.26	1.20
B^α_η (GPa)	2.20	3.37	3.05
c^α_ϵ (J/g K)	3.96	3.01	3.23
γ^α_0 (-)	0.132	0.276	0.231
$B^\alpha_{\eta\mathrm{p}}$ (-)	6.96	7.22	7.15
k^α_{V} (-)	7.0	6.0	...
μ^α_{S} (MPa)	...	0.27	0.20
μ^α_k (MPa)	...	1.64	1.20
k^α_k (-)	...	0.17	0.17
$\beta^\alpha_{\mathrm{S}1}$ (-)	...	100	100
$\beta^\alpha_{\Phi k,1}$ (-)	...	100	100
$\tau^\alpha_{\mathrm{S}1}$ (s)	...	1.0×10^{-3}	1.0×10^{-3}
$\tau^\alpha_{\Phi k,1}$ (s)	...	1.0×10^{-3}	1.0×10^{-3}
J_{C} (kJ/m^2)	...	1.0	1.0
l^α (mm)	...	0.04	0.04
ϑ^α (-)	...	2.0	2.0
$\epsilon^\alpha_{\mathrm{r}}$ (-)	...	0.15	0.15
$\bar{r}^\alpha = \tilde{r}^\alpha_k$ (-)	...	2.0	2.0

Experiments[18] and prior modeling[97] suggest that fiber fracture and debonding occur sooner than matrix rupture in tensile loading of rabbit skin. This implies that fibers should have lower toughness, and therefore lower fracture surface energy and cohesive energy, than the isolated matrix. Denote by $\phi_{\mathrm{F}} = \mathsf{J}^\alpha_{\mathrm{C}k}/\bar{\mathsf{J}}^\alpha_{\mathrm{C}}$ the ratio of toughness of a single fiber family k to that of the matrix, and assign the same regularization length $l^1 = \bar{l}^1 = l^1_1$ to all components of the solid phase $\alpha = 1$. Then with J_{C} the total measured fracture toughness of the skin,[223,238,239] assuming the fluid supports negligible tensile load in unconfined toughness experiments, and denoting by K_{F} the total number of fiber families, cohesive energies of matrix and fibers are estimated as

$$2l^1(1 + K_{\mathrm{F}}\phi_{\mathrm{F}})\bar{E}^1_{\mathrm{C}} = n^1_0\mathsf{J}_{\mathrm{C}}, \qquad E^1_{\mathrm{C}1} = \phi_{\mathrm{F}}\bar{E}^1_{\mathrm{C}}. \tag{343}$$

In the present application, $K_{\mathrm{F}} = 2$, and from previous work,[97] $K_{\mathrm{F}}\phi_{\mathrm{F}} = 0.84$. Degradation exponents $\vartheta^1 = \bar{\vartheta}^1 = \vartheta^1_1$ and quantities affecting the Finsler metric,

namely remnant strain $\epsilon_{\rm r}^1 = \bar{\epsilon}_{\rm r}^1 = \tilde{\epsilon}_{\rm r1}^1$ and exponential factor $\bar{r}^1 = \tilde{r}_1^1$, are also obtained from that reference.[97]

Lastly, parameters controlling momentum and energy exchange between solid and fluid are needed. For the former, in the first equality of Eq. 336, $\Xi = 1.76 \times 10^{-16} \mathrm{m}^2$ for skin,[225] a value intermediate among those reported in the literature.[17,227,229,230,240] For the latter, in the second equality in Eq. 336, $\kappa^{\rm fs} = 6\,\mathrm{W/m^2\,K}$ is estimated from Chato.[187] Applying a columnar idealization of the geometry of the fibrous microstructure of the dermis,[241] the surface area density is $\alpha_{\rm v} = 2n_0^{\rm f}/R_0$ with $R_0 = 5\,\mu$m the collagen fiber radius.[18]

Outcomes of the shock evolution analysis are reported in Table 5 and Fig. 8. The former is analogous to Table 3. It contains properties affecting shock decay as well as initial jumps in stress of Eq. 265, temperature of Eq. 267, matrix damage of Eq. 333, and fiber fracture of Eq. 334, each to $O(\llbracket J^\alpha \rrbracket^2)$ for initial strain jump $\Delta J_0^\alpha = -0.1$. Recall that if damage is rate dependent, its jumps are zero instead in the linearized weak-shock approximation. Results for the fluid phase do not depend at all on the shock direction. Nearly all results for the solid phase and homogenized mixture vary only slightly with orientation of the shock wave with respect to the microstructure. Fiber orientations only affect the deviatoric response.

Most quantities entering the shock-decay analysis are dominated by the bulk compressibility that is independent of fiber direction. A notable exception is the damage predicted for fibers in the bottom row of Table 5. Fiber fracture is most severe for loading parallel to Langer's lines. In this loading protocol, the fibers support relatively larger stress and thus contain the highest strain energy density that is a driving force for damage. Fiber damage is less severe for loading perpendicular to Langer's lines, as their strain energy is lower than that for the parallel loading. Fiber fractures are negligible for loading normal to the plane of the skin. This prediction is logical considering that the fibers should not stretch or compress under uniaxial strain perpendicular to their enclosing plane. Some fibers are dispersed out-of-plane, but their contribution to stiffness in the loading direction is zero to the present order of approximation for weak shocks.

Table 5 Shock evolution parameters for rabbit skin comprising ECF and solid ($n_0^1 = 0.73$). "Mixture" invokes same shock simultaneously to each phase. "Parallel" and "perpendicular" denote shock loading in orthogonal directions along and transverse to Langer's lines, respectively, with both directions in the plane of the skin tissue. "Normal" denotes shock loading orthogonal to plane of the skin. $(\Delta P)_0^\alpha$, $(\Delta\theta)_0^\alpha$, $(\Delta\bar{D})_0^\alpha$, and $(\Delta D_1)_0^\alpha$ are initial stress, temperature, and matrix and fiber damage jumps, respectively, for initial strain change $\Delta J_0^\alpha = [\![J^\alpha]\!](t=0) = -0.1$.

Property or		**Parallel**		**Perpendicular**		**Normal**	
prediction (units)	**ECF**	**Solid**	**Mixture**	**Solid**	**Mixture**	**Solid**	**Mixture**
ρ_0^α (g/cm^3)	0.278	0.922	1.200	0.922	1.200	0.922	1.200
$\hat{\mathsf{C}}^{\alpha+}$ (GPa)	0.594	2.509	3.103	2.495	3.089	2.453	3.047
$\hat{\mathsf{C}}'^{\alpha+}$ (GPa)	-4.728	-20.20	-24.93	-20.20	-24.93	-20.11	-24.84
$\mathcal{C}^\alpha$ (km/s)	1.462	1.650	1.608	1.645	1.604	1.631	1.593
$\hat{\mathsf{G}}^{\alpha+}$ (g K/cm^3)	-11.38	-78.89	-87.45	-78.89	-87.45	-78.89	-87.45
ω^α (1/s)	8.92×10^8	2.69×10^8	8.12×10^1	2.69×10^8	8.47×10^1	2.69×10^8	7.88×10^1
Λ^α (1/m)	3.07×10^5	8.10×10^4	2.51×10^{-2}	8.08×10^4	2.62×10^{-2}	8.05×10^4	2.43×10^{-2}
$(\Delta P)_0^\alpha$ (MPa)	83.0	364	447	363	446	359	442
$(\Delta\theta)_0^\alpha$ (K)	4.32	9.10	7.74	9.10	7.74	9.10	7.74
$(\Delta\bar{D})_0^\alpha$ (-) matrix	...	0.040	0.040	0.040	0.040	0.040	0.040
$(\Delta D_1)_0^\alpha$ (-) fibers	...	0.081	0.081	0.033	0.033	0.000	0.000

Normalized exponential decay of $[\![P^\alpha]\!]$ and $[\![\theta^\alpha]\!]$ calculated from Eq. 302 is shown for shocks applied individually to each constituent in Fig. 8a and to the homogenized mixture with equal velocities and temperatures among phases in Fig. 8b. For the former case, solid-fluid interactions are included, noting that interphase momentum drag is the primary impetus for transient decay of shock amplitudes when phases are shocked individually. Shock evolution in the latter case of Fig. 8b, wherein viscoelastic dissipation is the only source of decay, occurs over much greater distances (i.e., order of meters) than that in Fig. 8a (i.e., order of tens of micrometers). These trends agree with results for skeletal muscle and liver reported in Section 4.4.1. Differences in decay for different loading directions are barely discernible in Fig. 8a and are deemed very small in Fig. 8b.

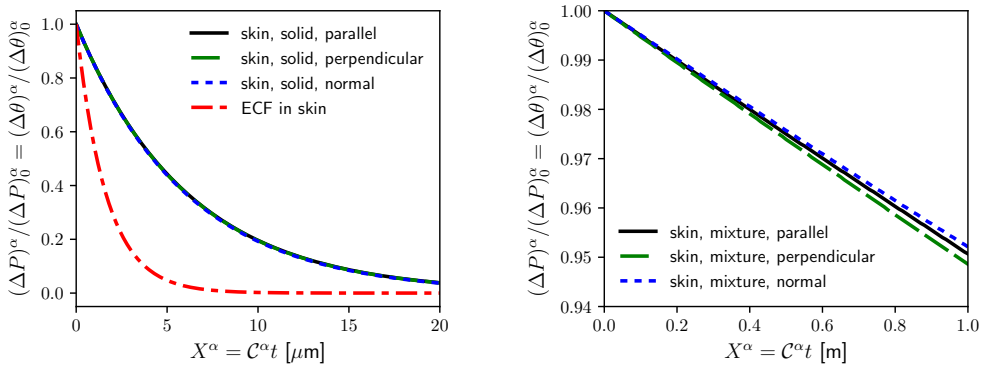

(a) skin, constituents

(b) skin, homogenized mixture

Fig. 8 Predicted ratio of jump in shock stress $(\Delta P)^\alpha$ or temperature $(\Delta\theta)^\alpha$ normalized by initial magnitude $(\Delta P)^\alpha_0$ or $(\Delta\theta)^\alpha_0$, for shock amplitude ΔJ^α_0 vs. propagation distance X^α in the weak shock limit: (a) shock applied individually to skin constituent α interacting with phase $\beta \neq \alpha$, (b) shock applied simultaneously to tied constituents of the skin in its homogenized mixture representation. Wave speed is $\mathcal{C}^\alpha$; different scales (i.e., μm or m) used for X^α. Shocks applied independently in directions parallel or perpendicular to Langer's lines in the plane of the skin, or normal to the plane of the skin.

Table 6 compares decay distances for shocks applied to isolated solid constituents (albeit with fluid-solid interactions) in skeletal muscle, liver, lung, and skin. Outcomes of the study of Section 4.4.1 are used for the first three materials and those of the present Section 4.4.2 are used for skin. Denote by Φ^α the normalized shock amplitude for constituent α with constant weak-shock velocity $\mathcal{C}^\alpha$ and decay constant ω^α. Inverting Eq. 302, the decay distance $X^\alpha = \mathcal{C}^\alpha t$ from a shock applied at

$t = 0$ is

$$X^\alpha = -(\mathcal{C}^\alpha/\omega^\alpha) \ln \Phi^\alpha. \tag{344}$$

Results in Table 6 for skin are for loading parallel to Langer's lines; differences for loading in other directions are negligible, on the order of 1% of X^α.

Substantial decay requires distances on the order of micrometers in solid tissues of skeletal muscle and skin. Decay takes place over distances of millimeters in liver. Significant shock evolution requires the largest distances in lung, on the order of centimeters. Recall from Figs. 6 and 8a that shocks in the fluid phase all decay over shorter distances than those in the solid phase. If isolated shocks degenerate over distances small relative to the dimensions of the microstructure, then a physically rational assumption is that macroscopic shock propagation can be modeled using the homogenized mixture approximation (e.g., a constrained mixture theory[145,146,188,189]). From results in Table 6, this "locally undrained" assumption, wherein fluid and solid phases move in concert with the same local velocity (i.e., fluid is entrapped or immobile with respect to the solid) and temperature, appears most-to-least appropriate in the following order: skeletal muscle, skin, liver parenchyma, and lung parenchyma.

Table 6 Decay distance X^α to attain fraction of initial shock strength Φ^α predicted for weak shocks in solid tissue phase ($\alpha = 1$)

Soft	**Decay distance X^α (units)**		
tissue	$\Phi^\alpha = 0.9$	$\Phi^\alpha = 0.5$	$\Phi^\alpha = 0.1$
Muscle	0.20 μm	1.32 μm	4.40 μm
Skin	0.65 μm	4.25 μm	14.12 μm
Liver	0.07 mm	0.43 mm	1.42 mm
Lung	1.55 cm	10.18 cm	33.81 cm

5. Conclusions

Presentation of a recent theoretical framework[1] is advanced for modeling multiphase soft biologic materials over wide ranges of loading rate and pressure. Classical continuum mixture theory of Bowen and Truesdell is augmented with internal variables that can address viscoelasticity, activation, growth and remodeling, and tissue degradation (e.g., the opposite of growth and remodeling). Dependence of free energy and external working on state variable gradients leads to Ginzburg–Landau-type kinetics for these state variables. The phase-field fracture theory distinguishes among order parameters associated with matrix and fiber damage, providing more physical insight than prior models that used only single damage order parameter. Permitting non-Euclidean metric tensors to depend on internal state can resolve residual (i.e., remnant) strain from growth, remodeling, or degradation. Fracture resistance increases in concert with remnant strain, similar to toughening seen in structural materials in concert with plastic strain. Usual incompressibility assumptions of soft-tissue mechanics and poromechanics are abandoned to permit modeling of shock waves and large (volumetric) compressions, the latter unrestricted by initial porosity of the drained solid medium.

Results for uniaxial-stress and shock loading agree with experimental data on biologic fluids and soft tissues. Fluids include water, ECF, and blood. Soft tissues include skeletal muscle infused with ECF, liver infused with blood, and lung permeated with air. New results on shock loading of skin, not addressed in the recent underlying theoretical article,[1] are also reported. Skin is modeled as a mixture comprised of ECF and a solid tissue phase, the latter represented by an isotropic matrix and two families of weakly dispersed collagen fibers furnishing orthotropic anisotropy.

Uniaxial-stress calculations reveal that damage, represented by order parameters for matrix rupture and fiber fractures, is strain-rate insensitive in muscle fibers but rate dependent in liver. Model results adequately match experimental data on these tissue types. Since the solid and fluid phases are of about the same bulk compressibility, and since both constituents are nearly incompressible (i.e., null or very small ratio of tangent shear modulus to bulk modulus), uniaxial stresses supported by the mixture are nearly indistinguishable whether the fluid phase is equilibrated to its partial atmospheric pressure or tied to deform laterally in lock-step with the solid

phase. In the latter undrained assumption, the total lateral pressure of the mixture is equilibrated to ambient atmospheric pressure (i.e., 1 atm) when simulating uniaxial-stress experiments.

A new analytical solution has been derived for shock evolution including phase interactions, viscoelasticity, and tissue damage. Closed-form results are obtained in the weak-shock limit. Calculations consider one of the two phases shock-loaded independently, albeit still interacting with the other initially quiescent phase, or a single shock wave applied simultaneously to all constituents in a homogenized material system. Model predictions for weak shocks reveal the dominance of interphase momentum and energy exchange over viscoelastic dissipation and effects of matrix and fiber damage for all two-phase materials. For muscle, liver, and skin, effects of interphase heat exchange on shock decay are small relative to effects of interphase viscous drag. For lung, thermal effects are not insignificant, but an uncertain value of the Grüneisen parameter, on the order of 0.1, is prescribed for the solid-tissue phase of the lung.

In all materials, decay distances for weak shocks in solid constituents are around one order of magnitude larger than those for fluid constituents. Weak shock decay in isolated constituents occurs over distances of micrometers in muscle and skin, over distances of millimeters in liver, and over distances of tens of centimeters in lung. An assumption that the mixture can be idealized as a single-phase material with homogenized properties therefore appears most valid for the dynamic response of skeletal muscle and skin tissue, less valid for liver, and least valid for lung. Numerical solutions for transient shock response obtained from poromechanics simulations[74,242–245] should confirm or refute these inferences in the future.

6. References

1. Clayton J. Universal phase-field mixture representation of thermodynamics and shock wave mechanics in porous soft biologic continua. Physical Review E. 2024;110:035001.

2. Fung YC. Biomechanics: Motion, flow, stress, and growth. Springer; 1990.

3. Fung YC. Biomechanics: Mechanical properties of living tissues. 2nd ed. Springer; 1993.

4. Cooper G, Jonsson A. Protection against blast injury. In: Cooper GJ, Dudley HAF, Gann DS, Little RA, Maynard RL, editors. Scientific foundations of trauma. Butterworth Heinemann; 1997. p. 258–283.

5. Saraf H, Ramesh K, Lennon A, Merkle A, Roberts J. Mechanical properties of soft human tissues under dynamic loading. Journal of Biomechanics. 2007;40:1960–1967.

6. Wilgeroth J, Hazell P, Appleby-Thomas G. The dynamic response and shock-recovery of porcine skeletal muscle tissue. AIP Conference Proceedings. 2012;1426:139–142.

7. Hampton C, Kleinberger M. Material models for the human torso finite element model. DEVCOM Army Research Laboratory (US); 2018. Report No.: ARL-TR-8338.

8. Clayton J, Banton R, Freed A. A nonlinear thermoelastic-viscoelastic continuum model of lung mechanics for shock wave analysis. AIP Conference Proceedings. 2020;2272:040001.

9. Brannen M, Kang G, Dutrisac S, Banton R, Clayton J, Petel O. The influence of the tertiary bronchi on dynamic lung deformation. Journal of the Mechanical Behavior of Biomedical Materials. 2022;130:105181.

10. Clayton J, Banton R, Goertz A. A continuum mechanical model of the human lung: implementation and parameterization. CCDC Army Research Laboratory (US); 2020. Report No.: ARL-TR-9138.

11. Freed A, Zamani S, Paul S, Clayton J. A dodecahedral model for alveoli. Part I. theory and numerical methods. CCDC Army Research Laboratory (US); 2021. Report No.: ARL-TR-9148.

12. Freed A, Clayton J. Coordinate indexing strategies for the Laplace stretch in two and three dimensions. DEVCOM Army Research Laboratory (US); 2022. Report No.: ARL-TR-9530.

13. Cowin S, Doty S. Tissue mechanics. Springer; 2007.

14. Ricken T, Dahmen U, Dirsch O. A biphasic model for sinusoidal liver perfusion remodeling after outflow obstruction. Biomechanics and Modeling in Mechanobiology. 2010;9:435–450.

15. Zheng Y, Jiang Y, Cao Y. A porohyperviscoelastic model for the shear wave elastography of the liver. Journal of the Mechanics and Physics of Solids. 2021;150:104339.

16. Holzapfel G, Ogden R. Constitutive modelling of passive myocardium: a structurally based framework for material characterization. Philosophical Transactions of the Royal Society A. 2009;367:3445–3475.

17. Sachs D, Wahlsten A, Kozerke S, Restivo G, Mazza E. A biphasic multilayer computational model of human skin. Biomechanics and Modeling in Mechanobiology. 2021;20:969–982.

18. Yang W, Sherman V, Gludovatz B, Schaible E, Stewart P, Ritchie R, Meyers M. On the tear resistance of skin. Nature Communications. 2015;6:6649.

19. Zubelewicz A. Liquid-liquid-solid transition in viscoelastic liquids. Scientific Reports. 2013;3:1323.

20. Varchanis S, Dimakopoulos Y, Wagner C, Tsamopoulos J. How viscoelastic is human blood plasma?. Soft Matter. 2018;14:4238–4251.

21. Van Liedekerkem P, Tijskens E, Ramon H, Ghysels P, Samaey G, Roose D. Particle-based model to simulate the micromechanics of biological cells. Physical Review E. 2010;81:061906.

22. Waugh R, Evans E. Thermoelasticity of red blood cell membrane. Biophysics Journal. 1979;26:115–131.

23. Holzapfel G, Gasser T, Ogden R. A new constitutive framework for arterial wall mechanics and a comparative study of material models. Journal of Elasticity. 2000;61:1–48.

24. Chagnon G, Rebouah M, Favier D. Hyperelastic energy densities for soft biological tissues: a review. Journal of Elasticity. 2015;120:129–160.

25. Rubin M, Bodner S. A three-dimensional nonlinear model for dissipative response of soft tissue. International Journal of Solids and Structures. 2002;39:5081–5099.

26. Flynn C, Rubin M. An anisotropic discrete fiber model with dissipation for soft biological materials. Mechanics of Materials. 2014;68:217–227.

27. Gultekin O, Sommer G, Holzapfel G. An orthotropic viscoelastic model for the passive myocardium: continuum basis and numerical treatment. Computer Methods in Biomechanics and Biomedical Engineering. 2016;19:1647–1664.

28. Gasser T, Ogden R, Holzapfel G. Hyperelastic modelling of arterial layers with distributed collagen fibre orientations. Journal of the Royal Society Interface. 2006;3:15–35.

29. Planas J, Guinea G, Elices M. Constitutive model for fiber-reinforced materials with deformable matrices. Physical Review E. 2007;76:041903.

30. Kalhofer-Kochling M, Bodenschatz E, Wang Y. Structure tensors for dispersed fibers in soft materials. Physical Review Applied. 2020;13:064039.

31. Ito D, Tanaka E, Yamamoto S. A novel constitutive model of skeletal muscle taking into account anisotropic damage. Journal of the Mechanical Behavior of Biomedical Materials. 2010;3:85–93.

32. Li W. Damage models for soft tissues: a survey. Journal of Medical and Biological Engineering. 2016;36:285–307.

33. Clayton J. Modeling lung tissue dynamics and injury under pressure and impact loading. Biomechanics and Modeling in Mechanobiology. 2020;19:2603–2626.

34. Clayton J, Freed A. Viscoelastic-damage theory based on a QR decomposition of deformation gradient. CCDC Army Research Laboratory (US); 2019. Report No.: ARL-TR-8840.

35. Clayton J, Freed A. A continuum mechanical model of the lung. CCDC Army Research Laboratory (US); 2019. Report No.: ARL-TR-8859.

36. Clayton J, Freed A. A constitutive model for lung mechanics and injury applicable to static, dynamic, and shock loading. Mechanics of Soft Materials. 2020;2:3.

37. Raina A, Miehe C. Rupture in soft biological tissues modeled by a phase-field method. Proceedings of Applied Math and Mechanics (PAMM). 2015;15:103–104.

38. Gultekin O, Hager S, Dal H, Holzapfel G. Computational modeling of progressive damage and rupture in fibrous biological tissues: application to aortic dissection. Biomechanics and Modeling in Mechanobiology. 2019;18:1607–1628.

39. Chittajallu S, Richhariya A, Tse K, Chinthapenta V. A review on damage and rupture modelling for soft tissues. Bioengineering. 2022;9:26.

40. Levitas V, Levin V, Zingerman K, Freiman E. Displacive phase transitions at large strains: phase-field theory and simulations. Physical Review Letters. 2009;103:025702.

41. Yang L, Dayal K. Formulation of phase-field energies for microstructure in complex crystal structures. Applied Physics Letters. 2010;96:081916.

42. Clayton J, Knap J. A phase field model of deformation twinning: nonlinear theory and numerical simulations. Physica D. 2011;240:841–858.

43. Clayton J, Knap J. Phase field analysis of fracture induced twinning in single crystals. Acta Materialia. 2013;61:5341–5353.

44. Acharya A, Vinals J. Field dislocation mechanics and phase field crystal models. Physical Review B. 2020;102:064109.

45. Karma A, Kessler D, Levine H. Phase-field model of mode III dynamic fracture. Physical Review Letters. 2001;87:045501.

46. Eastgate L, Sethna J, Rauscher M, Cretegny T, Chen CS, Meyers C. Fracture in mode I using a conserved phase-field model. Physical Review E. 2002;65:036117.

47. Henry H, Levine H. Dynamic instabilities of fracture under biaxial strain using a phase field model. Physical Review Letters. 2004;93:105504.

48. Marconi V, Jagla E. Diffuse interface approach to brittle fracture. Physical Review E. 2005;71:036110.

49. Spatschek R, Muller-Gugenberger C, Brener E. Phase field modeling of fracture and stress-induced phase transitions. Physical Review E. 2007;75:066111.

50. Clayton J, Knap J. A geometrically nonlinear phase field theory of brittle fracture. International Journal of Fracture. 2014;189:139–148.

51. Levitas V. Phase field approach to martensitic phase transformations with large strains and interface stresses. Journal of the Mechanics and Physics of Solids. 2014;70:154–189.

52. Levitas V, Idesman A, Palakala A. Phase-field modeling of fracture in liquid. Journal of Applied Physics. 2011;110:033531.

53. Santillan D, Mosquera JC, Cueto-Felgueroso L. Fluid-driven fracture propagation in heterogeneous media: Probability distributions of fracture trajectories. Physical Review E. 2017;96:053002.

54. Clayton J, Knap J. Nonlinear phase field theory for fracture and twinning with analysis of simple shear. Philosophical Magazine. 2015;95:2661–2696.

55. Clayton J, Knap J. Phase field modeling of coupled fracture and twinning in single crystals and polycrystals. Computer Methods in Applied Mechanics and Engineering. 2016;312:447–467.

56. Clayton J. Mesoscale models of interface mechanics in crystalline solids. Journal of Materials Science. 2018;53:5515–5545.

57. Needleman A. A continuum model for void nucleation by inclusion debonding. Journal of Applied Mechanics. 1987;54:525–531.

58. Clayton J, McDowell D. Homogenized finite elastoplasticity and damage: theory and computations. Mechanics of Materials. 2004;36:799–824.

59. Clayton J. Dynamic plasticity and fracture in high density polycrystals: constitutive modeling and numerical simulation. Journal of the Mechanics and Physics of Solids. 2005;53:261–301.

60. Clayton J. Modeling dynamic plasticity and spall fracture in high density polycrystalline alloys. International Journal of Solids and Structures. 2005;42:4613–4640.

61. Clayton J, Williams C. Deformation and failure of ductile and brittle solids in extreme dynamic environments. In: Silberschmidt V, editor. Comprehensive Mechanics of Materials; Vol. 1. Elsevier; 2024. p. 250–272.

62. Clayton J, Knap J, Leavy R. On rate dependence and anisotropy in phase field modeling of polycrystalline fracture. Mechanics of Materials. 2023;180:104606.

63. Clayton J, Leavy R, Knap J. Phase field theory for pressure-dependent strength in brittle solids with dissipative kinetics. Mechanics Research Communications. 2023;129:104097.

64. Biot M. General theory of three-dimensional consolidation. Journal of Applied Physics. 1941;12:155–164.

65. Truesdell C, Toupin R. The classical field theories. In: Flugge S, editor. Handbuch der Physik; Vol. III. Springer; 1960. p. 226–793.

66. Capriz G, Guidugli P. On the basic laws of reacting mixtures of structured continua. Meccanica. 1974;9:9–15.

67. Bowen R. Theory of mixtures. In: Eringen A, editor. Continuum Physics; Vol. 3. Academic Press; 1976. p. 1–127.

68. Bowen R. Compressible porous media models by use of the theory of mixtures. International Journal of Engineering Science. 1982;20:697–735.

69. Yang M, Taber L. The possible role of poroelasticity in the apparent viscoelastic behavior of passive cardiac muscle. Journal of Biomechanics. 1991;24:587–597.

70. Ehlers W. Foundations of multiphasic and porous materials. In: Ehlers W, Bluhm J, editors. Porous media: theory, experiments and numerical applications. Springer; 2002. p. 3–86.

71. Huyghe J, Arts T, Van Campen D, Reneman R. Porous medium finite element model of the beating left ventricle. American Journal of Physiology. 1992;262:H1256–H1267.

72. Regueiro R, Zhang B, Wozniak S. Large deformation dynamic three-dimensional coupled finite element analysis of soft biological tissues treated as biphasic porous media. Computer Modeling in Engineering Sciences (CMES). 2014;98:1–39.

73. MacMinn C, Dufresne E, Wettlaufer J. Large deformations of a soft porous material. Physical Review Applied. 2016;5:044020.

74. Irwin Z, Clayton J, Regueiro R. A large deformation multiphase continuum mechanics model for shock loading of soft porous materials. International Journal for Numerical Methods in Engineering. 2024;125:e7411.

75. Wilson Z, Landis C. Phase-field modeling of hydraulic fracture. Journal of the Mechanics and Physics of Solids. 2016;96:264–290.

76. Suh H, Sun W. Asynchronous phase field fracture model for porous media with thermally non-equilibrated constituents. Computer Methods in Applied Mechanics and Engineering. 2021;387:114182.

77. Terzaghi K. Theoretical soil mechanics. John Wiley and Sons; 1943.

78. Ehlers W, Wagner A. Modelling and simulation methods applied to coupled problems in porous-media mechanics. Archive of Applied Mechanics. 2021;89:609–628.

79. Fielding S, Cochran J, Huang J, Bi D, Marchetti M. Constitutive model for the rheology of biological tissue. Physical Review E. 2023;108:L042602.

80. Mulla Y, Oliveri G, Overvelde J, Koenderink G. Crack initiation in viscoelastic materials. Physical Review Letters. 2018;120:268002.

81. Bowen R, Wright T. Shock waves in a mixture of linear elastic materials. Rendiconti del Circolo Matematico di Palermo. 1972;21:209–234.

82. Baer M, Nunziato J. A two-phase mixture theory for the deflagration-to-detonation transition (DDT) in reactive granular materials. International Journal of Multiphase Flow. 1986;12:861–889.

83. Madjarevic D, Ruggeri T, Simic S. Shock structure and temperature overshoot in macroscopic multi-temperature model of mixtures. Physics of Fluids. 2014;26:106102.

84. Madjarevic D, Simic S. Entropy growth and entropy production rate in binary mixture shock waves. Physical Review E. 2019;100:023119.

85. Bowen R. Incompressible porous media models by use of the theory of mixtures. International Journal of Engineering Science. 1982;18:1129–1148.

86. Grillo A, Carfagna M, Federico S. An Allen-Cahn approach to the remodelling of fibre-reinforced anisotropic materials. Journal of Engineering Mathematics. 2018;109:139–172.

87. Clayton J. Analysis of shock waves in a mixture theory of a thermoelastic solid and fluid with distinct temperatures. International Journal of Engineering Science. 2022;175:103675.

88. Wilgeroth J, Hazell P, Appleby-Thomas G. On the behaviour of porcine skeletal muscle tissue under shock compression. International Journal of Impact Engineering. 2012;50:83–89.

89. Clayton J. A continuum description of nonlinear elasticity, slip and twinning, with application to sapphire. Proceedings of the Royal Society (London) A. 2009;465:307–334.

90. Clayton J, Williams C. Modelling the anomalous shock response of titanium diboride. Proceedings of the Royal Society of London A. 2022;478:20220253.

91. Boteler J, Sutherland G. Tensile failure of water due to shock wave interactions. Journal of Applied Physics. 2004;96:6919–6924.

92. Bejancu A. Finsler geometry and applications. Ellis Horwood; 1990.

93. Clayton J. Finsler-geometric continuum mechanics. DEVCOM Army Research Laboratory (US); 2016. Report No.: ARL-TR-7694.

94. Clayton J. Generalized Finsler geometric continuum physics with applications in fracture and phase transformations. Zeitschrift fur Angewandte Mathematik und Physik (ZAMP). 2017;68:9.

95. Clayton J. Finsler geometry of nonlinear elastic solids with internal structure. Journal of Geometry and Physics. 2017;112:118–146.

96. Clayton J. Finsler differential geometry in continuum mechanics: fundamental concepts, history, and renewed application to ferromagnetic solids. Mathematics and Mechanics of Solids. 2022;27:910–949.

97. Clayton J. Generalized Finsler geometry and the anisotropic tearing of skin. Symmetry. 2023;15:1828.

98. Takamizawa K, Matsuda T. Kinematics for bodies undergoing residual stress and its applications to the left ventricle. Journal of Applied Mechanics. 1990;57:321–329.

99. Yavari A. A geometric theory of growth mechanics. Journal of Nonlinear Science. 2010;20:781–830.

100. Sadik S, Angoshtari A, Goriely A, Yavari A. A geometric theory of nonlinear morphoelastic shells. Journal of Nonlinear Science. 2016;26:929–978.

101. Clayton J, Bammann D, McDowell D. Anholonomic configuration spaces and metric tensors in finite strain elastoplasticity. International Journal of Non-Linear Mechanics. 2004;39:1039–1049.

102. Clayton J, Bammann D, McDowell D. A geometric framework for the kinematics of crystals with defects. Philosophical Magazine. 2005;85:3983–4010.

103. Clayton J. Nonlinear mechanics of crystals. Springer; 2011.

104. Clayton J. Defects in nonlinear elastic crystals: differential geometry, finite kinematics, and second-order analytical solutions. Zeitschrift fur Angewandte Mathematik und Mechanik (ZAMM). 2015;95:476–510.

105. Clayton J. Nonlinear soft-tissue elasticity, remodeling, and degradation described by an extended Finsler geometry. arXiv preprint. 2024;https://doi.org/10.48550/arXiv.2408.15530.

106. Takano Y, Koibuchi H. J-shaped stress-strain diagram of collagen fibers: frame tension of triangulated surfaces with fixed boundaries. Physical Review E. 2017;95:042411.

107. Mitsuhashi K, Ghosh S, Koibuchi H. Mathematical modeling and simulations for large-strain J-shaped diagrams of soft biological materials. Polymers. 2008;10:715.

108. Ikeda S. A physico-geometrical consideration on the theory of directors in the continuum mechanics of oriented media. Tensor, N.S. 1973;27:361–368.

109. Ikeda S. On the conservation laws in the theory of fields in Finsler spaces. Journal of Mathematical Physics. 1981;22:1211–1214.

110. Eremeyev V, Konopinska-Zmyslowska V. On dynamic extension of a local material symmetry group for micropolar media. Symmetry. 2020;12:1632.

111. Clayton J. Finsler-geometric continuum dynamics and shock compression. International Journal of Fracture. 2017;208:53–78.

112. Clayton J. Finsler geometric-continuum mechanics and the micromechanics of fracture in crystals. Journal of Micromechanics and Molecular Physics. 2016;1:1640003.

113. Clayton J. Generalized pseudo-Finlser geometry applied to the nonlinear mechanics of torsion of crystalline solids. International Journal of Geometric Methods in Modern Physics. 2018;15:1850113.

114. Clayton J, Knap J. Continuum modeling of twinning, amorphization, and fracture: theory and numerical simulations. Continuum Mechanics and Thermodynamics. 2018;30:421–455.

115. Clayton J. Computational modeling of dual-phase ceramics with Finsler-geometric phase field mechanics. Computer Modeling in Engineering and Sciences (CMES). 2019;120:333–350.

116. Coleman B, Gurtin M. Thermodynamics and one dimensional shock waves in materials with memory. Proceedings of the Royal Society of London A. 1966;292:562–574.

117. Chen P, Gurtin M. Growth and decay of one-dimensional shock waves in fluids with internal state variables. Physics of Fluids. 1971;14:1091–1094.

118. Bowen R, Chen P. Shock waves in ideal fluid mixtures with several temperatures. Archive for Rational Mechanics and Analysis. 1974;53:277–294.

119. Rund H. The differential geometry of Finsler spaces. Springer-Verlag; 1959.

120. Amari S. A theory of deformations and stresses of ferromagnetic substances by Finsler geometry. In: Kondo K, editor. RAAG Memoirs; Vol. 3. Gakujutsu Bunken Fukyu-kai; 1962. p. 257–278.

121. Clayton J. Nonlinear elastic and inelastic models for shock compression of crystalline solids. Springer; 2019.

122. Grinfeld P. Introduction to tensor analysis and the calculus of moving surfaces. Springer; 2013.

123. Clayton J, Lloyd J. Finite strain continuum theory for phase transformations in ferromagnetic elastic-plastic solids. Continuum Mechanics and Thermodynamics. 2022;34:1579–1620.

124. Destrade M, Saccomandi G. Finite amplitude elastic waves propagating in compressible solids. Physical Review E. 2005;72:016620.

125. Ortega A, Lombardini M, Hill D. Converging shocks in elastic-plastic solids. Physical Review E. 2011;84:056307.

126. Taniguchi S, Arima T, Ruggeri T, Sugiyama M. Thermodynamic theory of the shock wave structure in a rarefied polyatomic gas: beyond the Bethe-Teller theory. Physical Review E. 2014;89:013025.

127. Davison L. Fundamentals of shock wave propagation in solids. Springer; 2008.

128. Annaidh A, Bruyere K, Destrade M, Gilchrist M, Maurini C, Ottenio M, Saccomandi G. Automated estimation of collagen fibre dispersion in the dermis and its contribution to the anisotropic behaviour of skin. Annals of Biomedical Engineering. 2012;40:1666–1678.

129. Burla F, Dussi S, Martinez-Torrez C, Tauber J, Gucht J, Koenderink G. Connectivity and plasticity determine collagen network fracture. Proceedings of the National Academy of Sciences USA. 2020;117:8326–8334.

130. Epstein M. The split between remodeling and aging. International Journal of Non-Linear Mechanics. 2009;44:604–609.

131. Epstein M. Mathematical characterization and identification of remodeling, growth, aging, and morphogenesis. Journal of the Mechanics and Physics of Solids. 2015;84:72–84.

132. Goriely A. The mathematics and mechanics of biological growth. Springer; 2017.

133. Hamedzadeh A, Gasser T, Federico S. On the constitutive modelling of recruitment and damage of collagen fibres in soft biological tissues. European Journal of Mechanics A Solids. 2018;72:483–496.

134. Hamedzadeh A, Grillo A, Epstein M, Federico S. Remodelling of biological tissues with fibre recruitment and reorientation in the light of the theory of material uniformity. Mechanics Research Communications. 2019;96:56–61.

135. Li K, Holzapfel G. Multiscale modeling of fiber recruitment and damage with a discrete fiber dispersion method. Journal of the Mechanics and Physics of Solids. 2019;126:226–244.

136. Kumar A, Yavari A. Nonlinear mechanics of remodeling. Journal of the Mechanics and Physics of Solids. 2023;181:105449.

137. Ambrosi D, Preziosi L, Vitale G. The insight of mixtures theory for growth and remodeling. Zeitschrift fur Angewandte Mathematik und Physik (ZAMP). 2010;61:177–191.

138. Grillo A, Prohl R, Wittum G. A poroplastic model of structural reorganisation in porous media of biomechanical interest. Continuum Mechanics and Thermodynamics. 2016;28:579–601.

139. Takamizawa K, Nakayama Y. Non-Euclidean stress-free configuration of arteries accounting for curl of axial strips sectioned from vessels. Journal of Biomechanical Engineering. 2013;135:114505.

140. Truesdell C. Rational thermodynamics. 2nd ed. Springer-Verlag; 1984.

141. Rajagopal K, Tao L. Mechanics of mixtures. World Scientific; 1995.

142. Hall R, Rajagopal K. Modeling approaches and some physical considerations concerning thermodynamics and the theory of mixtures applied to time-dependent behaviors in heterogeneous materials. Experimental Mechanics. 2020;60:591–609.

143. Hansen A, Crane R, Damson M, Donovan R, Horning D, Walker J. Some notes on a volume fraction mixture theory and a comparison with the kinetic theory of gases. International Journal of Engineering Science. 1991;29:561–573.

144. Liu IS. A solid-fluid mixture theory of porous media. International Journal of Engineering Science. 2014;84:133–146.

145. Humphrey J, Rajagopal K. A constrained mixture model for growth and remodeling of soft tissues. Mathematical Models and Methods in Applied Sciences. 2002;12:407–430.

146. Ateshian G, Zimmerman B. Continuum mechanics of constrained reactive mixtures. Journal of Biomechanical Engineering. 2022;144:041011.

147. Ruggeri T, Simic S. Average temperature and Maxwellian iteration in multi-temperature mixtures of fluids. Physical Review E. 2009;80:026317.

148. Gurtin M. Generalized Ginzburg-Landau and Cahn-Hilliard equations based on a microforce balance. Physica D. 1996;92:178–192.

149. Rund H. A divergence theorem for Finsler metrics. Monatshefte fur Mathematik. 1975;79:233–252.

150. Clayton J. Differential geometry and kinematics of continua. World Scientific; 2014.

151. Clayton J. Nonlinear thermodynamic phase field theory with application to fracture and dynamic inelastic phenomena in ceramic polycrystals. Journal of the Mechanics and Physics of Solids. 2021;157:104633.

152. Green A, Rivlin R. On Cauchy's equations of motion. Zeitschrift fur Angewandte Mathematik und Physik (ZAMP). 1964;15:290–292.

153. Marsden J, Hughes T. Mathematical foundations of elasticity. Prentice-Hall; 1983.

154. Eringen A. Nonlinear theory of continuous media. McGraw-Hill; 1962.

155. Truesdell C. Sulle basi della thermodinamica della miscele. Rendiconti Accademia Nazionale dei Lincei. 1968;44:381–383.

156. Grinfeld M. Thermodynamic methods in the theory of heterogeneous systems. Longman Scientific and Technical; 1991.

157. Casey J. On the derivation of jump conditions in continuum mechanics. International Journal of Structural Changes in Solids. 2011;3:61–84.

158. Kuhl E, Steinmann P. Mass- and volume-specific views on thermodynamics for open systems. Proceedings of the Royal Society of London A. 2003;459:2547–2568.

159. Volokh K. Stresses in growing soft tissues. Acta Biomaterialia. 2006;2:493–504.

160. Epstein M. The elements of continuum biomechanics. Wiley; 2012.

161. Dunn J, Serrin J. On the thermodynamics of interstitial working. Archive for Rational Mechanics and Analysis. 1985;88:95–133.

162. Bowen R, Rankin R. Acceleration waves in ideal fluid mixtures with several temperatures. Archive for Rational Mechanics and Analysis. 1973;51:261–277.

163. Simo J. On a fully three-dimensional finite-strain viscoelastic damage model: formulation and computational aspects. Computer Methods in Applied Mechanics and Engineering. 1987;60:153–173.

164. Holzapfel G, Simo J. A new viscoelastic constitutive model for continuous media at finite thermomechanical changes. International Journal of Solids and Structures. 1996;33:3019–3034.

165. Holzapfel G. On large strain viscoelasticity: continuum formulation and finite element applications to elastomeric structures. International Journal for Numerical Methods in Engineering. 1996;39:3903–3926.

166. Menzel A. Modelling of anisotropic growth in biological tissues. Biomechanics and Modeling in Mechanobiology. 2005;3:147–171.

167. Lubarda V, Hoger A. On the mechanics of solids with a growing mass. International Journal of Solids and Structures. 2002;39:4627–4664.

168. Coleman BD, Noll W. Archive for Rational Mechanics and Analysis. 1963;13:167.

169. Coleman B, Gurtin M. Thermodynaics with internal state variables. Journal of Chemical Physics. 1967;47:597–613.

170. Poirier JP, Tarantola A. A logarithmic equation of state. Physics of the Earth and Planetary Interiors. 1998;109:1–8.

171. Clayton J. Analysis of shock compression of strong single crystals with logarithmic thermoelastic-plastic theory. International Journal of Engineering Science. 2014;79:1–20.

172. Clayton J. Crystal thermoelasticity at extreme loading rates and pressures: analysis of higher-order energy potentials. Extreme Mechanics Letters. 2015;3:113–122.

173. Balzani D, Neff P, Schroder J, Holzapfel G. A polyconvex framework for soft biological tissues. adjustment to experimental data. International Journal of Solids and Structures. 2006;43:6052–6070.

174. Holzapfel G, Gasser T, Stadler M. A structural model for the viscoelastic behavior of arterial walls: continuum formulation and finite element analysis. European Journal of Mechanics A Solids. 2002;21:441–463.

175. Clayton J, Freed A. A constitutive framework for finite viscoelasticity and damage based on the Gram-Schmidt decomposition. Acta Mechanica. 2020;231:3319–3362.

176. Freed A. Soft solids. Springer; 2014.

177. Stalhand J, McMeeking R, Holzapfel G. On the thermodynamics of smooth muscle contraction. Journal of the Mechanics and Physics of Solids. 2016;94:490–503.

178. Martins J, Pires E, Salvado R, Dinis P. A numerical model of passive and active behavior of skeletal muscles. Computer Methods in Applied Mechanics and Engineering. 1998;151:419–433.

179. Franchini G, Breslavsky I, Giovanniello F, Kassab A, Holzapfel G, Amabili M. Role of smooth muscle activation in the static and dynamic mechanical characterization of human aortas. Proceedings of the National Academy of Sciences USA. 2022;119:2117232119.

180. Clayton J. Thermodynamic phase field models for fracture and inelasticity. DEVCOM Army Research Laboratory (US); 2021. Report No.: ARL-TR-9320.

181. Clayton J, Knap J. Phase field modeling of directional fracture in anisotropic polycrystals. Computational Materials Science. 2015;98:158–169.

182. Guo GJ, Zhang YG. Equilibrium molecular dynamics calculation of the bulk viscosity of liquid water. Molecular Physics. 2001;99:283–289.

183. Taniguchi T, Yamamoto S, Hayakawa A, Tanaka E, Kimpara H, Miki K. Strain-rate and muscle-tonus dependence of mechanical properties of rabbit tibialis anterior muscle. In: Proceedings of ATEM: Asian Conference on Experimental Mechanics. JSME-MMD; 2003. p. OS07W0228.

184. Clayton J, McDowell D, Bammann D. A multiscale gradient theory for single crystalline elastoviscoplasticity. International Journal of Engineering Science. 2004;42:427–457.

185. Epstein M, Maugin G. Thermomechanics of volumetric growth in uniform bodies. International Journal of Plasticity. 2000;16:951.

186. Xu F, Lu T, Seffen K. Biothermomechanics of skin tissue. Journal of the Mechanics and Physics of Solids. 2008;56:1852–1884.

187. Chato J. Heat transfer to blood vessels. Journal of Biomechanical Engineering. 1980;102:110–118.

188. Nims R, Ateshian G. Reactive constrained mixtures for modeling the solid matrix of biological tissues. Journal of Elasticity. 2017;129:69–105.

189. Humphrey J. Constrained mixture models of soft tissue growth and remodeling–twenty years after. Journal of Elasticity. 2021;145:49–75.

190. Cahn J, Hilliard J. Free energy of a nonuniform system. I. Interfacial free energy. Journal of Chemical Physics. 1958;28:258–267.

191. Zhu J, Chen LQ, Shen J, Tikare V. Coarsening kinetics from a variable-mobility Cahn-Hilliard equation: Application of a semi-implicit Fourier spectral method. Physical Review E. 1999;60:3564–3572.

192. Kell G. Density, thermal expansivity, and compressibility of liquid water from 0 to 150 c. correlations and tables for atmospheric pressure and saturation reviewed and expressed on 1968 temperature scale. Journal of Chemical Engineering Data. 1975;20:97–105.

193. Nagayama K, Mori Y, Shimada K, Nakahara M. Shock Hugoniot compression curve for water up to 1 GPa by using a compressed gas gun. Journal of Applied Physics. 2002;91:476–482.

194. Yao DK, Zhang C, Maslov K, Wang L. Photoacoustic measurement of the Grüneisen parameter of tissue. Journal of Biomedical Optics. 2014;19:017007.

195. Jones K, Nie W, Hu J, Turian J, Kassaee A, Sehgal C, Avery S. Acoustic-based proton range verification in heterogeneous tissue: simulation studies. Physics in Medicine and Biology. 2018;63:025018.

196. Morro A. Wave propagation in thermo-viscous materials with hidden variables. Archive of Mechanics. 1980;32:145–161.

197. Morro A. Shock waves in thermo-viscous fluids with hidden variables. Archive of Mechanics. 1980;32:193–199.

198. Nagoya H, Obara T, Takayama K. Underwater shock propagation and focusing in inhomogeneous media. In: Brun R, Dumitrescu LZ, editors. Shock-waves at Marseille; Vol. 3. Springer-Verlag; 1995. p. 439–444.

199. Neville M, Mathias R. The extracellular compartments of frog skeletal muscle. Journal of Physiology. 1979;288:45–70.

200. Song B, Chen W, Ge Y, Weerasooriya T. Dynamic and quasi-static compressive response of porcine muscle. Journal of Biomechanics. 2007;40:2999–3005.

201. Morrow D, Donahue T, Odegard G, Kaufman K. Transversely isotropic tensile material properties of skeletal muscle tissue. Journal of the Mechanical Behavior of Biomedical Materials. 2010;3:124–129.

202. Clayton J. Nonlinear thermomechanics for analysis of weak shock profile data in ductile polycrystals. Journal of the Mechanics and Physics of Solids. 2019;124:714–757.

203. Aryeetey O, Frank M, Lorenz A, Pahr D. Journal of the Mechanical Behavior of Biomedical Materials. 2022;135:105429.

204. Maher E, Early M, Creane A, Lally C, Kelly D. Site specific inelasticity of arterial tissue. Journal of Biomechanics. 2012;45:1393–1399.

205. Flory P, Spurr O. Melting equilibrium for collagen fibers under stress. elasticity in the amorphous state. Journal of the American Chemical Society. 1960;83:1308–1316.

206. Sanderson R, Foley R, McIvor G, Kirkaldy-Willis W. Histological response on skeletal muscle to ischemia. Clinical Orthopaedics and Related Research. 1975;113:27–35.

207. Winkler T, Roth P, Matziolis G, Schumann M, Hahn S, Strube P, Stoltenburg-Didinger G, Perka C, Duda G, Tohtz S. Time course of skeletal muscle regeneration after severe trauma: muscle function against the background of MRI and histological findings. Acta Orthopaedica. 2011;82:102–111.

208. Pervin F, Chen W, Weerasooriya T. Dynamic compressive response of bovine liver tissues. Journal of the Mechanical Behavior of Biomedical Materials. 2011;4:76–84.

209. Bonfiglio A, Leungchavaphongse K, Repetto R, Siggers J. Mathematical modeling of the circulation in the liver lobule. Journal of Biomechanical Engineering. 2010;132:111011.

210. Gao Z, Lister K, Desai J. Constitutive modeling of liver tissue: experiment and theory. Annals of Biomedical Engineering. 2010;38:505–516.

211. Soroushian B, Whelan W, Kolios M. Study of laser-induced thermoelastic deformation of native and coagulated ex-vivo bovine liver tissues for estimating their optical and thermomechanical properties. Journal of Biomedical Optics. 2010;15:065002.

212. Azar T, Hayward V. Estimation of the fracture toughness of soft tissue from needle insertion. In: Bello F, Edwards E, editors. Lecture Notes in Computer Science; Vol. 5104. Springer-Verlag; 2008. p. 166–175.

213. Rosen J, Brown J, De S, Sinanan M, Hannaford B. Biomechanical properties of abdominal organs in vivo and postmortem under compression loads. Journal of Biomechanical Engineering. 2008;130:021020.

214. Roan E, Vemaganti K. Strain rate-dependent viscohyperelastic constitutive modeling of bovine liver tissue. Medical and Biological Engineering and Computing. 2011;49:497–506.

215. Maleckova A, Kochova P, Palek R, Liska V, Mik P, Bonkowski T, Horak M, Tonar Z. Blunt injury of liver: mechanical response of porcine liver in experimental impact test. Physiological Measurement. 2021;42:025008.

216. Untaroiu C, Lu YC, Siripurapu S, Kemper A. Modeling the biomechanical and injury response of human liver parenchyma under tensile loading. Journal of the Mechanical Behavior of Biomedical Materials. 2015;41:280–291.

217. Lamsfuss J, Bargmann S. Computational modeling of damage in the hierarchical microstructure of skeletal muscles. Journal of the Mechanical Behavior of Biomedical Materials. 2022;134:105386.

218. Wang Q, Pei S, Lu X, Wang L, Wu Q. On the characterization of interstitial fluid flow in the skeletal muscle endomysium. Journal of the Mechanical Behavior of Biomedical Materials. 2020;102:103504.

219. Saha S, Francis I, Huang X, Paul A. Heat transfer and fluid flow analysis in a realistic 16-generation lung. Physics of Fluids. 2022;34:061906.

220. Khandagale P, Breitzman T, Majidi C, Dayal K. Statistical field theory for nonlinear elasticity of polymer networks with excluded volume interactions. Physical Review E. 2023;107:064501.

221. Joodaki H, Panzer M. Skin mechanical properties and modeling: a review. Proceedings of the Institution of Mechanical Engineers, Part H: Journal of Engineering in Medicine. 2018;232:323–343.

222. Lanir Y, Fung Y. Two-dimensional mechanical properties of rabbit skin—II. Experimental results. Journal of Biomechanics. 1974;7:171–182.

223. Tubon O J.D.T. Moreno-Flores, Sree V, Tepole A. Anisotropic damage model for collagenous tissues and its application to model fracture and needle insertion mechanics. Biomechanics and Modeling in Mechanobiology. 2022;21:1857–1872.

224. Annaidh A, Bruyère K, Destrade M, Gilchrist M, Otténio M. Characterization of the anisotropic mechanical properties of excised human skin. Journal of the Mechanical Behavior of Biomedical Materials. 2012;5:139–148.

225. Oftadeh R, Connizzo B, Nia H, Ortiz C, Grodzinsky A. Biological connective tissues exhibit viscoelastic and poroelastic behavior at different frequency regimes: application to tendon and skin biophysics. Acta Biomaterialia. 2018;70:249–259.

226. Lanir Y. The rheological behavior of the skin: experimental results and a structural model. Biorheology. 1979;16:191–202.

227. Oomens C. A mixture approach to the mechanics of skin and subcutis : a contribution to pressure sore research [thesis]. Eindhoven University of Technology; 1985.

228. Oomens C, Van Campen D, Grootenboer H. A mixture approach to the mechanics of skin. Journal of Biomechanics. 1987;20:877–885.

229. Oomens C, Van Campen D, Grootenboer H. In vitro compression of a soft tissue layer on a rigid foundation. Journal of Biomechanics. 1987;20:923–935.

230. Wahlsten A, Pensalfini M, Stracuzzi A, Restivo G, Hopf R, Massa E. On the compressibility and poroelasticity of human and murine skin. Biomechanics and Modeling in Mechanobiology. 2019;18:1079–1093.

231. Li C, Jiang J, Xu K. The variations of water in human tissue under certain compression studied with diffuse reflectance spectroscopy. Journal of Innovative Optical Health Sciences. 2013;6:1350005.

232. Samant P, Prausnitz M. Mechanisms of sampling interstitial fluid from skin using a microneedle patch. Proceedings of the National Academy of Sciences USA. 2018;115:4583–4588.

233. Moran C, Bush N, Bamber J. Ultrasonic propagation properties of excised human skin. Ultrasound in Medicine and Biology. 1995;21:1177–1190.

234. Moore D, Jerusalem A, Nyein M, Noels L, Jaffee M, Radovitzky R. Computational biology–modeling of primary blast effects on the central nervous system. NeuroImage. 2009;47:T10–T20.

235. Torvi D, Dale J. A finite element model of skin subjected to a flash fire. Journal of Biomechanical Engineering. 1994;116:250–255.

236. Cetingul M, Herman C. A heat transfer model of skin tissue for the detection of lesions: sensitivity analysis. Physics in Medicine and Biology. 2010;55:5933–5961.

237. Lim J, Hong J, Chen W, Weerasooriya T. Mechanical response of pig skin under dynamic tensile loading. International Journal of Impact Engineering. 2011;38:130–135.

238. Pereira B, Lucas P, Swee-Hin T. Ranking the fracture toughness of thin mammalian soft tissues using the scissors cutting test. Journal of Biomechanics. 1997;30:91–94.

239. Sree V, Ardekani A, Vlachos P, Tepole A. The biomechanics of autoinjector-skin interactions during dynamic needle insertion. Journal of Biomechanics. 2022;134:110995.

240. Weiss M, Shrestha P, Basak R, Stoeber B. Poroelastic behavior of skin tissue in response to pressure driven flow. Physics of Fluids. 2023;35:081902.

241. Oien A, Wiig H. Modeling in vivo interstital hydration-pressure relationships in skin and skeletal muscle. Biophysical Journal. 2018;115:924–935.

242. Irwin Z, Regueiro R, Clayton J. A large deformation multiphase continuum mechanics model for shock loading of lung parenchyma. Part I: Theory. DEVCOM Army Research Laboratory (US); 2023. Report No.: ARL-TR-9686.

243. Irwin Z, Regueiro R, Clayton J. A large deformation multiphase continuum mechanics model for shock loading of lung parenchyma. Part II: Numerical methods. DEVCOM Army Research Laboratory (US); 2023. Report No.: ARL-TR-9687.

244. Irwin Z, Regueiro R, Clayton J. A large deformation multiphase continuum mechanics model for shock loading of lung parenchyma. Part III: Numerical simulations. DEVCOM Army Research Laboratory (US); 2023. Report No.: ARL-TR-9688.

245. Irwin Z, Regueiro R, Clayton J. A large deformation multiphase continuum mechanics model for shock loading of lung parenchyma: Investigating the effects of fluid viscous stress. DEVCOM Army Research Laboratory (US); 2023. Report No.: ARL-TR-9815.

List of Symbols, Abbreviations, and Acronyms

TERMS:

1-D	one-dimensional
2-D	two-dimensional
3-D	three-dimensional
ARL	Army Research Laboratory
DEVCOM	US Army Combat Capabilities Development Command
ECF	extracellular fluid
EOS	equation of state

MATHEMATICAL SYMBOLS:

$(\square)^{\alpha}$	quantity for constituent or phase α
$(\square)_{k}$	quantity for fiber family k
$(\square)_{\mathrm{A}}$	quantity for active tension model
$(\square)_{\mathrm{D}}$	quantity for damage model
$(\square)_{\mathrm{F}}$	quantity for fiber hyperelasticity
$(\square)_{\mathrm{H}}$	quantity associated with Hugoniot response
$(\square)_{\mathrm{R}}$	quantity for isolated (i.e., real) constituent
$(\square)_{\mathrm{S}}$	quantity for deviatoric response
$(\square)_{\mathrm{V}}$	quantity for volumetric response
$(\square)_{\Gamma}$	quantity for matrix viscoelasticity
$(\square)_{\Phi}$	quantity for fiber viscoelasticity
$(\square)^{+}$	state quantity immediately ahead of shock front
$(\square)^{-}$	state quantity immediately behind shock front

$\nabla(\square)$	spatial gradient
$\nabla_0(\square)$	referential gradient
$\partial_t(\square)$	spatial time derivative
$D_t(\square)$	material time derivative with respect to constituent
$(\dot{\square})$	material time derivative with respect to mixture
$\delta_t(\square)$	moving time derivative at shock front
$(\square)^{\mathsf{T}}$	transpose
$(\square)^{-1}$	inverse
$\mathrm{tr}(\square)$	trace
$(\square)\cdot(\square)$	scalar product of vectors
$(\square):(\square)$	scalar product of second-order tensors
$(\square)\otimes(\square)$	outer (tensor) product of vectors
$\nabla\cdot(\square)$	spatial divergence
$[\![\square]\!]$	jump across singular surface
$\langle\square\rangle$	average across singular surface
$\mathrm{H}(\square)$	Heaviside unit step function
$\mathbf{1}$	unit tensor
a	generic dissipative internal variable
A	volumetric coefficient of thermal expansion
$\mathbf{b}$	spatial body force per unit mass
b	generic conservative internal variable
B_θ	isothermal bulk modulus
B_η	isentropic bulk modulus
$B_{\theta\mathrm{p}}$	pressure derivative of isothermal bulk modulus
$B_{\eta\mathrm{p}}$	pressure derivative of isentropic bulk modulus

$\hat{B}$	bulk Newtonian viscosity
$\tilde{\mathbf{B}}$	deviatoric Eulerian deformation tensor
c	mass supply rate
$\hat{c}$	modified mass supply rate
c_{B}	bulk sound speed
c_ϵ	specific heat per unit mass at constant strain
c_p	specific heat per unit mass at constant pressure
$\hat{C}$	total mass supply rate
$\mathbf{C}$	right Cauchy–Green tensor
$\bar{\mathbf{C}}$	right Cauchy–Green tensor excluding spatial Finsler metric
$\tilde{\mathbf{C}}$	deviatoric right Cauchy–Green tensor
C	longitudinal tangent modulus
$\mathbf{d}$	spatial deformation rate tensor
D	order parameter or damage measure for fiber fracture
$\bar{D}$	order parameter for matrix fracture or fluid cavitation
$\mathcal{C}$	longitudinal sound speed
$\mathcal{D}$	steady wave speed
$\mathfrak{D}$	dissipation per unit spatial volume
E_{C}	cohesive energy of fibers per unit reference volume
$\bar{E}_{\mathrm{C}}$	cohesive energy of matrix or fluid per unit reference volume
$\mathbf{F}$	deformation gradient
$\tilde{\mathbf{F}}$	deviatoric deformation gradient
g	determinant of spatial metric tensor
G	determinant of referential metric tensor
$\mathbf{g}$	spatial metric tensor

$\mathbf{G}$	referential metric tensor
$\bar{\mathbf{g}}$	Euclidean part of spatial metric tensor
$\bar{\mathbf{G}}$	Euclidean part of referential metric tensor
$\hat{\mathbf{g}}$	Finsler part of spatial metric tensor
$\hat{\mathbf{G}}$	Finsler part of referential metric tensor
G	longitudinal stress-entropy modulus
$\mathbf{h}$	momentum exchange per unit volume
$\mathbf{H}$	fiber structure tensor
I	scalar invariant
J	Jacobian determinant of deformation gradient
J_{C}	fracture toughness (energy per unit area)
k	fiber exponential stiffening constant
k_{V}	volumetric exponential stiffening constant
$\mathbf{l}$	spatial velocity gradient
l	regularization length for phase-field fracture of fibers
$\bar{l}$	regularization length for rupture of matrix or cavitation of fluid
m	current constituent mass concentration
m_0	referential constituent mass concentration
$\mathfrak{m}$	spatial manifold
$\mathfrak{M}$	referential manifold
n	current constituent volume fraction
n_0	referential constituent volume fraction
p	Cauchy pressure
P	longitudinal stress
$\mathbf{q}$	spatial heat flux vector

$\mathbf{Q}$	conjugate stress to viscoelastic configurational state variable
r	point heat source per unit mass
$\tilde{r}$	Finsler metric exponential constant for fibers
$\bar{r}$	Finsler metric exponential constant for matrix or fluid
$\mathfrak{R}$	ideal gas constant
t	time
u	internal energy per unit mass
U	internal energy per unit volume
$\mathcal{U}$	Eulerian shock speed
$\mathcal{U}^\alpha$	Lagrangian shock speed of constituent α
$\mathcal{U}_0$	Lagrangian shock speed of mixture
$\mathbf{x}$	spatial (i.e., Eulerian) coordinates
$\mathbf{X}$	referential (i.e., Lagrangian or material) coordinates
$\mathbf{z}$	generalized traction
α_{v}	interfacial surface contact area per unit volume
β	viscoelastic stiffness factor
$\boldsymbol{\beta}$	thermal stress tensor
$\boldsymbol{\chi}$	spatial motion
δ^i_j	Kronecker delta
Δ	internal variable for active tension
ϵ	energy exchange rate per unit volume
ϵ_{r}	remnant strain
ϕ_{F}	ratio of fiber toughness to matrix toughness
φ	half-angle between skin collagen fiber families
$\boldsymbol{\gamma}$	Grüneisen tensor

$\boldsymbol{\Gamma}$	viscoelastic configurational state variable
F	total conjugate force for Ginzburg–Landau kinetics
η	entropy per unit mass
$\boldsymbol{\iota}$	fiber direction
κ	fiber dispersion constant
κ_θ	thermal conductivity
κ^{fs}	interphase (fluid-solid) heat transfer coefficient
λ	stretch measure
$\lambda^{\alpha\beta}$	interphase momentum transfer coefficient
Λ	activation energy or critical strain gradient for steady shock
μ	shear modulus
$\hat{\mu}$	Newtonian shear viscosity
$\boldsymbol{\mu}$	diffusion velocity
ν	viscosity or kinetic parameter
ω	shock evolution (e.g., decay) coefficient
$\omega^{\alpha\beta}$	interphase energy exchange coefficient
Ω	spatial volume
Ω_0	referential volume
$\boldsymbol{\pi}$	generalized conjugate force to internal variable
θ	temperature
ϑ	damage degradation exponent
ρ	spatial mass density
ρ_0	referential mass density
$\boldsymbol{\sigma}$	total Cauchy stress tensor
$\bar{\boldsymbol{\sigma}}$	thermo-viscoelastic stress tensor

$\hat{\boldsymbol{\sigma}}$	viscous stress tensor
ς	degradation function
Σ	singular surface
τ	shear stress or viscoelastic relaxation time
$\boldsymbol{\upsilon}$	particle velocity
Υ	surface energy for fiber fracture
$\bar{\Upsilon}$	surface energy for matrix failure or fluid cavitation
$\boldsymbol{\xi}$	internal state variable or Finsler vector (spatial)
$\boldsymbol{\Xi}$	internal state variable or Finsler vector (referential)
Ξ	hydraulic permeability (dimensions of area)
ψ	Helmholtz free energy per unit mass
Ψ	Helmholtz free energy per unit volume
$\boldsymbol{\zeta}$	generalized conjugate force to gradient variable

1 (PDF)	DEFENSE TECHNICAL INFORMATION CTR DTIC OCA
1 (PDF)	DEVCOM ARL FCDD RLB CI TECH LIB